A STUDY OF LINEAR VS. NONLINEAR CONTROL TECHNIQUES FOR THE RECONFIGURATION OF SATELLITE FORMATIONS

THESIS

David J. Irvin, Jr., Captain, USAF

AFIT/GA/ENY/01M-02

DEPARTMENT OF THE AIR FORCE

AIR UNIVERSITY

AIR FORCE INSTITUTE OF TECHNOLOGY

Wright-Patterson Air Force Base, Ohio

APPROVED FOR PUBLIC RELEASE; DISTRIBUTION UNLIMITED

20010523 012

AFIT/GA/ENY/01M-02

A STUDY OF LINEAR VS. NONLINEAR CONTROL TECHNIQUES FOR THE RECONFIGURATION OF SATELLITE FORMATIONS

THESIS

Presented to the Faculty

Department of Aeronautics and Astronautics

Graduate School of Engineering and Management

Air Force Institute of Technology

Air University

Air Eductaion and Training Command

in Partial Fulfillment of the Requirements for the

Degree of Master of Science in Astronautical Engineering

David Jonathan Irvin, Jr., B.S.

Captain, USAF

March 2001

A STUDY OF LINEAR VS. NONLINEAR CONTROL TECHNIQUES FOR THE RECONFIGURATION OF SATELLITE FORMATIONS

David Jonathan Irvin, Jr., B.S.

Captain, USAF

Approved:

_____   7 MAR 01

Lt Col David Jacques   Date
Thesis Advisor

_____   7 MAR 01

Dr. Brad Liebst   Date
Committee Member

_____   7 March 2001

Dr. Meir Pachter   Date
Committee Member

Acknowledgements

It is with extreme appreciation that I thank my wonderful wife for her understanding and patience during this endeavor. She sacrificed daily to allow me to not only complete this thesis but be proud of it. If not for her, I never would have made it in one piece.

I would also express my sincere thanks to my advisor, Lt Col Dave Jacques, for the countless hours he spent letting me bounce ideas (both insightful and inane) off him and the guidance he provided over the entire course of this project. I am also thankful to Dr. Andrew Sparks upon whose work a majority of this thesis is based and for leading me toward some of the more important issues early on. I would like to give a special thanks to Dr. Steve Tragessor who, although he wasn't on my reading committee, provided invaluable insight on numerous topics over the last six months.

Finally, I would be extraordinarily remiss if I didn't thank Ralph, Sean, Mike, Mark, Dan, and the whole space ops crew who daily put it all in perspective with a good laugh.

David Jonathan Irvin, Jr.

Table of Contents

x

List of Symbols

Symbol	Page

List of Abbreviations

Abstract

This thesis investigates several linear and nonlinear feedback control methods for satellite formation reconfigurations and compares them to a near optimal open loop, discrete-time, impulsive maneuver. The reconfigurations are done in terms of a set of relative parameters that define an orbit about the leader satellite (or center reference position if a leader satellite does not exist at the center of the formation). The purpose of the study is two-fold, to compare the control usage of continuous feedback control methods versus a discrete burn method and to determine if nonlinear control techniques offer significant improvement over more conventional linear control laws. Linear Quadratic Regulators (LQR), LQR with linearizing feedback, State Dependent Riccati Equation (SDRE) and sliding mode controllers are considered. Simulations showed that reconfigurations for small relative orbits were adequately controlled using linear techniques.

A STUDY OF LINEAR VS. NONLINEAR CONTROL TECHNIQUES FOR THE RECONFIGURATION OF SATELLITE FORMATIONS

I. Introduction

The use of satellite formations to do the work of larger more costly single satellites has become a topic of great interest both for the Air Force and NASA. The potential benefits of using formations are numerous. Smaller, cheaper satellites lead to reduced launch and life cycle costs. Individual satellites can be replaced giving the formation the ability to upgrade without a manned mission to the satellite. Similarly, spare satellites can replace formation components as they fail. This creates added reliability and lifetime to a mission. From a military standpoint, a formation has a greater survivability than a single satellite as multiple satellites are often harder to destroy than a single one. Most pertinent to this thesis is the ability of a formation to reconfigure its relative geometry in order to meet changes in operational needs, adapt to the failure of a component, or allow for multi-mission capability. For example, a formation of satellites performing a mapping mission using synthetic aperture radar (SAR) could change its ground resolution by changing its relative positions (14). Although satellite formations are a relatively new concept, several applications have been offered. The Air Force is exploring formations for use in surveillance, passive radiometry, terrain mapping, navigation, communications, and ground target identification (22). In the civilian sector, satellite formations have been proposed as a way to provide users with remote sensing data in the visible and near infrared spectral bands (2) and to achieve high precision localization of beacon positions (8). Throughout this thesis the reference point by which relative motion is measured is called the "leader satellite" or simply "leader". Satellites occupying relative orbits about the leader satellite are referred to as "follower satellites" or "follower".

From a dynamics viewpoint, two of the larger obstacles to functioning satellite formations are the ability to keep each satellite in precise relative orbits (stationkeeping) and, if the need arises, to change those relative orbits (reconfiguration). Both of these problems

require accurate relative position and velocity data and control methods that use an acceptable amount of fuel. To produce relative position and velocity data, a formation could utilize a sensor on board the leader satellite (i.e. bouncing photons off follower satellites), or use a differential global positioning system (GPS) method. The filtering of this raw data for use in a control architecture is still the focus of intense research and will not be examined in this thesis. The control method will take the relative position and velocity data provided by the estimation technique, compare it to the desired relative orbit, and use that error to calculate the needed thrust inputs for stationkeeping and reconfiguration. This leads to the question: How will desired orbits of follower satellites be specified? Mission planners will most likely want to think about cluster configurations in terms of relative orbits about a leader as opposed to individually specified inertial orbits about the Earth. In this work, relative orbits will be defined in terms of a set of unique parameters that are discussed later. Whatever the desired relative orbit, the follower satellite must also be in a Keplarian orbit in the absence of control forces and perturbations. To keep a satellite in a non-Keplarian orbit requires continuous use of fuel, an unacceptable situation for a satellite. It is therefore important to find relative orbits that not only fulfill desired mission needs but also follow a Keplarian orbit. Only orbits that follow both a closed path inertial orbit about the Earth and a closed path relative orbit about the leader in the absence of control forces and perturbations will be examined here. The stationkeeping controller maintaining the relative orbit will most likely be separate from the reconfiguration controller and has been investigated by other researchers [(4),(27)]. Therefore, this thesis will concentrate on linear and nonlinear reconfiguration controllers with total fuel usage (proportional to ΔV) and settling time as the key parameters for comparison.

1.1 Background

The basic concepts behind relative satellite motion were developed in the 1960's by W.H. Clohessy and R.S. Wiltshire who were working on methods of rendezvous for orbital construction (6). Although developed specifically for rendezvous, these relative equations of motion work well in the design of useful relative orbits. The nonlinear form of the Clohessy-Whiltshire equations (henceforth known as CW equations) assumes that

the leader satellite exists in a circular orbit. A linear form of the CW equations can be derived if the additional assumption is made that the distance between the leader and follower satellite is small in comparison to their orbital radii. These are not limiting factors to most applications of satellite formations. One notable exception is the use of highly eccentric orbits commonly used to spend more time over a certain hemisphere for communications purposes (i.e. Molniya orbits (14)). This type of orbit obviously violates the first assumption and invalidates the CW equations.

Although the framework for developing satellite formations has been around since the 1960's, only recently has this problem gained widespread attention within the research community. Early research tackled the estimation problem. The Air Force sponsored work that determined the ability of an on-board U-D covariance Kalman filter algorithm based on the CW equations to estimate relative position to within 25 meters (about one quarter of a radar wavelength) for a ten satellite orbital formation. Results showed the position error well within the accuracy requirement (28). This research was expanded to include the use of additional measurement data from other satellites in the formation during the update cycle which produced a higher degree of accuracy in the relative position estimation (7). A later Air Force Institute of Technology (AFIT) thesis treated the Earth as an imperfect sphere as opposed to a point mass and thus developed a better truth model which included the J_2 term of the Earth's geopotential (17). The estimator used the same multiple satellite data and Kalman filter as used in (7). Independent investigation of an on-board relative position estimator, using a least-squares error analysis of short range satellite-to-satellite tracking between formation members was examined in (25).

Air Force interest in satellite formations is apparent in the TechSat 21 program which was created to explore the basic technologies required to create a viable satellite formation mission (15). The TechSat 21 program supports research into collaborative behavior of satellites, micro-propulsion, micro-satellite design, micro-electro-mechanical systems, smart mechanisms, multifunctional structures, and lightweight solar arrays (22). Some researchers have investigated the parameterization of the linearized version of the CW equations (more commonly known as Hill's equations) and used this parameterization to characterize the shapes of the relative orbits (31). Hill's equations have also been used to

3

design linear controllers to solve the stationkeeping problem (24). The Air Force Research Laboratory (AFRL) has supported research that more elegantly defines a perceptive frame which supports decentralized feedback (each satellite controls its own relative position error) based on real-time sensor data (11). This concept is expanded and used with an LQR controller on several simple reconfigurations (23). The research into satellite formations has matured to the point that realistic designs of the intersatellite links have been proposed. These are the communication links by which follower satellites would talk to the leader satellite and, if need be, each other (9). More recent attempts to define the problem have concentrated on finding equations of motion that are not constrained to circular leader orbits (30). Similar attempts have been made towards the estimation of relative position in elliptical orbits using Kalman filters (10). Although it is desirable to be able to generalize the satellite formation problem to handle elliptical (and thus more nonlinear) leader orbits, there are a myriad of applications for the constrained case which is, of course, much simpler to solve. This thesis will therefore concentrate on the constrained case. One final note about satellite formations; the European Space Agency (ESA) attempted to launch the "Cluster" series of four identical satellites aboard the maiden flight of the Ariane 5 as part of the Inter-Agency Solar Terrestrial Physics program (IASTP). These satellites were designed to take three-dimensional field and plasma measurements of the magnetosphere; however, the launch ended in failure with the four satellites destroyed in June 1996. Plans have been underway since November 1996 to build three new satellites to add to the preexisting ground spare (3). The new "Cluster" satellites were launched by two Russian Soyuz rockets (two satellites per rocket) on 16 July and 9 August 2000 from the Baikonur Cosmodrome in Kazakhstan. Their science mission commenced on 7 Feburary 2001 after an extensive checkout (1).

1.2 Objectives

This thesis will expand on previous works in two ways. First, it will compare reconfiguration simulations using both linear and nonlinear control techniques as applied to the constrained case in which the leader is in a circular orbit. It is important to determine if nonlinear control techniques provide enough of a benefit (i.e. lower fuel usage and recon-

4

figuration times versus linear techniques) to make their use attractive on an operational satellite. If not, a case for the simpler linear techniques will be made. These continuous control techniques will also be compared against a near optimal, open loop, discrete-time, impulsive maneuver (OLDTIM) which will be described in detail later. Second, this thesis will employ the use of relative parameters (from the parameterization of the linear equations of motion) to define the relative orbit. This is important from an operational standpoint, as users of satellite formations will most likely want to think in terms of relative orbits rather than Keplarian (Earth centered) orbits. Therefore, relative parameters are used to define the initial and final relative orbits of the follower about the leader satellite.

II. Relative Satellite Dynamics

The relative equations of motion are based on the inertial orbit equation (Derivation is in Appendix A)

$$\ddot{\vec{d}} = \frac{-\mu\vec{d}}{|\vec{d}|^3} + \vec{v}_c + \vec{v}_p \tag{1}$$

where μ is the gravitational parameter (for Earth $\mu = 398601\frac{km^3}{s^2}$), $\vec{d}$ is the position vector of the satellite, $\vec{v}_c$ is a vector of control forces per unit mass, and $\vec{v}_p$ is a vector of perturbation accelerations (oblate Earth effects, air drag, solar pressure, etc.). For now, assume that the satellite operates in a perturbations free environment ($\vec{v}_p = \vec{0}$). In "Terminal Guidance System for Satellite Rendezvous", (6) Clohessy and Wiltwhire used the inertial orbit equation to derive the equations of motion of a follower satellite about a leader satellite. These equations are the foundation upon which the control laws developed here are based; they are set up as follows: assume a moving reference frame centered on the leader satellite which is in a circular orbit about the Earth. The Radial, Cross Track, Out of Plane (RCO) coordinate frame is formed by the position vector of the leader satellite in inertial space $[\hat{R}]$, the velocity vector $[\hat{C}]$ (which for a circular orbit will always be perpendicular to the position vector), and the cross product of $\hat{R}$ and $\hat{C}$ which points out of the orbit plane $[\hat{O}]$ (same direction as the angular momentum vector of the leader satellite) as shown in Figure 1. In the RCO frame, the follower's relative equations of
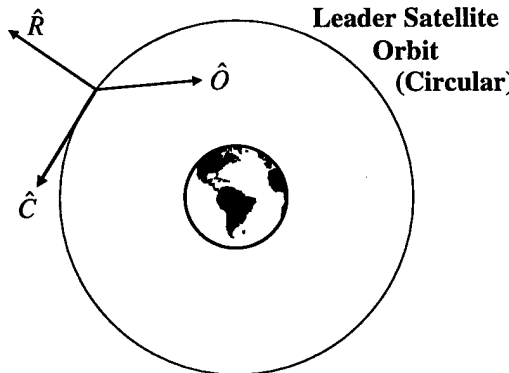
Figure 1   The RCO Frame

6

motion are [(6),(23)] (Derivation is in Appendix C):

$$\ddot{r} - 2\omega\dot{c} - \omega^2(k_o + r)\left[1 - \frac{k_o^3}{[(k_o+r)^2+c^2+o^2]^{\frac{3}{2}}}\right] - v_{c_r} = 0$$

$$\ddot{c} + 2\omega\dot{r} - \omega^2 c\left[1 - \frac{k_o^3}{[(k_o+r)^2+c^2+o^2]^{\frac{3}{2}}}\right] - v_{c_c} = 0 \qquad (2)$$

$$\ddot{o} + \omega^2 o\left[\frac{k_o^3}{[(k_o+r)^2+c^2+o^2]^{\frac{3}{2}}}\right] - v_{c_o} = 0$$

where r is the relative position in the radial direction, c is the relative position in the cross track direction, and o is out of the leader orbit plane. The remaining two variables are properties of the leader orbit: ω is the angular frequency (or mean motion) of the leader orbit and k_o is the radius of the leader orbit where the relationship between the two is based on Kepler's third law (29):

$$\omega = \sqrt{\frac{\mu}{k_o^3}} \qquad (3)$$

Equations 2 are used in the development of nonlinear controllers, but can be linearized to facilitate the use of linear control methods. When the distance between the follower and leader is small compared to the radii of their orbits, linearization yeilds (Derivation is in Appendix D):

$$\ddot{r} - 2\omega\dot{c} - 3\omega^2 r - v_{c_r} = 0$$

$$\ddot{c} + 2\omega\dot{r} - v_{c_c} = 0 \qquad (4)$$

$$\ddot{o} + \omega^2 o - v_{c_o} = 0$$

This is the more familiar form of the Clohessy-Wiltshire results commonly known as Hill's equations. If the control vector $\vec{v}_c$ is set to zero, the homogeneous form of Hill's equations can be parameterized as (31) (Derivation is in Appendix E):

$$r = \rho\sin(\omega t + \theta) + a$$

$$c = 2\rho\cos(\omega t + \theta) - \frac{3\omega}{2}at + b \qquad (5)$$

$$o = m\rho\sin(\omega t + \theta) + 2n\rho\cos(\omega t + \theta)$$

7

where

$$a = \frac{2\dot{c}_o + 4\omega r_o}{\omega} \tag{6}$$

$$b = \frac{\omega c_o - 2\dot{r}_o}{\omega} \tag{7}$$

$$\rho = \sqrt{(r_o - a)^2 + \left(\frac{\dot{r}_o}{\omega}\right)^2} \tag{8}$$

$$m = \frac{\dot{o}_o \dot{r}_o - o_o \omega^2 (a - r_o)}{\dot{r}_o^2 + \omega^2 (a - r_o)^2} \tag{9}$$

$$n = \frac{o_o \dot{r}_o \omega + \dot{o}_o \omega (a - r_o)}{2[\dot{r}_o^2 + \omega^2 (a - r_o)^2]} \tag{10}$$

$$\theta = \arctan\left[\frac{\omega(r_o - a)}{\dot{r}_o}\right] \tag{11}$$

which fall out of the derivation of Equations 5 (Note that the subscript o denotes initial conditions). In the simulations run for this thesis, a, b, and ρ are defined in kilometers, θ in degrees, and m and n in terms of a unitless slope (Appendix E.1). What we first notice about the parameterization is that the second equation has a term that grows linearly with time. Since ω will never be zero, it is easy to see that a must always equal zero or else the relative orbit will not follow a closed path. Thus there is an initial condition constraint that $\dot{c}_o = -2\omega r_o$. Further analysis of the follower orbit can be found in Section 2.1. Taking the derivatives of Equations 5 to find the relative velocity yields:

$$\dot{r} = \rho \omega \cos(\omega t + \theta)$$

$$\dot{c} = -2\rho \omega \sin(\omega t + \theta) - \frac{3\omega}{2} a \tag{12}$$

$$\dot{o} = m \rho \omega \cos(\omega t + \theta) - 2n \rho \omega \sin(\omega t + \theta)$$

Equations 5 and 12 can be used to convert desired relative orbits (in terms of relative parameters) into inertial position and velocity at a given time. First the RCO frame relationship to the inertial frame (IJK) is needed to find the transformation matrix $C^{FrameA-2-FrameB}$

$$^{IJK}Vector = C^{RCO2IJK} *^{RCO}Vector \tag{13}$$

$$C^{RCO2IJK} = [\hat{R}|\hat{C}|\hat{O}] \tag{14}$$

where $\hat{R}$, $\hat{C}$, and $\hat{O}$ are the unit vectors for each direction expressed in the IJK frame. Note that in the IJK system, $\hat{I}$ is in the direction of the first point of Aires, $\hat{J}$ is perpendicular to $\hat{I}$ in the Earth's equatorial plane and $\hat{K} = \hat{I} \times \hat{J}$ (29). If the leader satellite's inertial position and velocity are $^{IJK}\vec{L}$ and $^{IJK}\dot{\vec{L}}$ respectively and the follower's inertial position and velocity are $^{IJK}\vec{M}$ and $^{IJK}\dot{\vec{M}}$, all expressed in the IJK frame, then the radial unit direction is simply the unit vector of the leader's position

$$\hat{R} = \frac{^{IJK}\vec{L}}{|^{IJK}\vec{L}|} \tag{15}$$

If the leader is in a circular orbit (which is an assumption of the CW equations) then the velocity vector of the satellite will always be perpendicular to the position vector in the orbit plane thus

$$\hat{C} = \frac{^{IJK}\dot{\vec{L}}}{|^{IJK}\dot{\vec{L}}|} \tag{16}$$

and the out of plane direction is obtained via the cross product of the two

$$\hat{O} = \hat{R} \times \hat{C} \tag{17}$$

To find the inertial position of the follower in the IJK frame, the relative position vector is transformed to IJK and added to the leader's position

$$^{IJK}\vec{M} = C^{RCO2IJK} \begin{bmatrix} r \\ c \\ o \end{bmatrix} +^{IJK}\vec{L} \tag{18}$$

To find the inertial velocity we need to take the inertial derivative of the position vector.

$$^{IJK}\dot{\vec{M}} = \frac{d}{dt}\left(C^{RCO2IJK} \begin{bmatrix} r \\ c \\ o \end{bmatrix} \right) +^{IJK}\dot{\vec{L}} \tag{19}$$

To take the inertial derivative of a vector in a noninertial frame (like the RCO frame) we will use the following form

$$\dot{\vec{X}} = ^{RCO}\frac{d(\vec{X})}{dt} + N^{RCO-wrt-Inertial} \times \vec{X} \tag{20}$$

where N is the angular velocity of the RCO frame with respect to the inertial frame, in this case $N^{RCO-wrt-Inertial} = 0\hat{R} + 0\hat{C} + \omega\hat{O}$ where ω is the angular frequency of the leader satellite's orbit and is found via Equation 3. Thus

$$\frac{d}{dt}\left(C^{RCO2IJK} \begin{bmatrix} r \\ c \\ o \end{bmatrix} \right) = C^{RCO2IJK} \begin{bmatrix} \dot{r} \\ \dot{c} \\ \dot{o} \end{bmatrix} + \left(^{IJK}\omega \times C^{RCO2IJK} \begin{bmatrix} r \\ c \\ o \end{bmatrix} \right) \tag{21}$$

where angular frequency in the IJK frame is

$$^{IJK}\omega = C^{RCO2IJK} \begin{bmatrix} 0 \\ 0 \\ \omega \end{bmatrix} \tag{22}$$

Pulling out the common transformation matrix

$$\frac{d}{dt}\left(C^{RCO2IJK} \begin{bmatrix} r \\ c \\ o \end{bmatrix} \right) = C^{RCO2IJK} \left(\begin{bmatrix} \dot{r} \\ \dot{c} \\ \dot{o} \end{bmatrix} + \begin{bmatrix} 0 \\ 0 \\ \omega \end{bmatrix} \times \begin{bmatrix} r \\ c \\ o \end{bmatrix} \right) \tag{23}$$

and combining terms

$$\frac{d}{dt}\left(C^{RCO2IJK} \begin{bmatrix} r \\ c \\ o \end{bmatrix} \right) = C^{RCO2IJK} \begin{bmatrix} \dot{r} - c\omega \\ \dot{c} + r\omega \\ \dot{o} \end{bmatrix} \tag{24}$$

10

thus the inertial velocity of the follower satellite becomes

$$^{IJK}\dot{\vec{M}} = C^{RCO2IJK} \begin{bmatrix} \dot{r} - c\omega \\ \dot{c} + r\omega \\ \dot{o} \end{bmatrix} + ^{IJK}\dot{\vec{L}} \qquad (25)$$

Going from the inertial to the relative frame is a simple manipulation of the above equations and is shown in Appendix F.

2.1 The Relative Orbit

A manipulation of Equations 5 yields better insight into what path the follower will take about the leader and what each parameter represents. If a is set to zero, squaring the first two equations, adding them together, and using the trigonometric identity $\sin(\tau)^2 + \cos(\tau)^2 = 1$ yields

$$r^2 + \frac{(c-b)^2}{4} = \rho^2[\sin(\omega t + \theta)]^2 + \rho^2[\cos(\omega t + \theta)]^2 = \rho^2 \qquad (26)$$

Dividing both sides by ρ^2

$$\frac{r^2}{\rho^2} + \frac{(c-b)^2}{4\rho^2} = 1 \qquad (27)$$

Substituting $r = \rho\sin(\omega t + \theta)$ and $(c-b) = 2\rho\cos(\omega t + \theta)$ into the third equation

$$o = mr + n(c-b) \qquad (28)$$

Equation 27 shows that the path of the follower satellite in the radial/cross-track plane will be an ellipse with a semi minor axis equal to ρ and a semi major axis equal to 2ρ. Thus ρ defines the size the relative orbit. The b term defines an offset in the cross-track direction and shows that a closed path relative orbit can exist without the leader satellite located at the center of the ellipse. In fact, the center of the relative orbit can exist anywhere along the velocity direction of the leader provided it is not so far from the leader as to render Hill's equations invalid. The m and n terms in Equation 28 define the slope of the orbit of the radial/out-of-plane and cross-track/out-of-plane planes respectively. The θ term is

11

the initial angle with respect to the cross track direction and t is time. Figure 2 gives a graphical representation of Equation 27. The two foci of the ellipse fall on the major axis
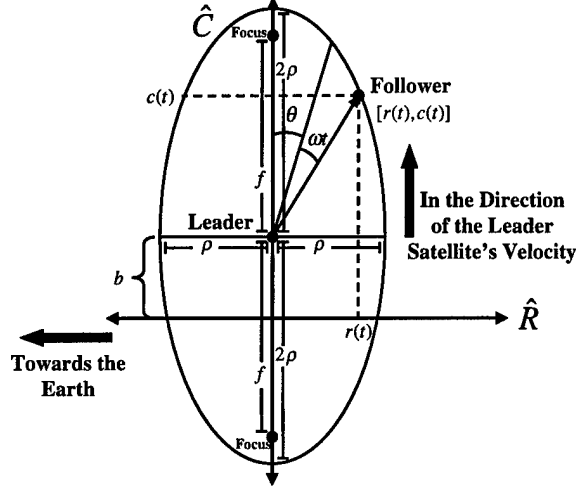
Figure 2   Path of Follower in R/C Plane

a distance f from the center of the ellipse where f is found via (13)

$$f^2 = (\text{Major Axis})^2 - (\text{Minor Axis})^2 \tag{29}$$

Thus

$$f = \sqrt{4\rho^2 - \rho^2} = \sqrt{3\rho^2} = \rho\sqrt{3} \tag{30}$$

The eccentricity of an ellipse is found with the following relationship (13).

$$e = \frac{f}{\text{Major Axis}} = \frac{\rho\sqrt{3}}{2\rho} = \frac{\sqrt{3}}{2} \tag{31}$$

Thus the eccentricity of the elliptical path in the R/C plane will always be $\frac{\sqrt{3}}{2}$. If m is set to zero, the follower track in the C/O plane will be a line of slope n. Likewise, if n is set to zero, the follower track in the R/O plane will be a line of slope m.

Other than the constraints on a (to prevent relative orbit drift), b, and ρ (to maintain the validity of the linear equations) a satellite formation mission planner is free to chose any set of parameters needed to create the relative orbit required by the mission. By choosing

a unique set of relative parameters, the user is choosing a unique set of initial conditions. The tradeoff for the ease of relative parameters is that the command signal is now based on the linear relative equations of motion, thus even at steady state conditions (i.e. no reconfiguration), there will always be error between the inertially propagated system and the commanded input. This error is quantified and discussed in the following section.

2.2 Error Using Linear vs. Nonlinear Equations

Linearizing the CW equations requires the assumption that the magnitude of the relative position vector is small compared to the radius of the leader orbit. In order to make valid conclusions about reconfigurations using a linear based command signal, it is important to quantify the error produced by using the linear equations as opposed to the nonlinear. The simulation shown in Figure 3 is used to quantify that error. The simulation
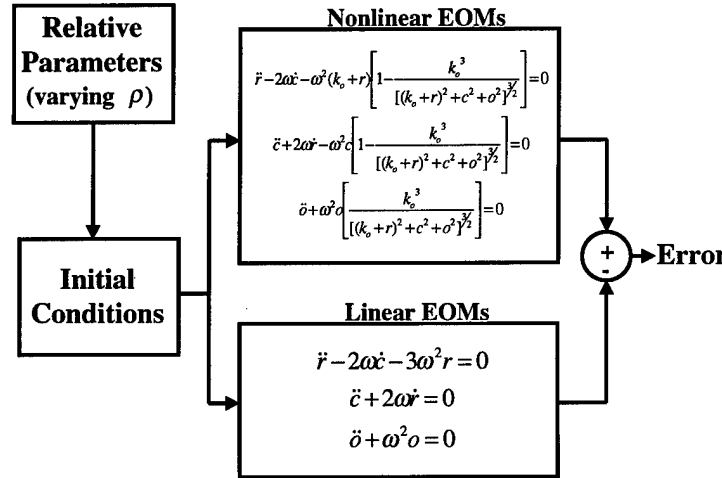
Figure 3   Error Analysis Simulation Setup

was run for various values of ρ (which defines the size of the relative orbit) and leader orbit radii. Relative parameters were used to determine initial conditions for both the linear and nonlinear equations of motion (EOMs) via Equations 5 and 12. These initial conditions are then used in both sets of equations (2 and 4) and propagated through two complete relative orbits. The error is the absolute value of the difference in the magnitude of the

13

position vectors. The relative parameters for each simulation are shown in Table 1. There

	Sim 1	Sim 2	Sim 3	Sim 4	Sim 5	Sim 6	Sim 7	Sim 8	Sim 9	Sim 10
ρ (km)	0.1	0.2	0.3	0.5	0.8	1	1.4	1.8	2.4	3
a (km)	0	0	0	0	0	0	0	0	0	0
θ (deg)	45	45	45	45	45	45	45	45	45	45
b (km)	0	0	0	0	0	0	0	0	0	0
m (unitless)	1	1	1	1	1	1	1	1	1	1
n (unitless)	0	0	0	0	0	0	0	0	0	0

Table 1   Absolute Error Simulation Relative Parameters

were three leader orbit radii used; a low Earth orbit (semi major axis = 6800 km), a geosynchronus orbit (semi major axis = 42241 km), and an orbit in between (semi major axis = 17720 km). For each orbit radius, ρ was varied from 0.1 to 3 km. The $\hat{R}$ and $\hat{O}$ directions showed periodic error patterns as shown in Figures 4 and 5 respectively where each line corresponds to a specific ρ and the error increases as ρ increases. The error in
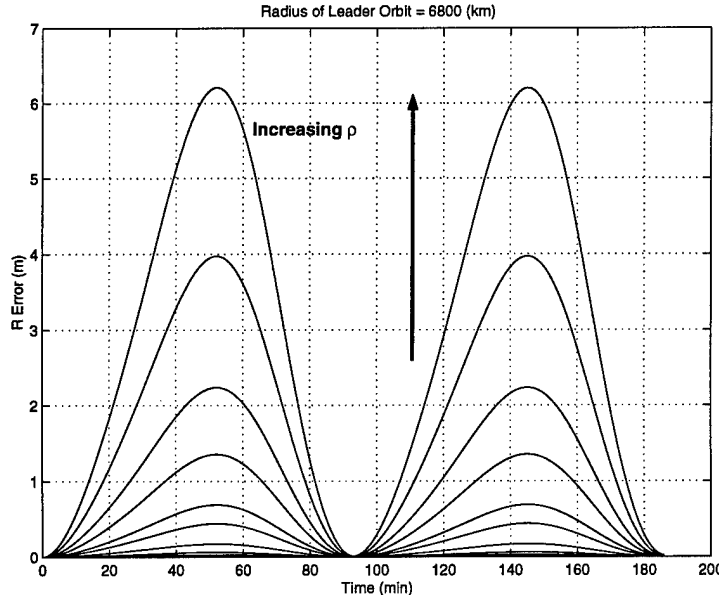
Figure 4 $\hat{R}$ Direction Absolute Position Error

the $\hat{C}$ direction has a secular growth element and is shown in Figure 6. Note that the cross track error is an order of magnitude greater than in the other two directions. The presence of this secular growth indicates that setting $a = 0$ (via $\dot{c}_o = -2\omega r_o$), does not eliminate all secular terms in the cross track direction (at least for the nonlinear equations). It is this
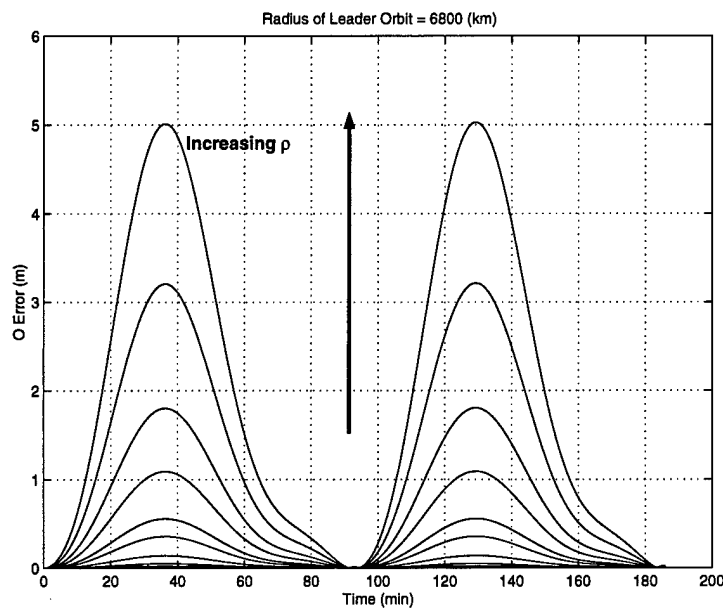
Figure 5 $\hat{O}$ Direction Absolute Position Error
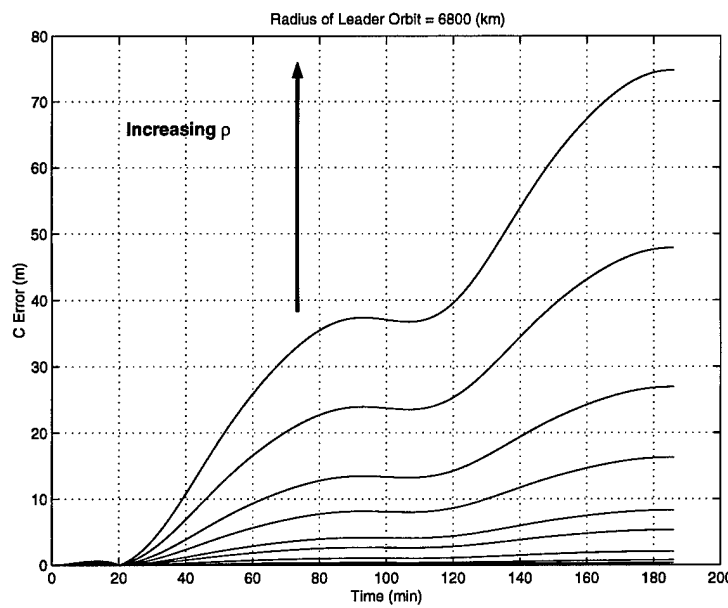
Figure 6 $\hat{C}$ Direction Absolute Position Error

growth in the error of the $\hat{C}$ direction that is the greatest concern. For one thing, creating initial conditions based solely on the relative parameters will not guarantee a stable relative orbit (that is an orbit that does not drift over time). From a classical orbital elements standpoint, this means that the follower and leader satellites have a different semi-major axis and thus different periods translating to a drift in their relative position. This is much more of a factor for stationkeeping controllers than reconfigurations since the former occurs over long time periods thus allowing cross track error to build up. Depending on the settling time of the controller, the cross track error during reconfiguration may be acceptable. Looking at the maximum error (peak of each absolute error curve) as a function of ρ produces Figures 7, 8, and 9. As expected, the larger the leader satellite orbit
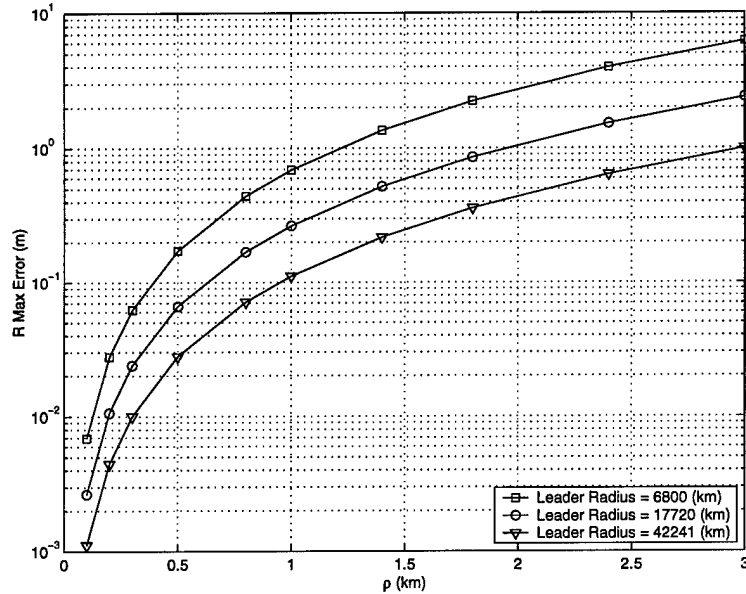
Figure 7 $\hat{R}$ Direction Max Error

and/or ρ, the smaller the max error between the linear and nonlinear equations. Note that in the $\hat{R}$ and $\hat{O}$ directions, the max error graph is valid for any number of relative orbits but in the $\hat{C}$ direction the graph would be shifted upwards for subsequent revolutions due to the growth term. In any case, the $\hat{C}$ direction error will be the determining factor in deciding how large ρ can be.

16
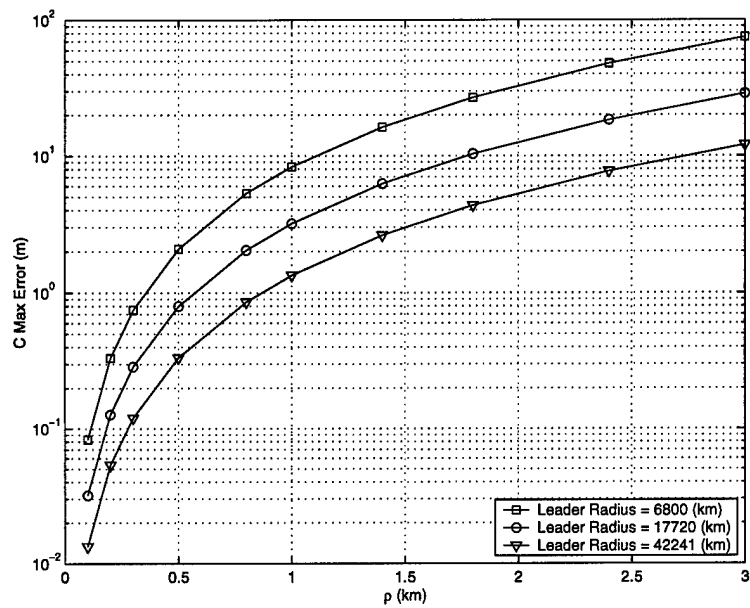
Figure 8 $\hat{C}$ Direction Max Error
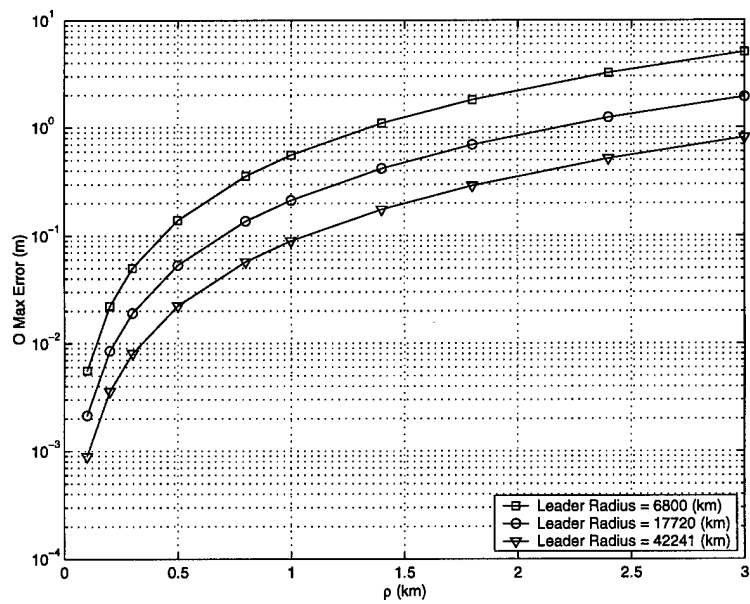
Figure 9 $\hat{O}$ Direction Max Error

2.3 Simulation Outline

The reconfiguration simulation used to obtain results for this thesis is setup according to Figure 10. Equations 5 and 12 are used to convert relative parameters and current time
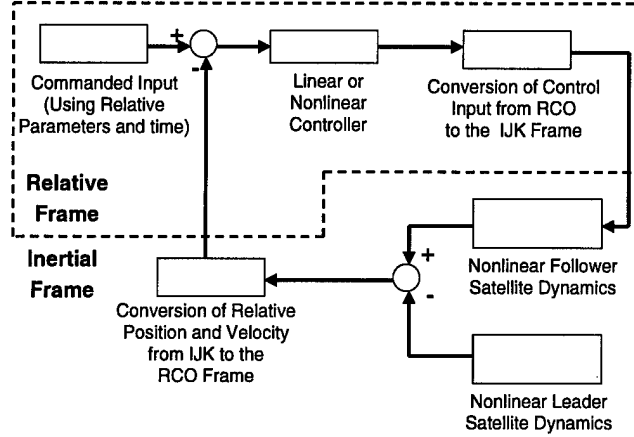
Figure 10   Reconfiguration Simulation Diagram

into a relative position and velocity (in the *RCO* frame). This is the command by which the relative measurement data is subtracted in order to produce an error signal. It is assumed that relative position and velocity data is available (i.e. full state feedback). The error signal is multiplied by the controller gain to find the control inputs. These inputs ($\vec{v}_c$) are converted to the *IJK* frame and used in the inertial orbit equation

$$\ddot{\vec{d}} = \frac{-\mu \vec{d}}{|\vec{d}|^3} + \vec{v}_c + \vec{v}_p \tag{32}$$

where $\vec{d}$ is the position of the satellite with respect to the Earth in the inertial frame and $\vec{v}_p$ is the perturbation acceleration. The orbits of both the leader and follower are propagated via Equation 32 (note that for the leader $\vec{v}_c = \vec{0}$) to find a new inertial position and velocity vector for the leader and follower which are differenced and transformed to the *RCO* frame (Appendix F explains the process). This is the measurement data compared against the command closing the loop. Although it may not be realistic to expect real time position and velocity data, the purpose of this research is to compare controller designs, not estimators.

18

Future work will include estimators that effectively deal with noise and propagate states between measurements. The results from each controller will also be compared against the near optimal open loop, discrete-time impulsive maneuver (OLDTIM) (Section 3.1). No claim is made that the discrete burn method used is optimal, only that it represents a recognized, efficient maneuver for orbit transfer.

The inertial orbit equation is propagated via the Dormand-Prince pair (an explicit Runge-Kutta formula). Since both follower and leader orbits are either circular or near circular, there is little need for a variable step solver. A fixed time step method was chosen to give the simulation user more control over the run time of the simulation. A time step of 15 seconds was selected for this thesis based on analysis of the integration error as a function of time step and because it provided reasonable run times. The simulation used to propagate the leader and follower inertial states was initialized for a circular orbit and run for one revolution. The position error is the maximum error between the magnitude of the position vector and the semi major axis of the circular orbit (used to find initial conditions) and is shown in Figure 11. The error simulation shows that for a 15 second
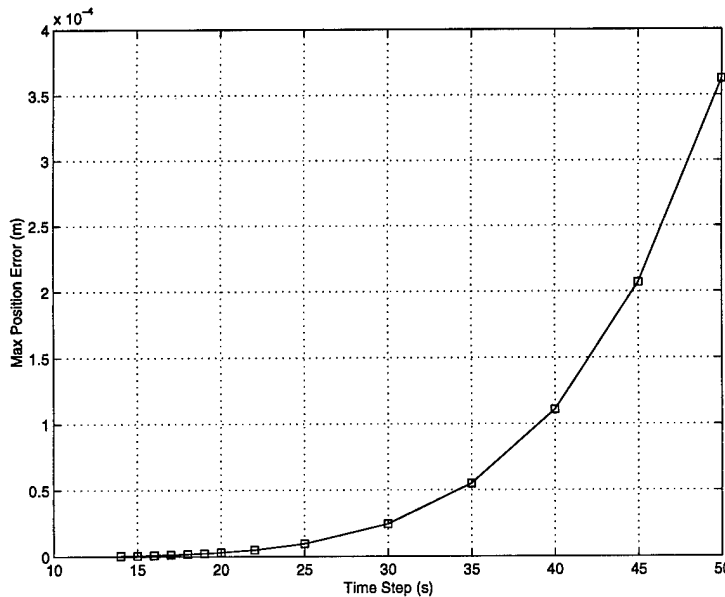
Figure 11   Integration Error vs. Time Step (Position)

time step, the error in the magnitude of the position vector is under 1×10^{-6}. The velocity error is the maximum error between the magnitude of the velocity vector and the expected

speed of the satellite based on the equation

$$V = \sqrt{\frac{\mu}{k_o}} \tag{33}$$

where k_o is the orbital radius (semi major axis). The velocity error is shown in Figure 12. The error simulation shows that for a 15 second time step, the error in the magnitude of
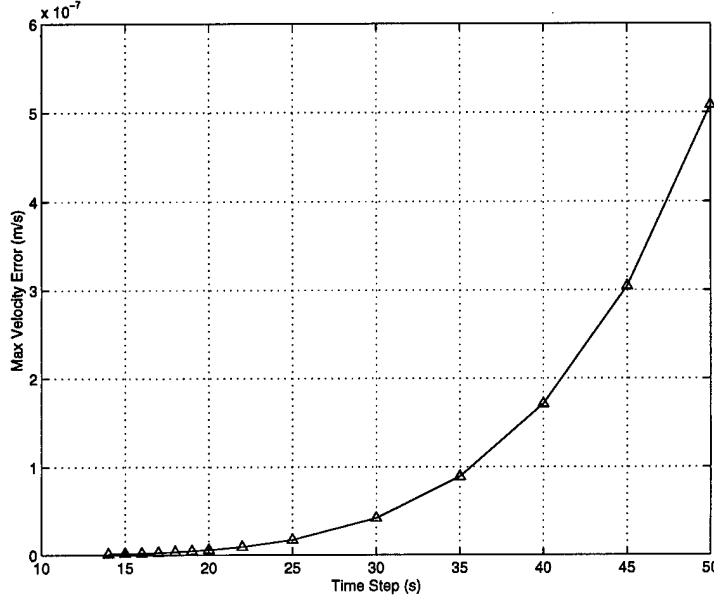
Figure 12   Integration Error vs. Time Step (Velocity)

the velocity vector is under 2×10^{-9}.

The rest of the Simulink simulation (Appendices K, L, M, and N) involves converting the data into relative parameters, classical orbital elements, and error signals.

III. Reconfiguration Control Laws

This chapter describes each of the four control techniques used to develop controllers for the relative orbit reconfiguration problem. The control techniques used for this thesis are the linear quadratic regulator (LQR), a nonlinear LQR technique using linearizing feedback, state dependent riccati equations (SDRE), and sliding mode control. The first section explains the assumptions and derives the equations used to calculate the OLDTIM maneuver ΔV and settling time. This is the open loop maneuver that will be used as a comparison point for the continuous feedback methods.

3.1 The Open Loop, Discrete-Time, Impulsive Maneuver

The open loop, discrete-time, impulsive maneuver (OLDTIM) consists of four separate burns. Experience with several simulation runs shows that all of the follower satellites' classical orbital elements (COEs) change during the reconfiguration except for the semi major axis. As discussed before, changes in the semi major axis would cause the relative orbit to drift as it would affect the period of the follower satellites' inertial orbit. True anomaly is not considered as it describes the position of a satellite within an orbit, not the size, shape, or attitude of the orbit. The change in eccentricity can be performed using a Hohmann transfer which is an optimal two burn maneuver for a circular to circular orbit transfer and near optimal for eccentric orbits. The inclination and longitude of the ascending node can be changed with a single burn given certain assumptions presented later. The final parameter, argument of perigee is changed with a single burn as well. The author is aware that other more optimal methods for discrete burns are available, however, this method allows for the fewest assumptions and is significantly easier to calculate. Given the fact that the OLDTIM maneuver is only a comparison point and not meant to bound an optimal transfer, the tradeoff is acceptable.

3.1.1 The Hohmann Maneuver (Eccentricity Change).
The Hohmann maneuver will perform the eccentricity change. To calculate the necessary ΔV, consider Figure 13 where r_a is the radius of apogee of the larger orbit and r_p is the radius of perigee of the
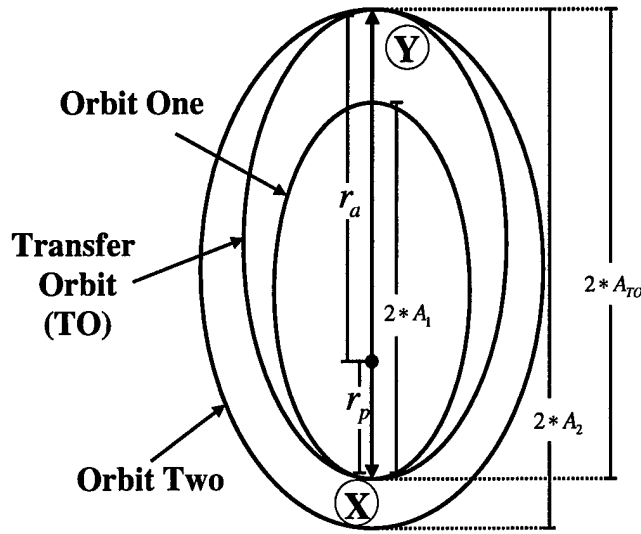
Figure 13   Hohmann Maneuver Setup

smaller orbit. These values are related to the semi major axis (A) and eccentricity (e) (29)

$$A_1 = A_2 = A \tag{34}$$

$$r_a = A_2(1 + e_2) = A(1 + e_2) \tag{35}$$

$$r_p = A_1(1 - e_1) = A(1 - e_1) \tag{36}$$

The total ΔV for the Hohmann maneuver will be

$$\Delta V_{Hohmann} = \Delta V_X + \Delta V_Y \tag{37}$$

To calculate the difference in orbital velocity at points X and Y, we need to find the velocity of the satellite at each point in its orbit (29)

$$V = \sqrt{\mu \left[\frac{2}{d} - \frac{1}{A} \right]} \tag{38}$$

22

where, μ is the gravitational constant and d is the magnitude of the position vector at the point of interest. Thus at point X

$$\Delta V_X = V_{TO_X} - V_{1_X} = \sqrt{\mu \left[\frac{2}{r_p} - \frac{1}{A_{TO}} \right]} - \sqrt{\mu \left[\frac{2}{r_p} - \frac{1}{A} \right]} \tag{39}$$

where

$$A_{TO} = \frac{r_a + r_p}{2} \tag{40}$$

The change in velocity at point Y is found the same way

$$\Delta V_Y = V_{2_Y} - V_{TO_Y} = \sqrt{\mu \left[\frac{2}{r_a} - \frac{1}{A} \right]} - \sqrt{\mu \left[\frac{2}{r_a} - \frac{1}{A_{TO}} \right]} \tag{41}$$

Thus the ΔV for the Hohmann maneuver is

$$\Delta V_{Hohmann} = \sqrt{\mu \left[\frac{2}{r_p} - \frac{1}{A_{TO}} \right]} - \sqrt{\mu \left[\frac{2}{r_p} - \frac{1}{A} \right]}$$
$$+ \sqrt{\mu \left[\frac{2}{r_a} - \frac{1}{A} \right]} - \sqrt{\mu \left[\frac{2}{r_a} - \frac{1}{A_{TO}} \right]} \tag{42}$$

Since this maneuver requires a burn at apogee and perigee, the "settling time" for the Hohmann is one half the period of the transfer orbit (29)

$$ST_{Hohmann} = \pi \sqrt{\frac{A_{TO}^3}{\mu}} \tag{43}$$

3.1.2 The Inclination/LAN Maneuver (Plane Change). The second maneuver will change the inclination and longitude of the ascending node through a plane change. Consider Figure 14 in which we assume that both the initial and final orbits are circular with the same radius. This is a good assumption as long as the relative orbit is small thus requiring a small eccentricity for the follower satellite. All possible orbits for a certain orbital radius exist on the surface of a sphere. In Figure 14, Ψ represents the angle between the planes of the two orbits, Ω is the longitude of the ascending node, and i is the

23
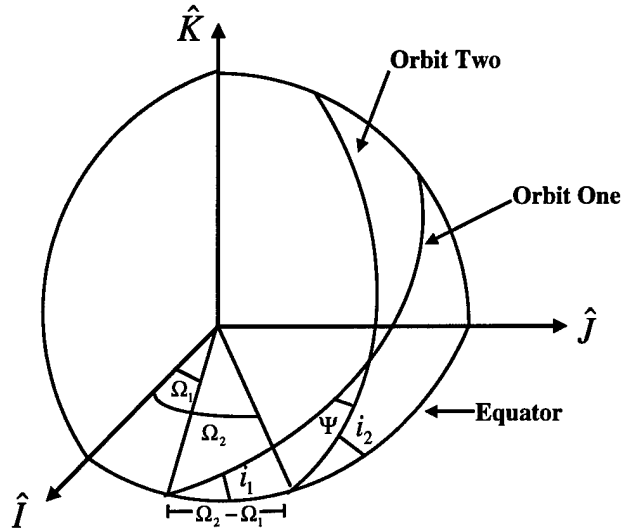
Figure 14   Inclination/Longitude of the Ascending Node Maneuver Setup

inclination. With spherical trigonometry (5)

$$\Psi = \arccos[\cos(i_1)\cos(i_2) + \sin(i_1)\sin(i_2)\cos(\Omega_2 - \Omega_1)] \qquad (44)$$

With the angle between the two planes known, the ΔV can be calculated. Consider Figure 15 where V_O is the speed of the satellite (constant for all points on the surface of the
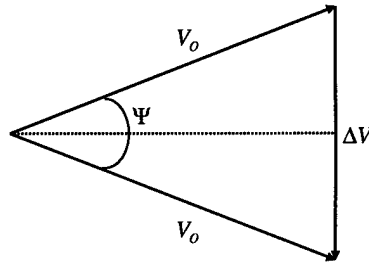
Figure 15   Inclination-LAN ΔV Calculation

sphere) and the dotted line bisects the angle Ψ. The speed of a satellite in a circular orbit

is found via (5)

$$V_O = \sqrt{\mu \left[\frac{2}{k_o} - \frac{1}{k_o} \right]} = \sqrt{\frac{\mu}{k_o}} \tag{45}$$

where k_o is the radius of the circular orbit. Using the trigonometric formula for the sine of an angle (Figure 15)

$$\sin\left(\frac{\Psi}{2}\right) = \frac{\frac{1}{2}\Delta V_{Inc/LAN}}{V_O} \tag{46}$$

Solving for ΔV

$$\Delta V_{Inc/LAN} = 2V_O \sin\left(\frac{\Psi}{2}\right) = 2\sqrt{\frac{\mu}{k_o}} \sin\left(\frac{\Psi}{2}\right) \tag{47}$$

Since this is a single instantaneous burn and will happen between the initial and final burns of the Hohmann, the settling time is zero.

3.1.3 The AP Maneuver (Orientation Change). The final discrete burn will change the angle of the line of perigee and is set up in Figure 16. Since only the argument
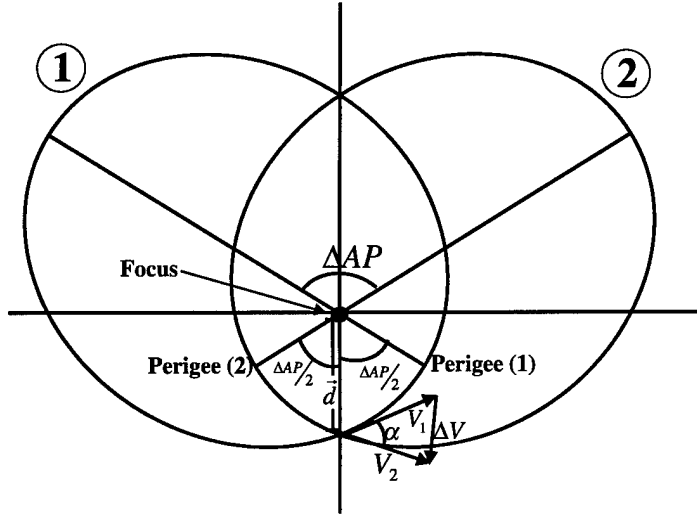
Figure 16   *AP* Maneuver Setup

25

of perigee (AP) changes, all other orbital elements will remain the same, thus

$$e_1 = e_2 = e \tag{48}$$

$$A_1 = A_2 = A \tag{49}$$

Since the semilatus rectum (p) is a function of e and A

$$p_1 = p_2 = p = A(1 - e^2) \tag{50}$$

Zooming in on Figure 16 the following relationships can be seen (Figure 17)
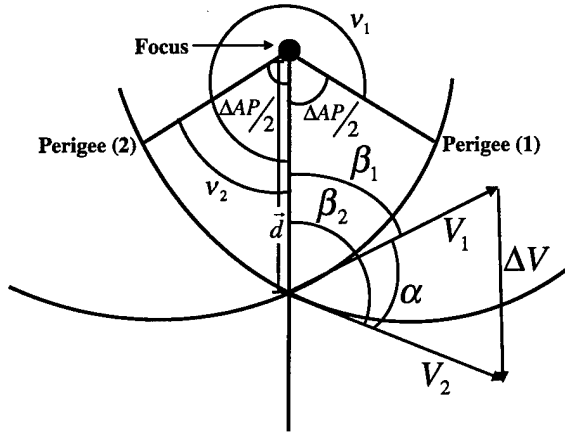
Figure 17 AP Maneuver Setup Zoom

$$\alpha = \beta_2 - \beta_1 \tag{51}$$

$$\nu_1 = 2\pi - \frac{\Delta AP}{2} \tag{52}$$

$$\nu_2 = \frac{\Delta AP}{2} \tag{53}$$

where β is the angle between the position and velocity vectors of each orbit and ν is the angle between the line of perigee and the position vector (also known as true anomaly).

Taking the cosine of both sides of Equations 52 and 53 (26)

$$\cos(\nu_1) = \cos\left(2\pi - \frac{\Delta AP}{2}\right) = \cos(2\pi)\cos\left(\frac{\Delta AP}{2}\right) + \sin(2\pi)\sin\left(\frac{\Delta AP}{2}\right)$$

$$= \cos\left(\frac{\Delta AP}{2}\right) \tag{54}$$

$$\cos(\nu_2) = \cos\left(\frac{\Delta AP}{2}\right) \tag{55}$$

Thus

$$\cos(\nu_1) = \cos(\nu_2) \tag{56}$$

$$\nu_1 = \nu_2 = \nu = \frac{\Delta AP}{2} . \tag{57}$$

Finally, looking at how β is constructed in Figure 18 we can say that
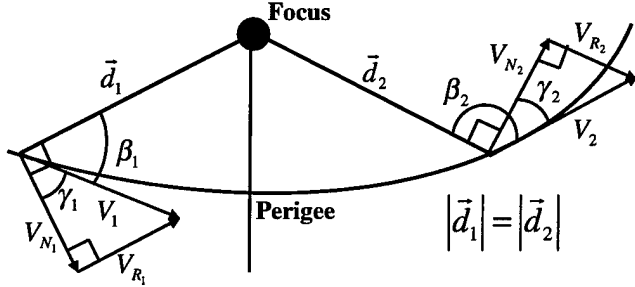
Figure 18 β Relationships

$$\beta_1 = \frac{\pi}{2} - \gamma_1 \tag{58}$$

$$\beta_2 = \frac{\pi}{2} + \gamma_2 \tag{59}$$

where γ is the flight path angle and is defined as

$$\gamma = \arccos\left(\frac{V_N}{V}\right) \tag{60}$$

27

where V_N is the velocity normal to the position vector (V_R is the velocity parallel to the position vector). Substituting Equations 58 and 59 into Equation 51

$$\alpha = \left(\frac{\pi}{2} + \gamma_2\right) - \left(\frac{\pi}{2} - \gamma_1\right) = \gamma_2 + \gamma_1 \tag{61}$$

All the angle relationships are now in place to solve for the ΔV of the AP change. Note on Figure 16 that at the maneuver point, the two orbits share a common position vector. Relating the position vector to conic section geometry (29)

$$|\vec{d_1}| = |\vec{d_2}| = d = \frac{A(1 - e^2)}{1 + e\cos(\nu)} = \frac{p}{1 + e\cos(\nu)} \tag{62}$$

Equation 38 shows that the magnitude of the velocity is a function of the magnitude of the position vector and the semi major axis, both of which are identical for orbit one and two. Solving for V and substituting in Equations 50 and 62

$$|\vec{V_1}| = |\vec{V_2}| = V = \sqrt{\mu\left[\frac{2}{d} - \frac{1}{A}\right]} = \sqrt{\mu\frac{1 + 2e\cos(\nu) + e^2}{p}} \tag{63}$$

Taking the cross product of the two position vectors with their respective velocity vectors yields the angular momentum

$$
\begin{aligned}
|\vec{d_1} \times \vec{V_1}| &= |\vec{H_1}| = dV\sin(\beta_1) = dV\sin\left(\frac{\pi}{2} - \gamma_1\right) \\
&= dV\left[\sin\left(\frac{\pi}{2}\right)\cos(\gamma_1) - \cos\left(\frac{\pi}{2}\right)\sin(\gamma_1)\right] = dV\cos(\gamma_1) \qquad (64) \\
|\vec{d_2} \times \vec{V_2}| &= |\vec{H_2}| = dV\sin(\beta_2) = dV\sin\left(\frac{\pi}{2} + \gamma_2\right) \\
&= dV\left[\sin\left(\frac{\pi}{2}\right)\cos(\gamma_2) + \cos\left(\frac{\pi}{2}\right)\sin(\gamma_2)\right] = dV\cos(\gamma_2) \qquad (65)
\end{aligned}
$$

The magnitude angular momentum ($\vec{H}$) is (5)

$$|\vec{H}| = \sqrt{\mu p} \tag{66}$$

Since $p_1 = p_2$

$$|\vec{H}_1| = |\vec{H}_2| \qquad (67)$$

$$dV\cos(\gamma_1) = dV\cos(\gamma_2) \qquad (68)$$

$$\gamma_1 = \gamma_2 = \gamma \qquad (69)$$

By Equation 60 this means that

$$V_{N1} = V_{N2} = V_N \qquad (70)$$

Substituting γ into Equation 61

$$\alpha = 2\gamma \qquad (71)$$

and relating γ to angular momentum

$$dV\cos(\gamma) = |\vec{H}| = \sqrt{\mu p} \qquad (72)$$

$$\cos(\gamma) = \frac{\sqrt{\mu p}}{dV} \qquad (73)$$

Substituting Equation 60 for $\cos(\gamma)$

$$\frac{V_N}{V} = \frac{\sqrt{\mu p}}{dV} \qquad (74)$$

Cancelling the V and substituting Equation 62 for d

$$V_N = \sqrt{\mu p}\frac{1 + e\cos(\nu)}{p} = \sqrt{\frac{\mu}{p}}[1 + e\cos(\nu)] \qquad (75)$$

Taking the cosine of Equation 71 and employing the double angle cosine trigonometric identity (26)

$$\cos(\alpha) = \cos(2\gamma) = 2[\cos(\gamma)]^2 - 1 \qquad (76)$$

Substituting Equation 60 for γ

$$\cos(\alpha) = 2\left[\cos\left(\arccos\left[\frac{V_N}{V}\right]\right)\right]^2 - 1 = 2\left[\frac{V_N}{V}\right]^2 - 1 = \frac{2V_N{}^2 - V^2}{V^2} \qquad (77)$$

29

Now that we have α, V_1, and V_2 the law of cosines states that

$$\Delta V_{AP}^2 = V_1^2 + V_2^2 - 2V_1 V_2 \cos(\alpha) = 2V^2(1 - \cos(\alpha)) \tag{78}$$

Substituting for $\cos(\alpha)$ (Equation 76)

$$\Delta V_{AP}^2 = 2V^2 \left[1 - \frac{2V_N^2 - V^2}{V^2} \right] = 4V^2 - 4V_N^2 \tag{79}$$

Expanding this with the values of V and V_N via Equations 63 and 75

$$\Delta V_{AP}^2 = 4 \left[\mu \frac{1 + 2e\cos(\nu) + e^2}{p} - \frac{\mu}{p}[1 + e\cos(\nu)]^2 \right] \tag{80}$$

Adding the fractions, expanding the squared term, and simplifying

$$\Delta V_{AP}^2 = 4\mu \left[\frac{e^2(1 - [\cos(\nu)]^2)}{p} \right] = \frac{4\mu e^2[\sin(\nu)]^2}{p} \tag{81}$$

Finally, taking the square root of both sides and substituting $\frac{\Delta AP}{2}$ for ν (per Equation 57)

$$\Delta V_{AP} = 2e\sqrt{\frac{\mu}{p}} \sin\left(\frac{\Delta AP}{2}\right) \tag{82}$$

or in terms of classical orbital elements

$$\Delta V_{AP} = 2e\sqrt{\frac{\mu}{A(1 - e^2)}} \sin\left(\frac{\Delta AP}{2}\right) \tag{83}$$

3.1.4 Total ΔV and Settling Time.   Adding Equations 42, 47, and 83 to get the total ΔV for the OLDTIM

$$\Delta V_{OLDTIM} = \Delta V_{Hohmann} + \Delta V_{Inc/LAN} + \Delta V_{AP} \tag{84}$$

To determine the total maneuver time (or settling time) visualize the following sequence. The first burn will place the spacecraft on the Hohmann transfer orbit and occurs at apogee of the initial orbit. There are two opportunities to do the Inclination/LAN burn located 180 degrees apart, therefore one opportunity will occur between apogee and perigee

30

and will not affect the maneuver time. The third burn occurs at perigee and places the spacecraft onto the final orbit. The fourth and final burn changes the argument of perigee. Figure 16 shows that the spacecraft either travels an angle of $\frac{\Delta AP}{2}$ from the third burn at perigee till the fourth burn or the fourth burn occurs before the final Hohmann burn. In the form case, the following relationship calculates the travel time (29)

$$ST_{AP} = \Delta t = \sqrt{\frac{A^3}{\mu}}[E - e\sin(E)] \tag{85}$$

where E is the eccentric anomaly and is equal to (29)

$$E = 2\arctan\left[\frac{\tan\left(\frac{\nu}{2}\right)}{\sqrt{\frac{1+e}{1-e}}}\right] \tag{86}$$

where $\nu = \frac{\Delta AP}{2}$. Thus the "settling time" of the OLDTIM maneuver is

$$ST_{OLDTIM} = ST_{Hohmann} + ST_{AP} \tag{87}$$

$$
\begin{aligned}
ST_{OLDTIM} &= \pi\sqrt{\frac{A_{TO}^3}{\mu}} + 2\sqrt{\frac{A^3}{\mu}}\arctan\left[\frac{\tan\left(\frac{\Delta AP}{4}\right)}{\sqrt{\frac{1+e_2}{1-e_2}}}\right] \\
&\quad - e_2\sqrt{\frac{A^3}{\mu}}\sin\left(2\arctan\left[\frac{\tan\left(\frac{\Delta AP}{4}\right)}{\sqrt{\frac{1+e_2}{1-e_2}}}\right]\right)
\end{aligned} \tag{88}
$$

3.2   Linear Quadratic Regulator

The Linear Quadratic Regulator (LQR) is based on linear, time-invarient systems of the form

$$\dot{x} = Ax + Bu \tag{89}$$

where x is a vector of states and u is a vector of control inputs. LQR minimizes the quadratic performance index

$$J = \frac{1}{2}\int\left(x^T Q x + u^T R u\right)dt \tag{90}$$

31

where Q is the state weighting matrix and R is the control weighting matrix. For the relative orbit reconfiguration problem, the states represent the relative position and velocity in the RCO frame and thus all states are weighed equally giving Q a diagonal form in which each diagonal element is the same magnitude. Likewise, excess control usage is equally bad in all three directions thus R has a diagonal form in which each diagonal element is the same magnitude. High values of the elements in the state weighting matrix result in faster movement from initial to desired states. High values of the elements in the control weighting matrix result in lower control usage. For the purposes of this simulation, Q is set to the identity matrix and the elements of R will be varied. Placing Hill's equations (4) in the form of Equation 89 yields

$$
\begin{bmatrix} \ddot{r} \\ \dot{r} \\ \ddot{c} \\ \dot{c} \\ \ddot{o} \\ \dot{o} \end{bmatrix} = \begin{pmatrix} 0 & 3\omega^2 & 2\omega & 0 & 0 & 0 \\ 1 & 0 & 0 & 0 & 0 & 0 \\ -2\omega & 0 & 0 & 0 & 0 & 0 \\ 0 & 0 & 1 & 0 & 0 & 0 \\ 0 & 0 & 0 & 0 & 0 & -\omega^2 \\ 0 & 0 & 0 & 0 & 1 & 0 \end{pmatrix} \begin{bmatrix} \dot{r} \\ r \\ \dot{c} \\ c \\ \dot{o} \\ o \end{bmatrix} + \begin{pmatrix} 1 & 0 & 0 \\ 0 & 0 & 0 \\ 0 & 1 & 0 \\ 0 & 0 & 0 \\ 0 & 0 & 1 \\ 0 & 0 & 0 \end{pmatrix} \begin{bmatrix} v_r \\ v_c \\ v_o \end{bmatrix} \tag{91}
$$

With A, B, Q, and R an algebraic Riccati equation is solved to find S

$$
SA + A^T S + Q - SBR^{-1}B^T S = 0 \tag{92}
$$

The static gain controller matrix is then

$$
K = R^{-1}B^T S \tag{93}
$$

The control inputs will therefore be (18)

$$
\begin{bmatrix} v_r \\ v_c \\ v_o \end{bmatrix} = -K \begin{bmatrix} \dot{r} - \dot{r}_{com} \\ r - r_{com} \\ \dot{c} - \dot{c}_{com} \\ c - c_{com} \\ \dot{o} - \dot{o}_{com} \\ o - o_{com} \end{bmatrix}
\tag{94}
$$

where the subscript *com* represents the commanded states.

3.3 Linear Quadratic Regulator With Linearizing Feedback

In order to use a linear technique such as LQR without losing the nonlinear aspects of the dynamics, we can use linearizing feedback (LF). This technique is useful only if the nonlinear equations can be split into linear and nonlinear parts. Standard linear techniques can then be applied to that part of the problem while nonlinear terms are added in after control is calculated. Starting with the nonlinear CW equations (2), assume the control inputs (v_{r_c}, v_{c_c}, v_{o_c}) have the form

$$
\begin{aligned}
v_{c_r} &= -\omega^2(k_o + r)\left[1 - \frac{k_o^3}{[(k_o+r)^2+c^2+o^2]^{\frac{3}{2}}}\right] + 3\omega^2 r + v_r' \\
v_{c_c} &= -\omega^2 c\left[1 - \frac{k_o^3}{[(k_o+r)^2+c^2+o^2]^{\frac{3}{2}}}\right] + v_c' \\
v_{c_o} &= -\omega^2 o\left[\frac{k_o^3}{[(k_o+r)^2+c^2+o^2]^{\frac{3}{2}}}\right] + v_o'
\end{aligned}
\tag{95}
$$

Substituting Equations 95 into Equations 2 produces Hill's equations (4)

$$
\begin{aligned}
\ddot{r} - 2\omega\dot{c} - 3\omega^2 r - v_r' &= 0 \\
\ddot{c} + 2\omega\dot{r} - v_c' &= 0 \\
\ddot{o} + \omega^2 o - v_o' &= 0
\end{aligned}
\tag{96}
$$

33

The static gain controller matrix is found using the same LQR process as outlined in Section 3.2 but now the linearizing feedback must be added to the output of the controller to find the control signal

$$
\begin{bmatrix} v_{c_r} \\ v_{c_c} \\ v_{c_o} \end{bmatrix} = \begin{bmatrix} -\omega^2(k_o + r)\left[1 - \frac{k_o^3}{[(k_o+r)^2+c^2+o^2]^{\frac{3}{2}}}\right] + 3\omega^2 r \\ -\omega^2 c\left[1 - \frac{k_o^3}{[(k_o+r)^2+c^2+o^2]^{\frac{3}{2}}}\right] \\ -\omega^2 o\left[\frac{k_o^3}{[(k_o+r)^2+c^2+o^2]^{\frac{3}{2}}}\right] \end{bmatrix} - K \begin{bmatrix} \dot{r} - \dot{r}_{com} \\ r - r_{com} \\ \dot{c} - \dot{c}_{com} \\ c - c_{com} \\ \dot{o} - \dot{o}_{com} \\ o - o_{com} \end{bmatrix}
\tag{97}
$$

where the subscript *com* represents the commanded states.

3.4 State Dependent Riccati Equations

The State Dependent Riccati Equation (SDRE) technique uses the nonlinear CW equations.

$$
\begin{aligned}
\ddot{r} &= 2\omega\dot{c} + \omega^2(k_o + r)\left[1 - \frac{k_o^3}{[(k_o+r)^2+c^2+o^2]^{\frac{3}{2}}}\right] + v_{c_r} \\
\ddot{c} &= -2\omega\dot{r} + \omega^2 c\left[1 - \frac{k_o^3}{[(k_o+r)^2+c^2+o^2]^{\frac{3}{2}}}\right] + v_{c_c} \\
\ddot{o} &= -\omega^2 o\left[\frac{k_o^3}{[(k_o+r)^2+c^2+o^2]^{\frac{3}{2}}}\right] + v_{c_o}
\end{aligned}
\tag{98}
$$

Assume the following simplification

$$
\sigma_o = \frac{k_o^3}{[(k_o+r)^2+c^2+o^2]^{\frac{3}{2}}}
\tag{99}
$$

$$
\sigma_c = 1 - \sigma_o
\tag{100}
$$

$$
\sigma_r = \left(\frac{k_o}{r} + 1\right)\sigma_c
\tag{101}
$$

Substituting these equations into Equations 98 yields

$$
\ddot{r} = 2\omega\dot{c} + \omega^2\sigma_r r + v_{c_r}
$$

$$
\ddot{c} = -2\omega\dot{r} + \omega^2\sigma_c c + v_{c_c}
\tag{102}
$$

34

$$\ddot{o} = -\omega^2 \sigma_o o + v_{c_o}$$

In matrix form

$$
\begin{bmatrix} \ddot{r} \\ \dot{r} \\ \ddot{c} \\ \dot{c} \\ \ddot{o} \\ \dot{o} \end{bmatrix} =
\begin{pmatrix}
0 & \omega^2 \sigma_r & 2\omega & 0 & 0 & 0 \\
1 & 0 & 0 & 0 & 0 & 0 \\
-2\omega & 0 & 0 & \omega^2 \sigma_c & 0 & 0 \\
0 & 0 & 1 & 0 & 0 & 0 \\
0 & 0 & 0 & 0 & 0 & -\omega^2 \sigma_o \\
0 & 0 & 0 & 0 & 1 & 0
\end{pmatrix}
\begin{bmatrix} \dot{r} \\ r \\ \dot{c} \\ c \\ \dot{o} \\ o \end{bmatrix} +
\begin{pmatrix}
1 & 0 & 0 \\
0 & 0 & 0 \\
0 & 1 & 0 \\
0 & 0 & 0 \\
0 & 0 & 1 \\
0 & 0 & 0
\end{pmatrix}
\begin{bmatrix} v_{c_r} \\ v_{c_c} \\ v_{c_o} \end{bmatrix}
\quad (103)
$$

Since σ_r, σ_c, and σ_o change at each time step, the SDRE technique continuously updates Equation 103 and finds a new controller gain matrix via the Riccati equation discussed in Section 3.2 and uses the new gain to find the control signal.

$$
\begin{bmatrix} v_{c_r} \\ v_{c_c} \\ v_{c_o} \end{bmatrix} = -K
\begin{bmatrix}
\dot{r} - \dot{r}_{com} \\
r - r_{com} \\
\dot{c} - \dot{c}_{com} \\
c - c_{com} \\
\dot{o} - \dot{o}_{com} \\
o - o_{com}
\end{bmatrix}
\quad (104)
$$

where the subscript *com* represents the commanded states.

For LQR, LQR with linearizing feedback, and SDRE, the control weight (R) will be varied for each simulation run. Trial runs show that a range of about 10^9 to 10^{13} produce acceptable results. Lower than 10^9 results in unacceptably high control usage while larger than 10^{13} translates to unacceptable settling times. The specifics can be found in Chapter IV.

3.5 Sliding Mode Control

Sliding mode control (SMC) is a nonlinear control technique for imprecise systems. Since the commanded input is based on linear equations (creating an imprecise system)

this type of controller is a candidate. SMC is derived by defining a time varying surface upon which the system has some desired dynamics (21) and is defined as

$$s(x,t) = \left(\frac{d}{dt} + \lambda \right)^{n-1} \tilde{x} \tag{105}$$

where $\tilde{x}$ is the tracking error

$$\tilde{x} = \begin{bmatrix} \dot{r} - \dot{r}_{com} \\ r - r_{com} \\ \dot{c} - \dot{c}_{com} \\ c - c_{com} \\ \dot{o} - \dot{o}_{com} \\ o - o_{com} \end{bmatrix} \tag{106}$$

where the subscript *com* represents the commanded states, n is the order of the system (in this case $n = 2$) and λ are the real poles that determine the system dynamics on the surface $s(x,t)$. Since the system order in this case is two, Equation 105 reduces to

$$s = \dot{\tilde{x}} + \lambda \tilde{x} \tag{107}$$

The goal of SMC is to drive $\dot{s}$ to zero

$$\dot{s} = \ddot{\tilde{x}} + \lambda \dot{\tilde{x}} = 0 \tag{108}$$

The sliding mode function from the Nonlinear Synthesis toolbox from Optimal Synthesis Inc was used to implement sliding mode control for this simulation. The function required a pole (λ) for each direction, a parameter η which designates the rates at which the system will converge to the sliding surface, and ϵ which designates the boundary layer of the sliding surface (16). Within the boundary layer defined by ϵ, no control is used.

Trial runs using sliding mode control on the nonlinear CW equations showed the best η and ϵ are

$$\eta = 10^{-5.8}$$

$$\epsilon = 10^{-6}$$

Instead of varying the control weight (R) as in LQR and SDRE techniques, the pole locations are varied for each sliding mode run. Trial runs showed that the poles should exist no farther from the $j\omega$ axis than -0.003 for acceptable control usage and settling time results.

The Nonlinear Synthesis toolbox requires a formulation of the problem such that the states are driven to zero; therefore the states need to be modified so that they are equal to the error signal instead of the relative position and velocity of the follower satellite. Starting with the nonlinear CW equations

$$
\begin{aligned}
\ddot{r} &= 2\omega\dot{c} + \omega^2(k_o + r)\left[1 - \frac{k_o^3}{[(k_o+r)^2+c^2+o^2]^{\frac{3}{2}}}\right] + v_{c_r} \\
\ddot{c} &= -2\omega\dot{r} + \omega^2 c\left[1 - \frac{k_o^3}{[(k_o+r)^2+c^2+o^2]^{\frac{3}{2}}}\right] + v_{c_c} \\
\ddot{o} &= -\omega^2 o\left[\frac{k_o^3}{[(k_o+r)^2+c^2+o^2]^{\frac{3}{2}}}\right] + v_{c_o}
\end{aligned}
\tag{109}
$$

The modified states and their derivative are

$$
x = \begin{bmatrix} \dot{r}_{com} - \dot{r} \\ r_{com} - r \\ \dot{c}_{com} - \dot{c} \\ c_{com} - c \\ \dot{o}_{com} - \dot{o} \\ o_{com} - o \end{bmatrix} \quad
\dot{x} = \begin{bmatrix} \ddot{r}_{com} - \ddot{r} \\ \dot{r}_{com} - \dot{r} \\ \ddot{c}_{com} - \ddot{c} \\ \dot{c}_{com} - \dot{c} \\ \ddot{o}_{com} - \ddot{o} \\ \dot{o}_{com} - \dot{o} \end{bmatrix}
\tag{110}
$$

Making the same simplifications as in the SDRE derivation

$$\sigma_o = \frac{k_o^3}{[(k_o+r)^2+c^2+o^2]^{\frac{3}{2}}} \tag{111}$$

$$\sigma_c = 1 - \sigma_o \tag{112}$$

$$\sigma_r = \left(\frac{k_o}{r} + 1\right)\sigma_c \tag{113}$$

yields

$$\ddot{r} = 2\omega\dot{c} + \omega^2\sigma_r r + v_{c_r}$$

$$\ddot{c} = -2\omega\dot{r} + \omega^2\sigma_c c + v_{c_c} \tag{114}$$

$$\ddot{o} = -\omega^2\sigma_o o + v_{c_o}$$

Substituting the commanded and actual states in Equations 109 (note that $\vec{v}_{c_{com}} = 0$)

$$\begin{aligned}
\ddot{r}_{com} - \ddot{r} &= [2\omega\dot{c}_{com} + \omega^2\sigma_{r_{com}}r_{com}] - [2\omega\dot{c} + \omega^2\sigma_r r + v_{c_r}] \\
&= 2\omega(\dot{c}_{com} - \dot{c}) + \omega^2(\sigma_{r_{com}}r_{com} - \sigma_r r) - v_{c_r}
\end{aligned} \tag{115}$$

$$\begin{aligned}
\ddot{c}_{com} - \ddot{c} &= [-2\omega\dot{r}_{com} + \omega^2\sigma_{c_{com}}c_{com}] - [-2\omega\dot{r} + \omega^2\sigma_c c + v_{c_c}] \\
&= -2\omega(\dot{r}_{com} - \dot{r}) + \omega^2(\sigma_{c_{com}}c_{com} - \sigma_c c) - v_{c_c}
\end{aligned} \tag{116}$$

$$\begin{aligned}
\ddot{o}_{com} - \ddot{o} &= [-\omega^2\sigma_{o_{com}}o_{com}] - [-\omega^2\sigma_o o + v_{o_c}] \\
&= -\omega^2(\sigma_{o_{com}}o_{com} - \sigma_o o) - v_{o_c}
\end{aligned} \tag{117}$$

The Nonlinear Synthesis toolbox requires a function file that passes the derivative of the state ($\dot{x}$) given the current state (x) and a vector of controls ($\vec{v}_c$), thus this function would pass back the following vector

$$\dot{x} = \begin{bmatrix} \ddot{r}_{com} - \ddot{r} \\ \dot{r}_{com} - \dot{r} \\ \ddot{c}_{com} - \ddot{c} \\ \dot{c}_{com} - \dot{c} \\ \ddot{o}_{com} - \ddot{o} \\ \dot{o}_{com} - \dot{o} \end{bmatrix} = \begin{bmatrix} 2\omega(\dot{c}_{com} - \dot{c}) + \omega^2(\sigma_{r_{com}}r_{com} - \sigma_r r) \\ x(1) \\ -2\omega(\dot{r}_{com} - \dot{r}) + \omega^2(\sigma_{c_{com}}c_{com} - \sigma_c c) \\ x(3) \\ -\omega^2(\sigma_{o_{com}}o_{com} - \sigma_o o) \\ x(5) \end{bmatrix} - \begin{bmatrix} v_{c_r} \\ 0 \\ v_{c_c} \\ 0 \\ v_{c_o} \\ 0 \end{bmatrix} \tag{118}$$

IV. Results

The following chapter presents a comparison of the different control techniques for several different types of reconfigurations. Important information about how well each controller performs the reconfiguration can also be found by examining the control usage and state/COE time histories as well as other data produced during each simulation. For this reason, each control technique has an appendix where the complex parameter change reconfiguration (Section 4.4) is presented and discussed in more detail.

- LQR in Appendix G

- LQR with linearizing feedback in Appendix H

- SDRE in Appendix I

- Sliding Mode in Appendix J

The settling time for each maneuver is measured from the start of the reconfiguration not $t = 0$, likewise, the ΔV listed for each reconfiguration is the total ΔV measured at the settling time minus the total ΔV measured at the reconfiguration start time. This means the ΔV does not include any of the steady state control energy used to correct the error between the linear and nonlinear equations before or after the reconfiguration. Of course due to the linear command signal there will always be additional error that the controller is forced to deal with as shown in Section 2.2. The first section of this chapter will characterize this error and discuss its effects on ΔV for each controller.

4.1 The Impact of Using Linear vs. Nonlinear Equations on ΔV

In the reconfiguration simulation, the command signal is based on the parameterized Hill's equations (linear EOMs) while the orbits are propagated inertially (nonlinear EOMs). This causes an error between the commanded and the actual relative positions even without a reconfiguration and requires control usage. It is this control usage (and subsequent ΔV costs) that is of particular interest and must be quantified. Running the reconfiguration simulation without a change in the commanded relative parameters is used to examine the ΔV costs of the indicated errors. Using the relative parameters listed in Table 2, a

simulation was run using a time step of 15 seconds. The slope for each compensator is

ρ (km)	0.5
a (km)	0
θ (deg)	45
b (km)	0
m (unitless)	1
n (unitless)	0

Table 2 ΔV Error Simulation Relative Parameters

determined via a least squares line fit and is listed in Table 3. The use of ΔV to null out the command error is fairly linear for all values of control weight. For the LQR and SDRE techniques, smaller values of R (which translate to higher control usage) resulted in higher slopes while the reverse was true for LQR with LF (Figure 19). The converse was true for larger values of R (Figure 20). Experience shows that the total ΔV expended during a
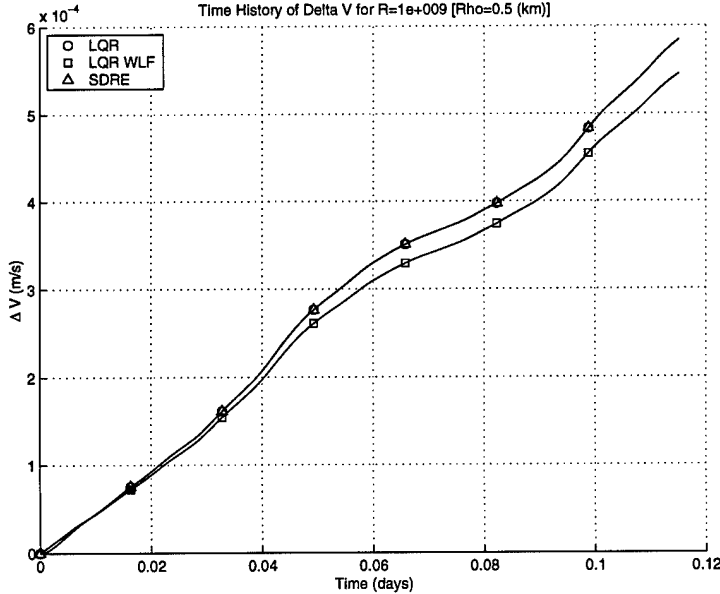
Figure 19   Gain Methods Steady State ΔV Costs $R = 10^9$

reconfiguration using LQR, LQR with LF, or SDRE is several orders of magnitude greater than the ΔV used to correct for the linear command. For this reason and the fact that these three compensators have similar slopes, the excess ΔV usage will be accepted. The sliding mode steady state costs are much more significant. Using the parameters in Table 2, the slopes for sliding mode are listed in Table 4. It is obvious that the sliding mode

40
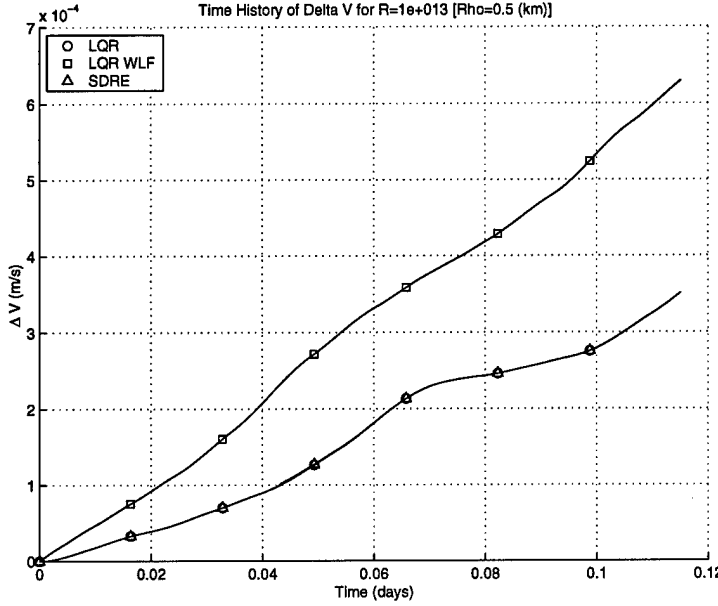
Figure 20   Gain Method Steady State ΔV Costs $R = 10^{13}$

ΔV Usage ($\frac{m}{s}$ per day)	LQR	LQR with LF	SDRE
$R = 10^9$	0.0049646	0.0046246	0.0049634
$R = 10^{10}$	0.0062665	0.0054137	0.0062631
$R = 10^{11}$	0.0061623	0.0054478	0.0061552
$R = 10^{12}$	0.0049441	0.0054484	0.004938
$R = 10^{13}$	0.0031391	0.0054485	0.0031386

Table 3   Steady State ΔV Slopes (Gain Methods)

controller is using a large amount of control energy during steady state conditions. This is due to excess chatter on the sliding mode surface; a known problem with sliding mode control. The negative effects of this chatter will become obvious in the example simulations and is the main reason that the sliding mode technique requires higher ΔVs than LQR, LQR with LF, and SDRE. The slopes seem to increase as the sliding mode pole moves away from the $j\omega$ axis. Figures 21 and 22 show the steady state ΔV cost for the highest (P=-0.003) and lowest (P=-0.0006) SMC slopes respectively.
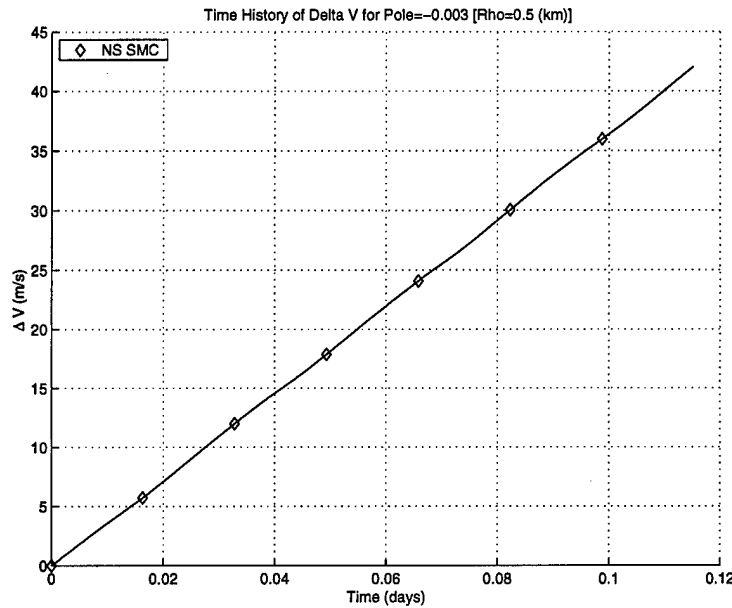
Figure 21   Pole Method Steady State ΔV Costs $(P = -0.003)$
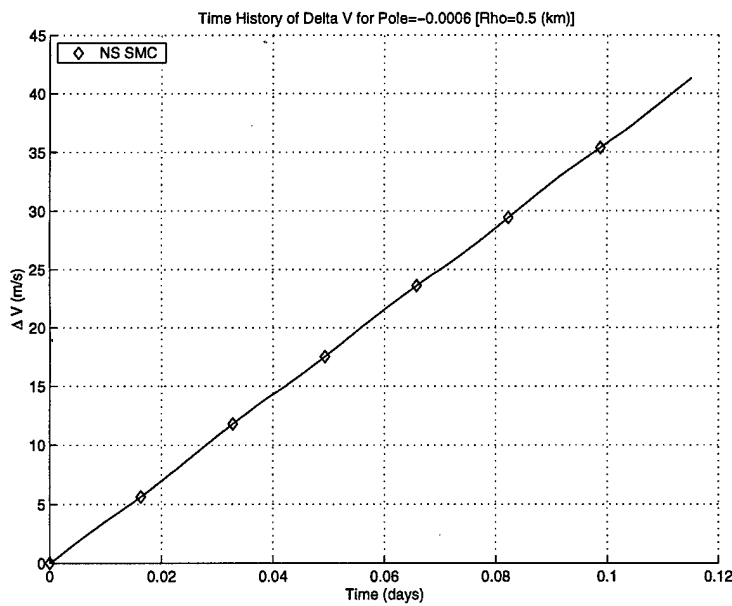
Figure 22   Pole Method Steady State ΔV Costs $(P = -0.0006)$

ΔV Usage ($\frac{m}{s}$ per day)	LQR
Pole=-0.0006	358.9385
Pole=-0.0012	361.1704
Pole=-0.0018	363.4057
Pole=-0.0024	364.9747
Pole=-0.003	365.577

Table 4   Steady State ΔV Slopes (Pole Method)

4.2 Simple ρ Reconfiguration (Small Relative Orbit)

This reconfiguration changed only the parameter ρ thereby changing the semi major/minor axes of the relative orbit. The choice of the initial and final ρ are small enough that the linear Hill's equations are very close to the nonlinear CW equations. From the error analysis done in Section 2.2 , we expect no more than a 1 meter error in the $\hat{R}$ and $\hat{O}$ directions and up to 10 meters in the $\hat{C}$ direction (depending on settling time) for a 10,000 km leader orbit. The initial and final relative parameters are given in Table 5. The simulation uses a 15 second time step with the leader in a circular orbit with classical orbital elements (COEs) listed in Table 6.   The ΔV results for controllers in which

	Initial	Final
ρ (km)	0.5	1.5
a (km)	0	0
θ (deg)	45	45
b (km)	0	0
m (slope)	1	1
n (slope)	0	0

Table 5   Small Orbit ρ Simulation Initial and Final Parameters

Semi-Major Axis	10000 km
Eccentricity	0
Inclination	10 deg
Argument of Perigee	0 deg
Longitude of the Ascending Node	0 deg
Initial True Anomaly	10 deg

Table 6   Small Orbit ρ Simulation Leader COEs

control weight was varied are listed in Table 7. The results show that for higher values of R, the two nonlinear methods do provide a lower ΔV as compared to LQR, however,

43

ΔV (m/s)	OLDTIM	LQR	LQR With LF	SDRE
$R = 10^9$	0.632092	13.8110215	13.8110284	13.8110049
$R = 10^{10}$	0.632092	7.8518765	7.8519592	7.8518429
$R = 10^{11}$	0.632092	4.2552826	4.2552369	4.2551942
$R = 10^{12}$	0.632092	2.3860346	2.3855585	2.3859874
$R = 10^{13}$	0.632092	1.7847727	1.7842614	1.7847499

Table 7   Small Orbit ρ Simulation ΔV Results (Control Weight Methods)

this improvement is on the order of 10^{-6} and thus negligible. The ΔV results for sliding mode control (which varied pole placement) are listed in Table 8. The sliding mode

ΔV (m/s)	OLDTIM	SMC
Pole=-0.0006	0.632092	36.5888133
Pole=-0.0012	0.632092	19.9482038
Pole=-0.0018	0.632092	15.3333261
Pole=-0.0024	0.632092	14.2883201
Pole=-0.003	0.632092	13.8828796

Table 8   Small Orbit ρ Simulation ΔV Results (Pole Method)

method shows a significant increase in control energy as opposed to the gain techniques. Section 4.1 shows that compared to the gain techniques, sliding mode control expends a large amount of control energy even during steady state conditions due to the chattering effect. The controller is required to expand even more energy on top of this to do the reconfiguration and thus at a disadvantage compared to the gain techniques.

The OLDTIM ΔV can be broken out into its three separate discrete burn maneuvers and is shown in Table 9. The changes in the COEs of the follower satellite upon which the OLDTIM maneuver is based are listed in Table 10.   The OLDTIM break out shows

Hohmann ΔV	0.000417502 (m/s)
Inc/LAN ΔV	0.631353 (m/s)
AP ΔV	0.000320607 (m/s)
Total	0.632092 (m/s)

Table 9   Small Orbit ρ Simulation OLDTIM ΔV

that a majority of the control energy in the discrete burn is used to change the inclination and longitude of the ascending node even though they are relatively small angle changes. Plane changes are usually more ΔV intensive than coplanar maneuvers.

	Initial	Final	Δ
Semi-Major Axis (km)	10000	10000	N/A
Eccentricity	0.0000499951	0.000149973	0.0000999777
Inclination (deg)	10.0023	10.007	0.00469583
Argument of Perigee (deg)	304.987	304.929	0.0581968
Longitude of the Ascending Node (deg)	-0.00945911	-0.0283561	0.018897

Table 10   Small Orbit ρ Simulation Follower COEs Changes

The settling time results are listed in Tables 11 and 12. The criteria for settling time is that the position error for each direction in the RCO frame falls and remains within +/- 10 meters. It is assumed that at this point a stationkeeping controller will take over and reduce or maintain the error to required levels.   As expected after seeing the ΔV

Settling Time (min)	OLDTIM	LQR	LQR With LF	SDRE
$R = 10^9$	82.933410	20.00	20.00	20.00
$R = 10^{10}$	82.933410	36.50	36.50	36.50
$R = 10^{11}$	82.933410	62.00	62.00	62.00
$R = 10^{12}$	82.933410	107.50	107.25	107.50
$R = 10^{13}$	82.933410	287.75	288.00	287.75

Table 11   Small Orbit ρ Simulation Settling Time Results (Control Weight Methods)

Settling Time (min)	OLDTIM	SMC
Pole=-0.0006	82.933410	146.00
Pole=-0.0012	82.933410	82.25
Pole=-0.0018	82.933410	65.25
Pole=-0.0024	82.933410	65.00
Pole=-0.003	82.933410	69.00

Table 12   Small Orbit ρ Simulation Settling Time Results (Pole Method)

costs, the linear and nonlinear gain controllers continue to perform virtually identically. To see a few other trends, this data is presented graphically in Figures 23 and 24 for ΔV and Figures 25 and 26 for settling time. Notice that for the control weight methods, the total ΔV for the reconfiguration approaches the OLDTIM ΔV nearly asymptotically as R increases. Also note that as ΔV decreases, settling time increases (a normal tradeoff in designing controllers). This is not the case for sliding mode control where ΔV and settling time decrease as the poles move from the origin to around -0.002 on the real axis. Since the steady state ΔV usage of sliding mode is so high, the quicker it settles to the commanded

45

orbit, the less ΔV it requires. The large amount of energy expended by the sliding mode controller during steady state is overwhelming its ability to control the follower satellite at a reasonable ΔV cost. To compare all the methods together and determine their
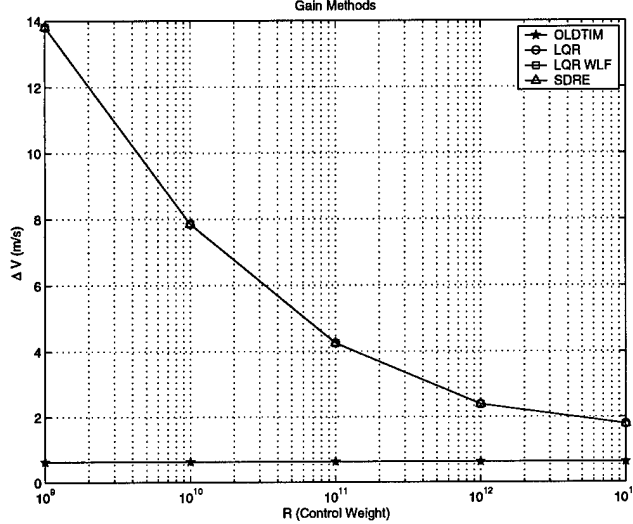
Figure 23   Small Orbit ρ Simulation ΔV (Control Weight Methods)
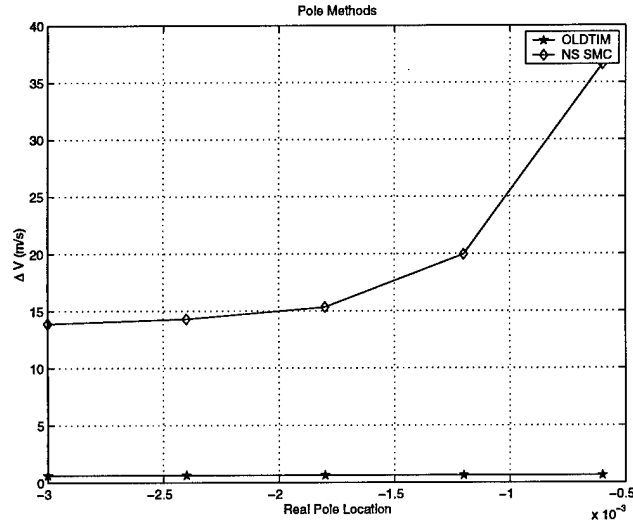
Figure 24   Small Orbit ρ Simulation ΔV (Pole Method)

best operating point (R or pole location), each method is graphed via ΔV versus settling time (Figure 27). Note that the closer the curve comes to the origin, the better the overall performance of the method. Once a specific method is determined, a designer can find the
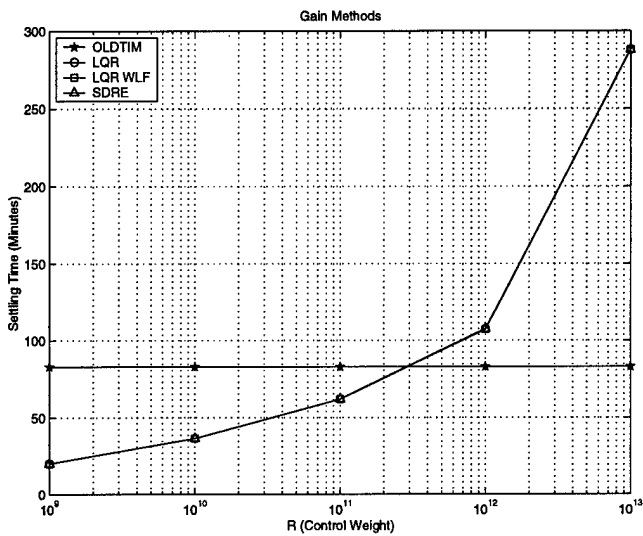
Figure 25   Small Orbit ρ Simulation Settling Time (Control Weight Methods)
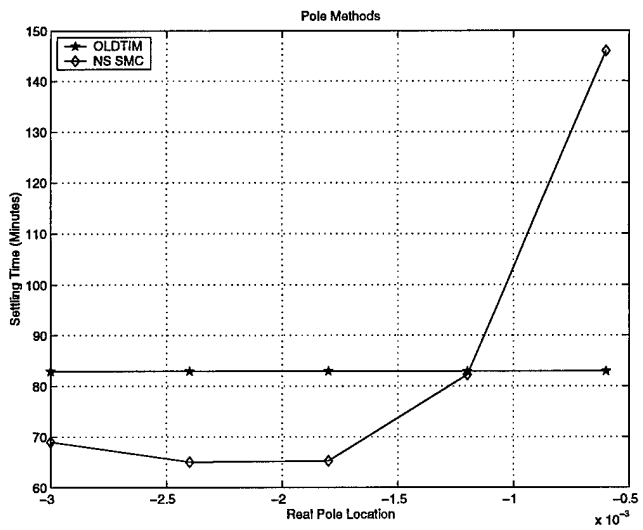
Figure 26   Small Orbit ρ Simulation Settling Time (Pole Method)

47
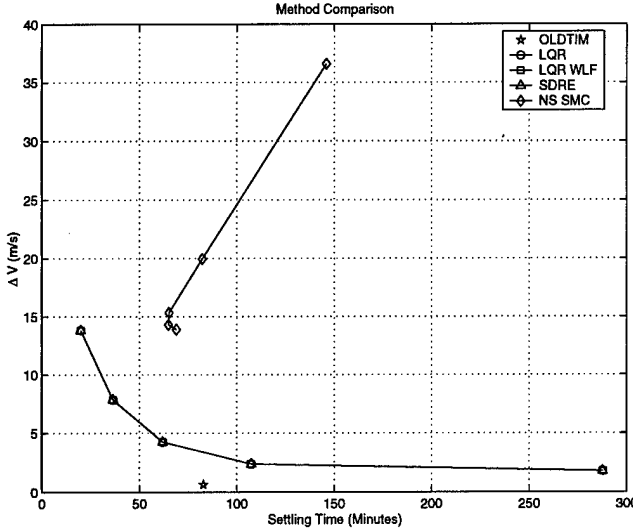
Figure 27   Small Orbit ρ Simulation Method Comparison

point at which the tradeoff between ΔV and settling time is acceptable based on mission parameters (on board fuel, acceptable off line times, frequency of reconfigurations, etc.).

For this reconfiguration in which ρ is changed and the relative orbit is small compared to the radius of the leader orbit, LQR, LQR with linearizing feedback, and SDRE work significantly better than sliding mode control (again, mostly due to chatter problems). Each of these three methods produces virtually identical results, thus there is no advantage to using nonlinear techniques over linear ones in this case. This is not a surprising result as the relative orbit is small enough that the linear equations of motion are a very good approximation.

4.3   Simple ρ Reconfiguration (Large Relative Orbit)

The next relative orbit reconfiguration changed the parameter ρ by the same amount as in the first simulation, however, in this case the initial and final ρ are much larger thus creating more error between the linear and nonlinear EOMs. For this larger ρ, error analysis shows that we can expect an almost 1200 meter error in the $\hat{R}$ and $\hat{O}$ directions and up to 14,000 meters in the $\hat{C}$ direction (depending on settling time) for a 10,000 km leader orbit. The initial and final relative parameters are given in Table 13. The simulation uses a 15 second time step with the leader in a circular orbit with classical orbital elements

48

(COEs) listed in Table 14. The ΔV results for controllers in which control weight was

	Initial	Final
ρ (km)	40.5	41.5
a (km)	0	0
θ (deg)	45	45
b (km)	0	0
m (slope)	1	1
n (slope)	0	0

Table 13   Large Orbit ρ Simulation Initial and Final Parameters

Semi-Major Axis	10000 km
Eccentricity	0
Inclination	10 deg
Argument of Perigee	0 deg
Longitude of the Ascending Node	0 deg
Initial True Anomaly	10 deg

Table 14   Large Orbit ρ Simulation Leader COEs

varied are listed in Table 15. The control usage in this simulation is much different than in

ΔV (m/s)	OLDTIM	LQR	LQR With LF	SDRE
$R = 10^9$	1.260372	15.6921806	13.6182920	15.6912682
$R = 10^{10}$	1.260372	11.4366934	7.7630169	11.4385323
$R = 10^{11}$	1.260372	9.3192450	4.7136968	9.3163821
$R = 10^{12}$	1.260372	9.0168279	3.9794505	9.0305245
$R = 10^{13}$	1.260372	10.1362775	8.1898422	10.1407846

Table 15   Large Orbit ρ Simulation ΔV Results (Control Weight Methods)

the near linear case of the first simulation. The LQR and SDRE controllers showed near identical ΔVs, but LQR with LF proved to use significantly less total control energy. The ΔV results for sliding mode control (which varied pole placement) are listed in Table 16. As before, sliding mode control shows a significant increase in expended control energy as compared to the gain techniques due to the chattering effect discussed in Section 4.1.

The ΔV for each of the OLDTIM maneuvers is shown in Table 17. The changes in the COEs of the follower satellite upon which the OLDTIM maneuver is based are listed in Table 18. The OLDTIM breakout is significantly different than the first simulation. Both the Hohmann and AP maneuvers require two orders of magnitude more control

49

ΔV (m/s)	OLDTIM	SMC
Pole=-0.0006	1.260372	38.8888040
Pole=-0.0012	1.260372	19.6637421
Pole=-0.0018	1.260372	16.1290137
Pole=-0.0024	1.260372	14.7930510
Pole=-0.003	1.260372	14.3854720

Table 16   Large Orbit ρ Simulation ΔV Results (Pole Method)

Hohmann ΔV	0.182102 (m/s)
Inc/LAN ΔV	0.667614 (m/s)
AP ΔV	0.410657 (m/s)
Total	1.260372 (m/s)

Table 17   Large Orbit ρ Simulation OLDTIM ΔV

energy while the plane change ΔV only marginally increased. Note that their is more error associated with the initial and final COEs as they too are a calculated from the linear command signal. Thus the OLDTIM ΔV calculation has a larger margin of error as well.

The settling time results are listed in Tables 19 and 20. The criteria for settling time is that the position error for each direction in the RCO frame falls and remains within +/- 10 meters after which a stationkeeping controller will take over and reduce the error to required levels. An analysis of the position error history shows that only LQR with LF and sliding mode control are able to reduce the position error to the prescribed +/- 10 meters. The error plots of LQR and SDRE show that the error will oscillate with a fixed amplitude (Figure 28) about the zero axis with no apparent dampening. The settling times of LQR and SDRE are consequently approximately equal to the simulation run time and meaningless. Analysis of the position error at different gains indicates that the amplitude is a function of the control weight R. Lower values of R (less restrictive on control usage) will allow both controllers to keep error within +/- 10 meters but at unacceptable ΔV costs. To see the trends in ΔV and settling time, this data is presented graphically in Figures 29 and 30 for ΔV and Figures 31 and 32 for settling time. The inability of LQR and SDRE to damp the position and velocity state error means that ΔV will not approach OLDTIM value. LQR with LF also does not approach OLDTIM asymptotically and instead appears to have a local minimum at around $R = 10^{12}$. As before, the settling time increases as R

	Initial	Final	Δ
Semi-Major Axis (km)	10000	10000	N/A
Eccentricity	0.00401814	0.0041296	0.000111458
Inclination (deg)	10.1916	10.1968	0.00517635
Argument of Perigee (deg)	303.981	303.054	0.927511
Longitude of the Ascending Node (deg)	-0.743455	-0.761246	0.0177914

Table 18   Large Orbit ρ Simulation OLDTIM ΔV

Settling Time (min)	OLDTIM	LQR	LQR With LF	SDRE
$R = 10^9$	82.946683	90.50	20.00	90.50
$R = 10^{10}$	82.946683	158.25	36.50	158.25
$R = 10^{11}$	82.946683	216.00	62.00	216.00
$R = 10^{12}$	82.946683	331.00	107.25	331.00
$R = 10^{13}$	82.946683	576.00	288.00	576.00

Table 19   Large Orbit ρ Simulation Settling Time Results (Control Weight Methods)

Settling Time (min)	OLDTIM	SMC
Pole=-0.0006	82.946683	152.25
Pole=-0.0012	82.946683	79.75
Pole=-0.0018	82.946683	68.50
Pole=-0.0024	82.946683	66.75
Pole=-0.003	82.946683	70.75

Table 20   Large Orbit ρ Simulation Settling Time Results (Pole Method)
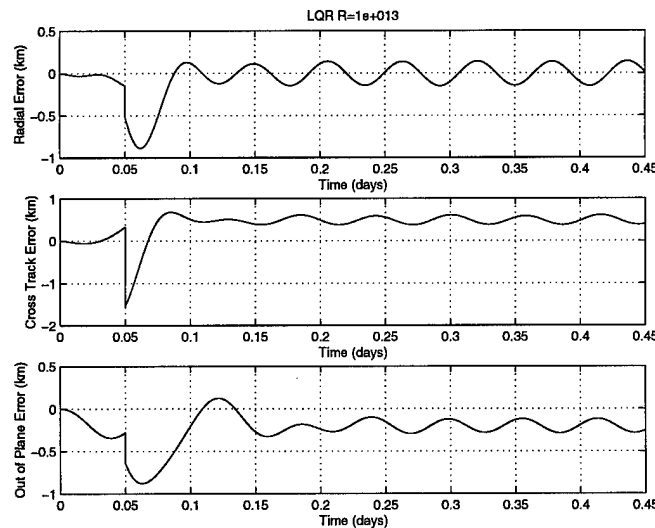
Figure 28   LQR Position Error for the Large Orbit ρ Simulation ($R = 10^{13}$)

51

increases. Sliding mode also damps out the error signal to zero but at a ΔV cost an order of magnitude above LQR with LF and appears to asymptotically approach a minimum ΔV value as the pole moves from the origin. Unlike LQR with LF, the ΔV decreases with shorter settling times due to the high steady state ΔV cost discussed in Section 4.1.

Graphing all of the methods together for comparison and optimal point determination
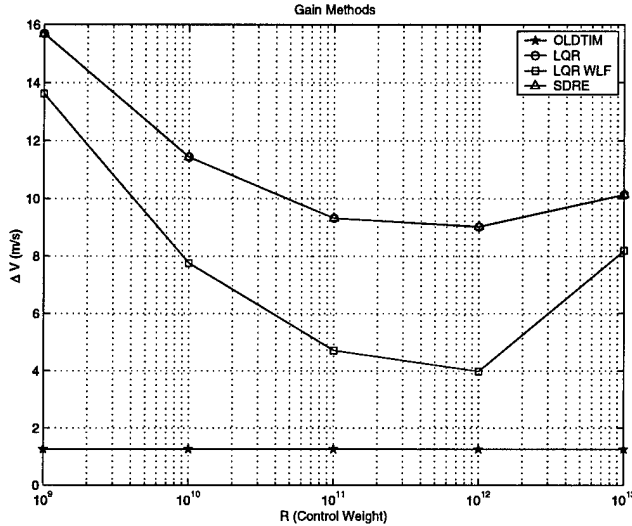
Figure 29   Large Orbit ρ Simulation ΔV (Control Weight Methods)
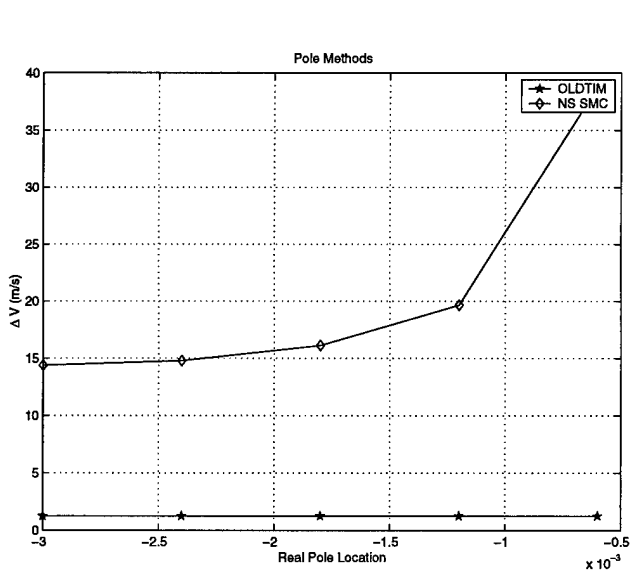
Figure 30   Large Orbit ρ Simulation ΔV (Pole Method)

yields Figure 33. Note that the closer the curve comes to the origin, the better the overall
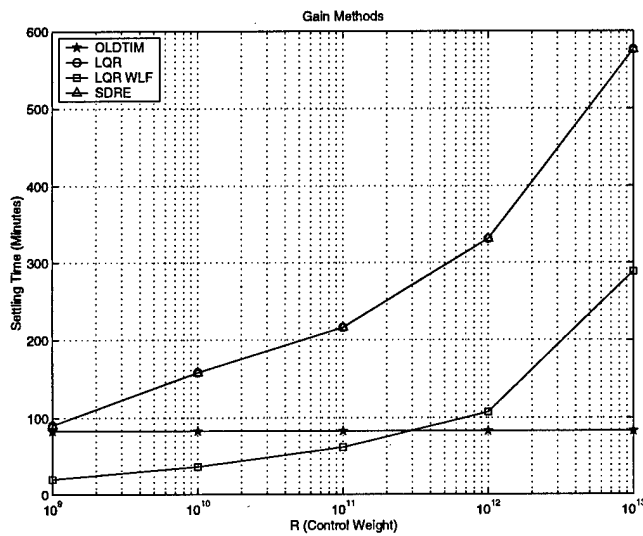
Figure 31   Large Orbit ρ Simulation Settling Time (Control Weight Methods)
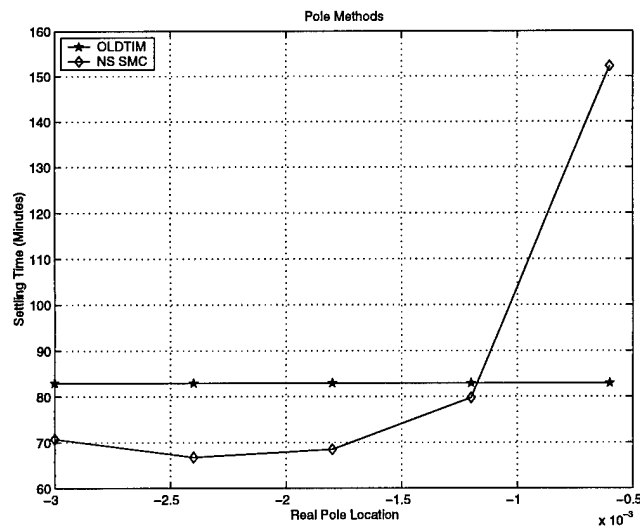
Figure 32   Large Orbit ρ Simulation Settling Time (Pole Method)
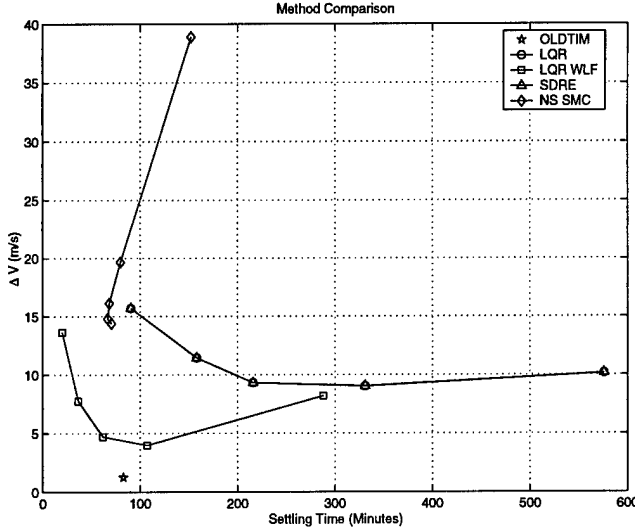
Figure 33   Large Orbit ρ Simulation Method Comparison

performance of the method.

Although the change in relative parameters for this simulation is identical to the first simulation, it is clear that using linear techniques will not be adequate. The command signal is based on the linear EOMs and thus the expended control energy will increase as the relative orbit size becomes a significant percentage of the orbit radius. Only LQR with LF and sliding mode were able to perform the reconfiguration to within the specified error tolerance and of these two, LQR with LF did the maneuver with significantly less ΔV and in an acceptable settling time.

4.4   Complex Parameter Reconfiguration

This simulation presents a more general relative orbit reconfiguration in which all parameters change except for a and b (thus leaving the leader satellite at the center of the formation). Like the first simulation, the choice of initial and final ρ is small enough that the linear Hill's equations are a very close approximation of the nonlinear CW equations. The small relative position magnitude means that we expect no more than a 1 meter error in the $\hat{R}$ and $\hat{O}$ directions and 10 meters in the $\hat{C}$ direction for a 10,000 km orbit. The initial and final relative parameters are given in Table 21. The simulation uses a 15 second time step with the leader in a circular orbit with classical orbital elements (COEs) listed

54

in Table 22. The ΔV results for controllers in which control weight was varied are listed

	Initial	Final
ρ (km)	0.5	1.5
a (km)	0	0
θ (deg)	45	60
b (km)	0	0
m (slope)	1	1.5
n (slope)	0	1

Table 21   Complex Simulation Initial and Final Parameters

Semi-Major Axis	10000 km
Eccentricity	0
Inclination	10 deg
Argument of Perigee	0 deg
Longitude of the Ascending Node	0 deg
Initial True Anomaly	10 deg

Table 22   Complex Simulation Leader COEs

in Table 23. The results show once again that the gain techniques are nearly equal in

ΔV (m/s)	OLDTIM	LQR	LQR With LF	SDRE
$R = 10^9$	2.351894	31.4307824	31.4307616	31.4307437
$R = 10^{10}$	2.351894	17.2212144	17.2213265	17.2211453
$R = 10^{11}$	2.351894	9.2636521	9.2637386	9.2635397
$R = 10^{12}$	2.351894	5.2854682	5.2845003	5.2854414
$R = 10^{13}$	2.351894	4.2184381	4.2181246	4.2185121

Table 23   Complex Simulation ΔV Results (Control Weight Methods)

their reconfiguration performance and no one method stands out. The ΔV results for sliding mode control (which varied pole placement) are listed in Table 24. The sliding mode method once again requires a much greater ΔV expenditure as compared to the gain methods due to the chattering and steady state problems discussed earlier.

The OLDTIM ΔV breakout is shown in Table 25. The changes in the COEs of the follower satellite upon which the OLDTIM maneuver is based are listed in Table 26. The OLDTIM shows that as in the first simulation, the majority of the discrete burn ΔV is going towards the plane change with the other two maneuvers several orders of magnitude smaller.

ΔV (m/s)	OLDTIM	SMC
Pole=-0.0006	2.351894	40.4172759
Pole=-0.0012	2.351894	24.1352993
Pole=-0.0018	2.351894	20.6293084
Pole=-0.0024	2.351894	21.2748060
Pole=-0.003	2.351894	23.4297615

Table 24   Complex Simulation ΔV Results (Pole Method)

Hohmann ΔV	0.00055705 (m/s)
Inc/LAN ΔV	2.26933 (m/s)
AP ΔV	0.0820091 (m/s)
Total	2.351894 (m/s)

Table 25   Complex Simulation OLDTIM ΔV

The settling time results are listed in Tables 27 and 28. The criteria for settling time is that the position error for each direction in the *RCO* frame falls and remains within +/- 10 meters after which a stationkeeping controller will take over and reduce the error to required levels. As with the ΔV costs, the linear and nonlinear gain controller settling times are virtually identically. To see the trends, the data is graphed in Figures 34 and 35 for ΔV and Figures 36 and 37 for settling time. Similar to the simple ρ parameter change, the gain techniques appear to asymptotically approach the OLDTIM maneuver as control usage is tightened and settling time increases. The sliding mode method has a local minimum for both ΔV and settling time at about P=-0.0018 on the real axis. All methods are compared against each other and the OLDTIM maneuver in Figure 38. Note that the closer the curve comes to the origin, the better the overall performance of the method. Once a specific method is determined, a designer can find the point at which the tradeoff between ΔV and settling time is acceptable based on mission parameters (on board fuel, acceptable off line times, frequency of reconfigurations, etc.). For the complex reconfiguration, the gain methods worked significantly better than the sliding mode method. Between the three gain methods, there was no clear advantage to using the nonlinear techniques.

	Initial	Final	Δ
Semi-Major Axis (km)	10000	10000	0.0017649
Eccentricity	0.0000499951	0.000149848	0.0000998524
Inclination (deg)	10.0023	9.99514	0.00721041
Argument of Perigee (deg)	304.987	319.916	14.9285
Longitude of the Ascending Node (deg)	-0.00945911	-0.120565	0.111106

Table 26   Complex Simulation Follower COEs Changes

Settling Time (min)	OLDTIM	LQR	LQR With LF	SDRE
$R = 10^9$	82.933415	21.25	21.25	21.25
$R = 10^{10}$	82.933415	37.50	37.50	37.50
$R = 10^{11}$	82.933415	86.50	86.50	86.50
$R = 10^{12}$	82.933415	152.50	152.50	152.50
$R = 10^{13}$	82.933415	407.25	407.75	407.25

Table 27   Complex Simulation Settling Time Results (Control Weight Methods)

Settling Time (min)	OLDTIM	SMC
Pole=-0.0006	82.933415	166.00
Pole=-0.0012	82.933415	107.75
Pole=-0.0018	82.933415	99.00
Pole=-0.0024	82.933415	107.00
Pole=-0.003	82.933415	123.00

Table 28   Complex Simulation Settling Time Results (Pole Method)
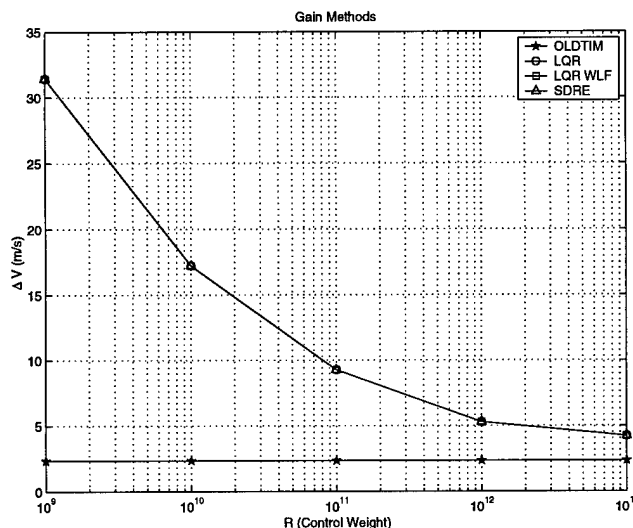

Figure 34   Complex Simulation ΔV (Control Weight Methods)
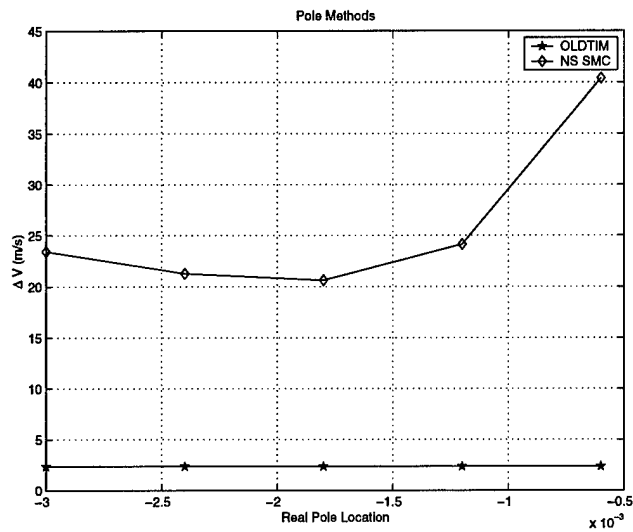
Figure 35   Complex Simulation ΔV (Pole Method)
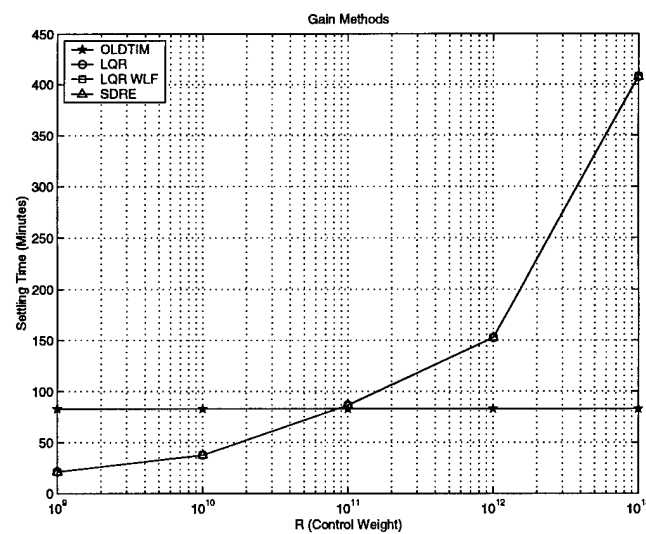

Figure 36   Complex Simulation Settling Time (Control Weight Methods)
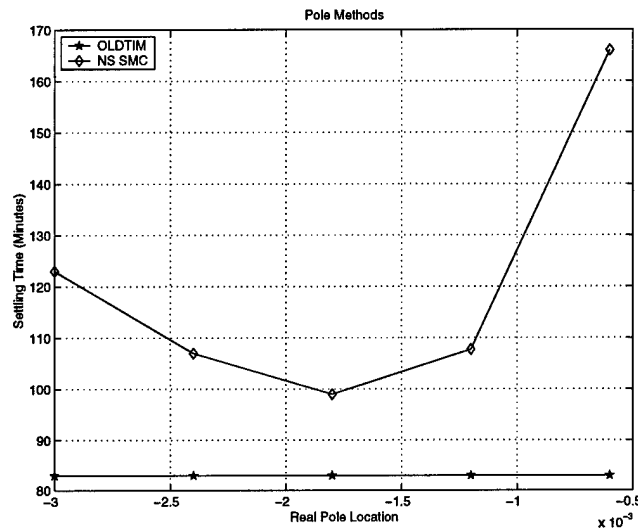
Figure 37   Complex Simulation Settling Time (Pole Method)
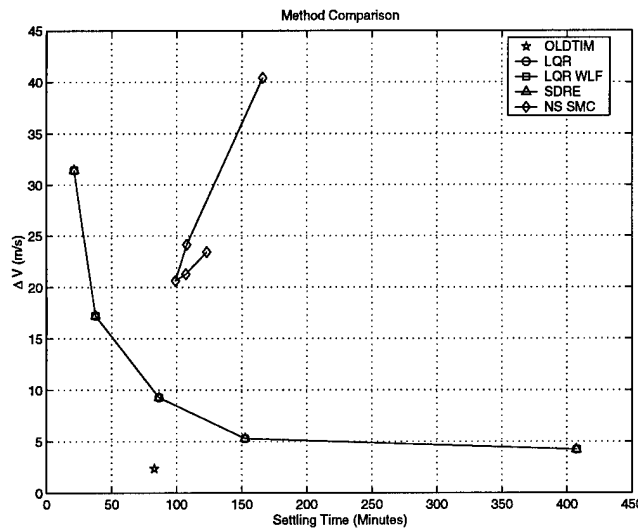
Figure 38   Complex Simulation Method Comparison

59

4.5 Simple θ Reconfiguration

The final relative orbit reconfiguration changed only the parameter θ. The θ parameter defines the angle that the follower satellite's position vector makes with $\hat{C}$ at $t = 0$. Changing θ does not change the size, shape, or orientation of the relative orbit only the follower satellites' starting position within the relative orbit. If the formation included multiple follower satellites, changing θ would change that follower's position relative to the other satellites in the formation. The choice of the initial and final ρ are small enough that the linear Hill's equations are a very close approximation of the nonlinear CW equations. From the error analysis done in Section 2.2, we expect no more than a 1 meter error in the $\hat{R}$ and $\hat{O}$ directions and 10 meters in the $\hat{C}$ direction for a 10,000 km leader orbit. The initial and final relative parameters are given in Table 29. The simulation uses a 15 second time step with the leader in a circular orbit with classical orbital elements (COEs) listed in Table 30. The ΔV results for controllers in which control weight was varied are

	Initial	Final
ρ (km)	0.5	0.5
a (km)	0	0
θ (deg)	30	60
b (km)	0	0
m (slope)	1	1
n (slope)	0	0

Table 29 θ Simulation Initial and Final Parameters

Semi-Major Axis	10000 km
Eccentricity	0
Inclination	10 deg
Argument of Perigee	0 deg
Longitude of the Ascending Node	0 deg
Initial True Anomaly	10 deg

Table 30 θ Simulation Leader COEs

listed in Table 31. The results once again show only the slightest of performance increases by using the nonlinear gain techniques over LQR (on the order of 10^{-6}). The ΔV results for sliding mode control (which varied pole placement) are listed in Table 32. The sliding mode results are an order of magnitude higher than the gain method controllers with

ΔV (m/s)	OLDTIM	LQR	LQR With LF	SDRE
$R = 10^9$	0.326750	3.6062904	3.6062857	3.6062818
$R = 10^{10}$	0.326750	2.1439774	2.1439539	2.1439696
$R = 10^{11}$	0.326750	1.3546992	1.3546386	1.3547005
$R = 10^{12}$	0.326750	0.8592822	0.8591845	0.8592881
$R = 10^{13}$	0.326750	0.5046080	0.5044617	0.5045870

Table 31 θ Simulation ΔV Results (Control Weight Methods)

ΔV (m/s)	OLDTIM	SMC
Pole=-0.0006	0.326750	22.9683408
Pole=-0.0012	0.326750	11.6012523
Pole=-0.0018	0.326750	7.8489131
Pole=-0.0024	0.326750	6.3261655
Pole=-0.003	0.326750	5.2428135

Table 32 θ Simulation ΔV Results (Pole Method)

no decrease in settling time. The chatter and steady state problems associated with the sliding mode controller drive up total ΔV costs once again.

Each of the OLDTIM maneuvers is shown in Table 33. The changes in the COEs of the follower satellite upon which the OLDTIM maneuver is based are listed in Table 34.

Hohmann ΔV	0.00000576885 (m/s)
Inc/LAN ΔV	0.163404 (m/s)
AP ΔV	0.16334 (m/s)
Total	0.326750 (m/s)

Table 33 θ Simulation OLDTIM ΔV

In this case the OLDTIM break out shows a nearly even split in control energy between the plane change (inclination and LAN) and orientation change (AP).

The settling time results are listed in Tables 35 and 36. The criteria for settling time is that the position error for each direction in the *RCO* frame falls and remains within +/- 10 meters. It is assumed that at this point a stationkeeping controller will take over and reduce the error to required levels. As with previous examples, the linear and nonlinear gain controller settling times are virtually identically. Finally, the data is presented graphically in Figures 39 and 40 for ΔV and Figures 41 and 42 for settling time. Similar to the ρ parameter change, the gain techniques appear to asymptotically

	Initial	Final	Δ
Semi-Major Axis (km)	10000	10000	0.0000182746
Eccentricity	0.0000499945	0.0000499943	2.56005×10^{-10}
Inclination (deg)	10.0027	10.0018	0.000850248
Argument of Perigee (deg)	289.986	319.977	29.9911
Longitude of the Ascending Node (deg)	-0.00563948	-0.0126345	0.00699506

Table 34 θ Simulation Follower COEs

Settling Time (min)	OLDTIM	LQR	LQR With LF	SDRE
$R = 10^9$	82.933394	15.75	15.75	15.75
$R = 10^{10}$	82.933394	28.75	28.75	28.75
$R = 10^{11}$	82.933394	48.75	48.75	48.75
$R = 10^{12}$	82.933394	83.25	83.25	83.25
$R = 10^{13}$	82.933394	180.25	180.25	180.25

Table 35 θ Simulation Settling Time Results (Control Weight Methods)

Settling Time (min)	OLDTIM	SMC
Pole=-0.0006	82.933394	91.50
Pole=-0.0012	82.933394	46.00
Pole=-0.0018	82.933394	32.00
Pole=-0.0024	82.933394	26.00
Pole=-0.003	82.933394	22.50

Table 36 θ Simulation Settling Time Results (Pole Method)

approach the OLDTIM maneuver as control usage is tightened and settling time increases. The sliding mode method appears to approach asymptotically as the poles on the real axis move farther from the origin but a much slower rate than the gain methods.   Figure
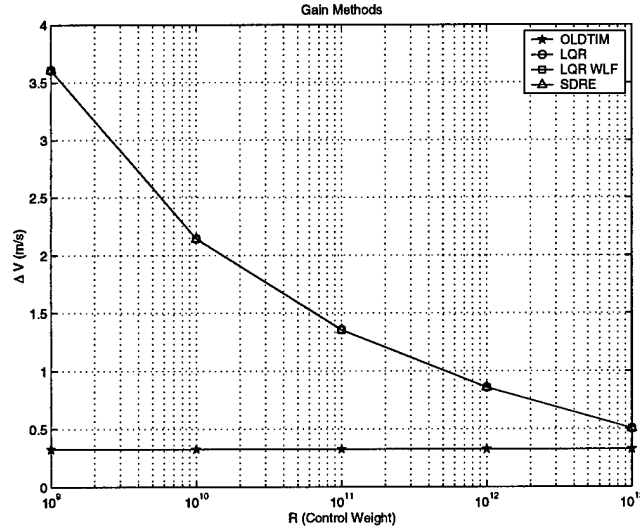

Figure 39 θ Simulation ΔV (Control Weight Methods)
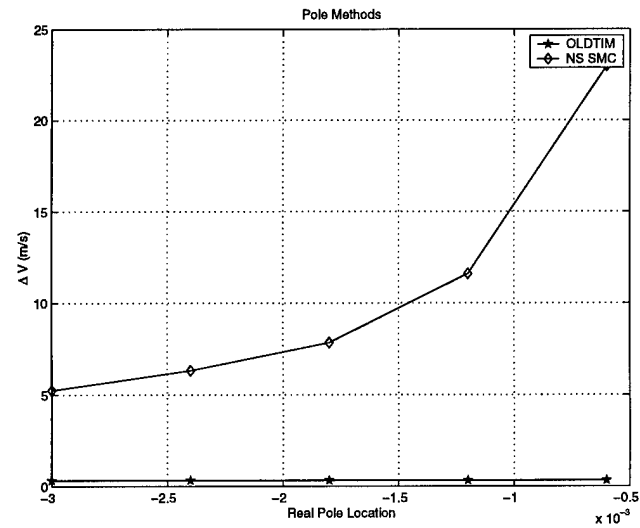

Figure 40 θ Simulation ΔV (Pole Method)

43 shows each method graphed with ΔV versus settling time. Note that the closer the curve comes to the origin, the better the overall performance of the method. Using this criteria to compare methods, it is easy to see that for the θ change simulation LQR, LQR
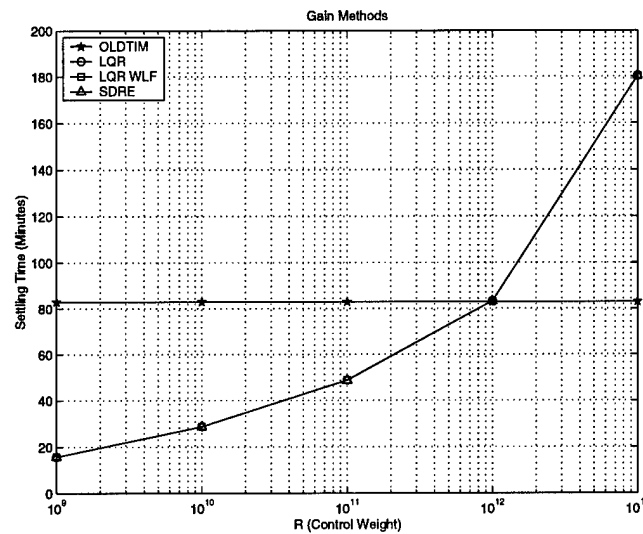
Figure 41 θ Simulation Settling Time (Control Weight Methods)


Figure 42 θ Simulation Settling Time (Pole Method)

64
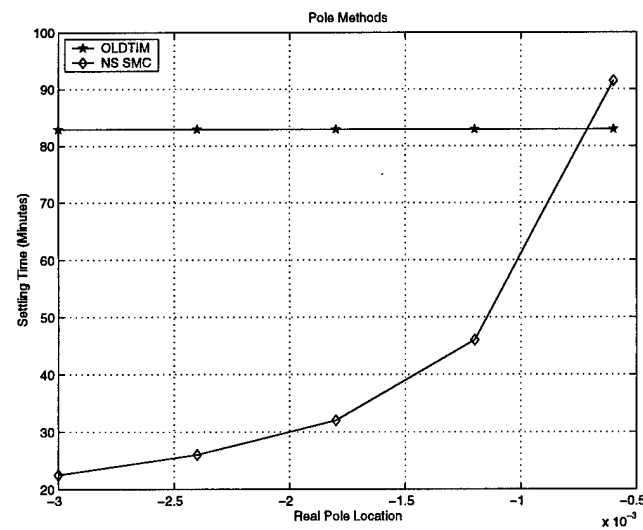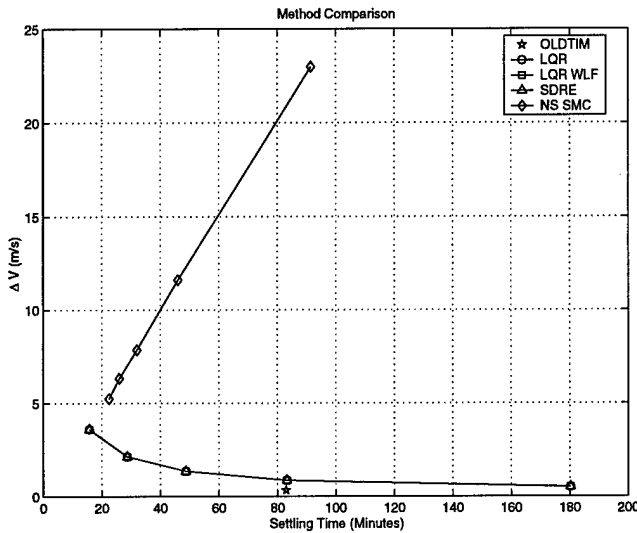
Figure 43 θ Simulation Method Comparison

with linearizing feedback, and SDRE work significantly better than sliding mode control (which once again must deal with chattering and steady state problems). Much like the first simulation, each of these three methods produces virtually identical results, thus there is no advantage to using nonlinear techniques over linear ones.

4.6   The Effect of J_2 on Reconfiguration

The results presented assume the ideal orbit model; the Earth is a point source and no other forms of perturbations exist (drag, third body effects, solar wind, etc.). There are two ways to approach the perturbations problem in the relative dynamics frame. The first is to have both the leader and follower correct for perturbations while still maintaining the proper relative alignment. The second is to accept drift due to perturbations and have the follower satellite only correct for the difference in the perturbations between the two satellites. With either, the equations of motion used to derive the controller must include the perturbations model. Effects caused by the Earth being an oblate sphere as opposed to a point mass are the strongest of the perturbations encountered by operational satellites.

Its derivation can be found in Appendix B and in the IJK frame is

$$\vec{v}_p = \frac{\mu J_2 R_e^2}{2} \begin{bmatrix} \frac{15z^2x}{d^7} - \frac{3x}{d^5} \\ \frac{15z^2y}{d^7} - \frac{3y}{d^5} \\ \frac{15z^3}{d^7} - \frac{9z}{d^5} \end{bmatrix} \quad (119)$$

where R_e is the radius of the Earth, J_2 is a constant coefficient found through observation of satellite orbits and is equal to 0.0010826 (unitless), and the coordinates of the satellite are x, y, and z measured in the inertial IJK frame $\left(|\vec{d}| = d = \sqrt{x^2 + y^2 + z^2}\right)$. Thus the equation of motion for a satellite in inertial space with only J_2 is

$$\ddot{\vec{d}} = \frac{-\mu\vec{d}}{d^3} + \frac{\mu J_2 R_e^2}{2} \begin{bmatrix} \frac{15z^2x}{d^7} - \frac{3x}{d^5} \\ \frac{15z^2y}{d^7} - \frac{3y}{d^5} \\ \frac{15z^3}{d^7} - \frac{9z}{d^5} \end{bmatrix} + \vec{v}_c \quad (120)$$

These modified equations of motion are not incorporated into the development of the controllers used in this thesis (Chapter III), however simulations were run with J_2 included into the inertial propagation of both leader and follower to show its effect. Two cases are presented here; both are LQR controllers at two different control weights ($R = 10^9$ and $R = 10^{13}$) for a simple ρ change reconfiguration ($\rho = 0.5 \rightarrow 1.5$). Both controllers were able to deal with J_2 to varying degrees of success. The $R = 10^9$ brought the error within 10 meters and the $R = 10^{13}$ to within 15 meters. The J_2 perturbation creates a drift in the argument of perigee (AP) and longitude of the ascending node (LAN) (5). The controllers were able to transform the AP drift to a periodic oscillation but did little to correct the LAN drift. As with making linear assumptions for the CW equations, accepting this drift term is an engineering tradeoff for reducing the complexity of the system. Given the relatively short period of time that reconfigurations occur over and the fact that only the difference in the J_2 effect between the leader and follower has to be incorporated into the controller, there is not an enormous need to include J_2 into the relative model. Not surprisingly, the J_2 effect prevents the controller from dampening the error to zero and creates a periodic error with an amplitude of approximately 1.2 meters for $R = 10^9$ and 25 meters for $R = 10^{13}$. The small abnormalities can best be seen by looking at the COE

time history in Figures 44 and 45 Note the scale for each graph and that the oscillations
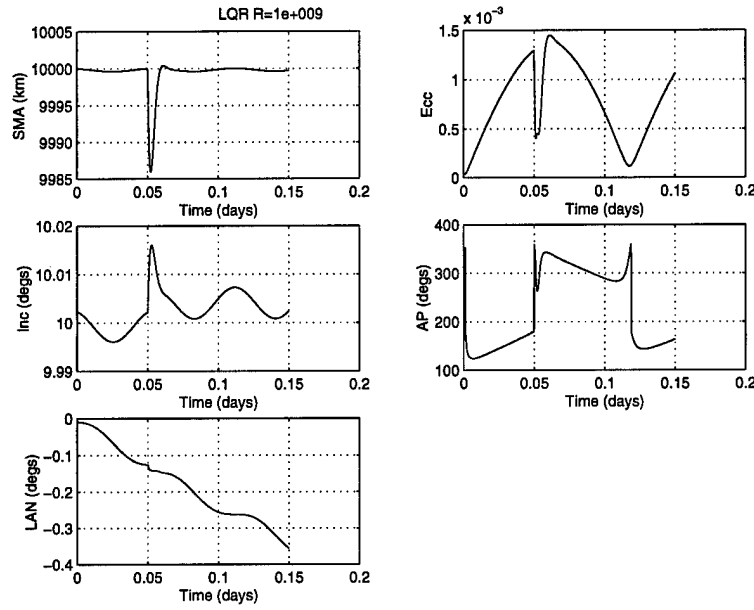
Figure 44   COE Time History with J_2 (LQR $R = 10^9$)

while present are not very large. Both controllers still do the job of controlling to the commanded relative parameters as seen in Figures 46 and 47
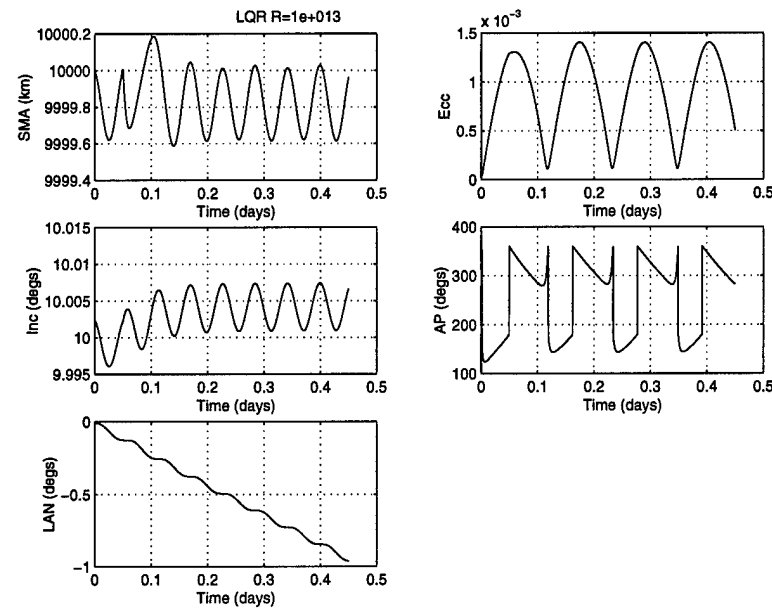
Figure 45   COE Time History with J_2 (LQR $R = 10^{13}$)
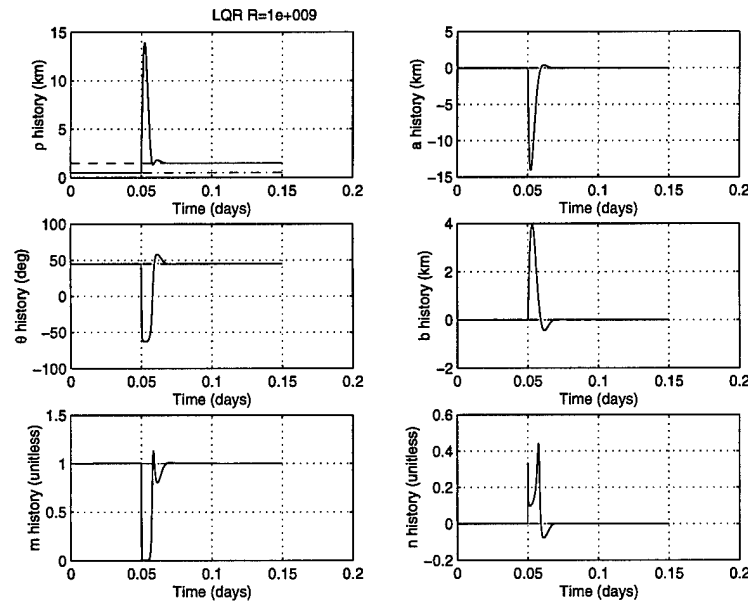
Figure 46   Relative Parameter Time History with J_2 (LQR $R = 10^9$)
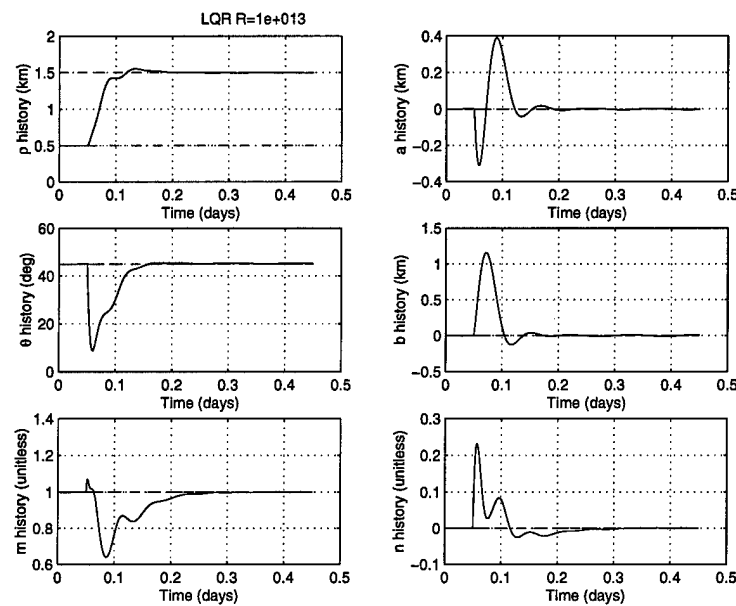
Figure 47   Relative Paramter Time History with J_2 (LQR $R = 10^{13}$)

V. Conclusions and Recommendations

Several conclusions can be made from the data produced by this thesis. The first is that continuous feedback control will burn considerably more fuel than the discrete burn method described in Section III. Although it must be stated again that the discrete method used in this thesis is not an optimal method, the comparison of it to the continuous feedback ΔVs seems to indicate that there are more optimal ways to reconfigure relative orbits. The feedback controllers do offer some advantages; namely the ability to control relative position error to a leader or another follower within the formation. The biggest problem with continuous feedback controllers is that the controller output is proportional to the error without regard for the best place in the orbit to do a burn. For example, to change the size of an orbit via the Hohmann method (an optimal method for same plane circular to circular orbits), thrusting occurs at apogee and perigee. A continuous feedback controller would continue to thrust throughout the transfer orbit until the desired size change was attained, burning much more fuel in the process. Truly optimal controllers will need to take into account not only the magnitude of the error to be corrected but also the best time within an orbit to make that correction. Further, if continuous methods are used for small relative orbits, nonlinear control techniques currently offer no clear advantage to standard linear controllers, and may in fact produce inferior results. This comes as no surprise given that with smaller relative orbits, the linear Hill's equations are a very good approximation of the nonlinear CW equations. The only time nonlinear controllers prove superior is when the relative orbit is large enough to create large errors between the linear and nonlinear EOMs. As ρ becomes larger (creating a larger relative orbit), LQR with LF becomes increasingly more efficient as compared to the linear LQR technique. Since the command signal is based on the linear EOMs, this simulation, as implemented, is ideally suited for small relative orbit reconfigurations. For those small orbit reconfigurations, LQR (a linear method) is as good as or better than the nonlinear methods tested here as well as significantly simpler to implement. Of course, this thesis did not exhaust the numerous nonlinear control techniques applicable to this problem. These controllers should be explored before nonlinear techniques are completely discarded. Also, in order to model more realistic conditions, measurement noise should be added and/or

70

an estimator used instead of assuming full state feedback. Finally, there is great research potential in exploring the nonlinear EOMs in order to develop command signals that are valid for larger relative orbits. Perhaps a Keplerian type formulation of the nonlinear EOMs based on an elliptical orbit. If nothing else, techniques need to be developed to choose appropriate initial conditions such that the secular drift term in the $\hat{C}$ direction is nulled out.

Appendix A. The Two Body Problem

To find the acceleration of a satellite relative to a much larger primary body due to the force of gravity, consider Figure 48 where $\vec{d_1}$ and $\vec{d_2}$ are position vectors in inertial space.
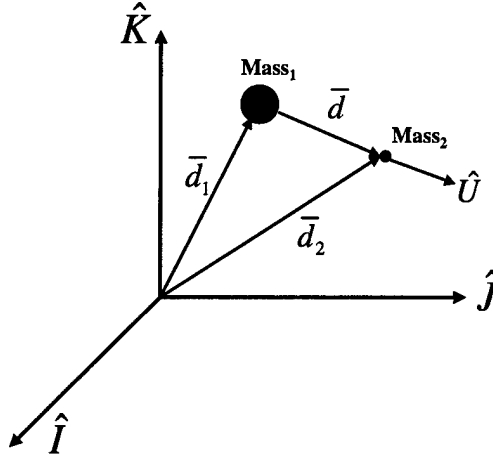
Figure 48   Two Body Problem

By Newton's second law (19)

$$\sum \vec{F} = mass * \vec{acc} \tag{121}$$

$$\vec{F_g} + \vec{f_c} + \vec{f_p} = mass * \vec{acc} \tag{122}$$

where $\vec{F_g}$ is the force due to gravity, $\vec{f_c}$ is a vector of control forces, and $\vec{f_p}$ is a vector of perturbative forces. Gravitational forces follow an inverse square law (19). Using Figure 48

$$|\vec{F_g}| \propto \frac{Mass_1 * Mass_2}{|\vec{d}|^2} \tag{123}$$

To make this an equality the universal constant of gravitation G is used $\left(G = 6.672 \times 10^{-11} \frac{N \cdot m^2}{kg^2} \right)$

$$|\vec{F_g}| = \frac{G * Mass_1 * Mass_2}{|\vec{d}|^2} \tag{124}$$

72

Subbing into Equation 122 for both masses

$$\left[\frac{G * Mass_1 * Mass_2}{|\vec{d}|^2}\right]\hat{U} + \vec{f}_{c1} + \vec{f}_{p1} = Mass_1 * \ddot{\vec{d}}_1$$

$$\left[\frac{G * Mass_1 * Mass_2}{|\vec{d}|^2}\right](-\hat{U}) + \vec{f}_{c2} + \vec{f}_{p2} = Mass_2 * \ddot{\vec{d}}_2 \qquad (125)$$

where $\hat{U}$ is a unit vector parallel to $\vec{d}$ and gives the scaler force of gravity a direction. Making the following substitution

$$\hat{U} = \frac{\vec{d}}{|\vec{d}|} \qquad (126)$$

yields

$$\left[\frac{G * Mass_1 * Mass_2}{|\vec{d}|^2}\right] * \frac{\vec{d}}{|\vec{d}|} + \vec{f}_{c1} + \vec{f}_{p1} = Mass_1 * \ddot{\vec{d}}_1$$

$$-\left[\frac{G * Mass_1 * Mass_2}{|\vec{d}|^2}\right] * \frac{\vec{d}}{|\vec{d}|} + \vec{f}_{c2} + \vec{f}_{p2} = Mass_2 * \ddot{\vec{d}}_2 \qquad (127)$$

Combining terms and dividing through by the masses to isolate the acceleration

$$\ddot{\vec{d}}_1 = \left[\frac{G * Mass_2}{|\vec{d}|^3}\right] * \vec{d} + \frac{\vec{f}_{c1}}{Mass_1} + \frac{\vec{f}_{p1}}{Mass_1}$$

$$\ddot{\vec{d}}_2 = \left[\frac{-G * Mass_1}{|\vec{d}|^3}\right] * \vec{d} + \frac{\vec{f}_{c2}}{Mass_2} + \frac{\vec{f}_{p2}}{Mass_1} \qquad (128)$$

Since $\vec{d} = \vec{d}_2 - \vec{d}_1$, taking the derivative twice yields

$$\ddot{\vec{d}} = \ddot{\vec{d}}_2 - \ddot{\vec{d}}_1 \qquad (129)$$

Subbing Equations 128 into the above equation

$$\ddot{\vec{d}} = \left[\frac{-G * Mass_1}{|\vec{d}|^3}\right] * \vec{d} + \frac{\vec{f}_{c2}}{Mass_2} + \frac{\vec{f}_{p2}}{Mass_2} - \left[\frac{G * Mass_2}{|\vec{d}|^3}\right] * \vec{d} - \frac{\vec{f}_{c1}}{Mass_1} - \frac{\vec{f}_{p1}}{Mass_1} \qquad (130)$$

Combining terms

$$\ddot{\vec{d}} = \frac{-G(Mass_1 + Mass_2)\vec{d}}{|\vec{d}|^3} - \frac{\vec{f}_{c1}}{Mass_1} - \frac{\vec{f}_{p1}}{Mass_1} + \frac{\vec{f}_{c2}}{Mass_2} + \frac{\vec{f}_{p2}}{Mass_2} \qquad (131)$$

If first body is the Earth and the second body a satellite orbiting the Earth then $Mass_1 = Mass_{Earth}$, $Mass_2 = Mass_{Sat}$, $f_{c1} = f_{EarthControl}$, $f_{c2} = f_{SatControl}$, $f_{p1} = f_{EarthPert}$, and $f_{p2} = f_{SatPert}$

$$
\begin{aligned}
\ddot{\vec{d}} \;=\; & \frac{-G(Mass_{Earth} + Mass_{Sat})\vec{d}}{|\vec{d}|^3} - \frac{\vec{f}_{EarthControl}}{Mass_{Earth}} - \frac{\vec{f}_{EarthPert}}{Mass_{Earth}} \\
& + \frac{\vec{f}_{SatControl}}{Mass_{Sat}} + \frac{\vec{f}_{SatPert}}{Mass_{Sat}}
\end{aligned}
\tag{132}
$$

Since $Mass_{Earth} \gg Mass_{Sat}$ we can say that $Mass_{Earth} + Mass_{Sat} \approx Mass_{Earth}$, further, if the Earth is being used as the inertial reference frame for the satellite then $\vec{f}_{EarthControl} = 0$ and $\vec{f}_{EarthPert} = 0$.

$$
\ddot{\vec{d}} = \frac{-G * Mass_{Earth} * \vec{d}}{|\vec{d}|^3} + \frac{\vec{f}_{SatControl}}{Mass_{Sat}} + \frac{\vec{f}_{SatPert}}{Mass_{Sat}}
\tag{133}
$$

If we define the constant μ

$$
\mu = G * Mass_{Earth} = 6.672 \times 10^{-11} \tfrac{N \cdot m^2}{kg^2} \times 5.974236 \times 10^{24} kg
$$
$$
\mu = 3.98601 \times 10^{14} \tfrac{m^3}{s^2} = 398601 \tfrac{km^3}{s^2}
\tag{134}
$$

and define the specific forces

$$
\vec{v}_c = \frac{\vec{f}_{SatControl}}{Mass_{Sat}}
\tag{135}
$$

$$
\vec{v}_p = \frac{\vec{f}_{SatPert}}{Mass_{Sat}}
\tag{136}
$$

Then the equation of motion for a satellite about the Earth with control input of $\vec{v}_c$ and a perturbative acceleration of $\vec{v}_p$ is

$$
\ddot{\vec{d}} = \frac{-\mu \vec{d}}{|\vec{d}|^3} + \vec{v}_c + \vec{v}_p
\tag{137}
$$

Appendix B. The J_2 Perturbation

Because gravity is a conservative force, it can be derived from the gradient of a scalar potential function (20). Looking at Equation 137 without any control inputs

$$\ddot{\vec{d}} = \frac{-\mu \vec{d}}{|\vec{d}|^3} + \vec{v}_p \tag{138}$$

Expanding in the inertial reference frame shown in Figure 48 and noting that $|\vec{d}| = d = \sqrt{x^2 + y^2 + z^2}$ where x, y, and z are the position of the satellite in the inertial frame IJK

$$
\begin{aligned}
\ddot{\vec{d}} =\ & \left[\frac{-\mu x}{[x^2 + y^2 + z^2]^{\frac{3}{2}}} + \vec{v}_{pI} \right] \hat{I} + \left[\frac{-\mu y}{[x^2 + y^2 + z^2]^{\frac{3}{2}}} + \vec{v}_{pJ} \right] \hat{J} \\
& + \left[\frac{-\mu z}{[x^2 + y^2 + z^2]^{\frac{3}{2}}} + \vec{v}_{pK} \right] \hat{K}
\end{aligned}
\tag{139}
$$

Noting that

$$
\begin{aligned}
\frac{\partial}{\partial x} \left(\frac{\mu}{|\vec{d}|} + B \right) &= \left[\frac{\sqrt{x^2 + y^2 + z^2} * (0) - \mu[1/2(\sqrt{x^2 + y^2 + z^2})^{-1/2}]2x}{x^2 + y^2 + z^2} \right] + \vec{v}_{pJ} \\
&= \frac{-\mu x}{[x^2 + y^2 + z^2]^{\frac{3}{2}}} + \vec{v}_{pI}
\end{aligned}
\tag{140}
$$

where B is a potential function such that

$$\nabla B = \vec{v}_p \tag{141}$$

Similarly

$$\frac{\partial}{\partial y} \left(\frac{\mu}{d} + B \right) = \frac{-\mu y}{[x^2 + y^2 + z^2]^{\frac{3}{2}}} + \vec{v}_{pJ} \tag{142}$$

$$\frac{\partial}{\partial z} \left(\frac{\mu}{d} + B \right) = \frac{-\mu z}{[x^2 + y^2 + z^2]^{\frac{3}{2}}} + \vec{v}_{pK} \tag{143}$$

Therefore the inertial acceleration is the gradient of the potential function $\frac{\mu}{d} + B$

$$\ddot{\vec{d}} = \nabla \left(\frac{\mu}{d} + B \right) \tag{144}$$

75

The B term comes about by modeling the Earth not as a point mass but as an oblate body with nonhomogeneous mass distribution (Figure 49) and is the sum on the infinite series
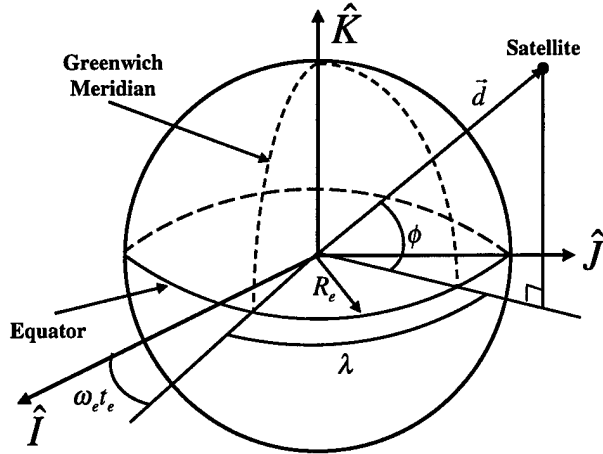

Figure 49   Oblate Earth Coordinate Frame

$$B = \frac{-\mu}{d} \left\{ \sum_{n=2}^{\infty} \left[\left(\frac{R_e}{d} \right)^n J_n P_n(\sin\phi) + \sum_{m=1}^{n} \left(\frac{R_e}{d} \right)^n (C_{nm}\cos\varphi + S_{nm}\sin\varphi) P_{nm}(\sin\phi) \right] \right\}$$

(145)

$$\varphi = m\lambda + \omega_e t_e$$

(146)

where R_e is the mean equatorial radius of the Earth, ϕ is the geocentric latitude of the satellite (measured from the equator), λ is the geographical longitude (measured from the prime meridian), d is the satellite position vector magnitude, ω_e is the rotation rate of the Earth, t_e is the time since the $\hat{I}$ direction lined up with the Greenwich meridian, J_n is the zonal harmonic coefficients of order 0, P_n is a Legendre polynomial of degree n and order 0, P_{nm} is a Legendre polynomial of degree n and order m, C_{nm} is the tesseral harmonic coefficient for $n \neq m$, and S_{nm} is the sectorical harmonic coefficents for $n = m$.

Measurements of the zonal, tesseral and sectorial coefficients (J_n, C_{nm}, and S_{nm}) reveal that the J_2 term is at least 400 times larger than the next most significant term. Thus for applications such as satellite reconfigurations which occur over relatively short time periods all higher terms can be ignored. Using this assumption, Equation 145 reduces

to

$$B = \frac{-\mu}{d} \sum_{n=2}^{2} \left[\left(\frac{R_e}{d} \right)^n J_n P_n(\sin\phi) \right] = \frac{-\mu}{d} \left(\frac{R_e}{d} \right)^2 J_2 P_2(\sin\phi) \qquad (147)$$

where $J_2 = 0.0010826$ and the 2nd Legendre polynomial has the form (12)

$$P_2(X) = \frac{1}{2}(3X^2 - 1) \qquad (148)$$

Using this Legendre polynomial in Equation 147

$$B = \frac{-\mu}{d} \left(\frac{R_e}{d} \right)^2 J_2 \frac{1}{2} \left[3(\sin\phi)^2 - 1 \right] \qquad (149)$$

rearranging terms in B

$$B = \frac{J_2 R_e^2}{2} \left(\frac{-\mu}{d^3} \left[3(\sin\phi)^2 - 1 \right] \right) \qquad (150)$$

By geometry in Figure 49

$$\sin\phi = \frac{z}{d} \qquad (151)$$

which means

$$B = \frac{J_2 R_e^2}{2} \left(\frac{-\mu}{d^3} \left[3\frac{z^2}{d^2} - 1 \right] \right) = \frac{\mu J_2 R_e^2}{2} \left(\frac{-3z^2 + d^2}{d^5} \right) \qquad (152)$$

Now that B is in cartesian coordinates, $\vec{v}_p$ is found by taking the gradient of B

$$\vec{v}_p = \nabla B = \begin{bmatrix} \frac{\partial}{\partial x} B \\ \frac{\partial}{\partial y} B \\ \frac{\partial}{\partial z} B \end{bmatrix} = \frac{\mu J_2 R_e^2}{2} \begin{bmatrix} \frac{d^5(2d\frac{x}{d}) - (-3z^2 + d^2)5d^4\frac{x}{d}}{d^{10}} \\ \frac{d^5(2d\frac{y}{d}) - (-3z^2 + d^2)5d^4\frac{y}{d}}{d^{10}} \\ \frac{d^5(-6z + 2d\frac{z}{d}) - (-3z^2 + d^2)5d^4\frac{z}{d}}{d^{10}} \end{bmatrix} \qquad (153)$$

Simplifying

$$\vec{v}_p = \frac{\mu J_2 R_e^2}{2} \begin{bmatrix} \frac{15z^2 x}{d^7} - \frac{3x}{d^5} \\ \frac{15z^2 y}{d^7} - \frac{3y}{d^5} \\ \frac{15z^3}{d^7} - \frac{9z}{d^5} \end{bmatrix} \qquad (154)$$

77

Appendix C.   Clohessy-Wiltshire Derivation

Assume the relationship between the leader and follower satellite shown in Figure 50 and that the leader satellite is in a circular orbit about the Earth (Section 1.1). In the *RCO*
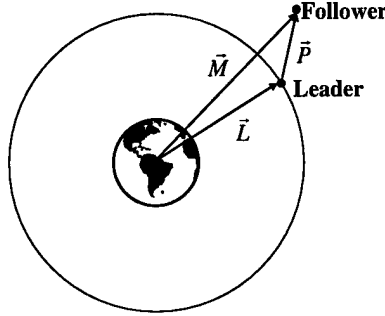

Figure 50   Clohessy-Wiltshire Setup

frame (Figure 1) the position vectors are:

$$\vec{L} = k_o\hat{R} + 0\hat{C} + 0\hat{O} \tag{155}$$

$$\vec{P} = r\hat{R} + c\hat{C} + o\hat{O} \tag{156}$$

$$\vec{M} = \vec{L} + \vec{P} = (k_o + r)\hat{R} + c\hat{C} + o\hat{O} \tag{157}$$

where k_o is the orbit radius of the leader satellite. To take the inertial derivative of a vector:

$$\dot{\vec{X}} = {}^{RCO}\frac{d(\vec{X})}{dt} + N^{RCO-wrt-Inertial} \times \vec{X} \tag{158}$$

where N is the angular velocity of the *RCO* frame with respect to the inertial frame, in this case $N^{RCO-wrt-Inertial} = 0\hat{R} + 0\hat{C} + \omega\hat{O}$ where ω is the angular frequency of the leader satellite's orbit and is found via Equation 3. Taking the inertial derivative of Equation 157 yields the velocity:

$$\dot{\vec{M}} = {}^{RCO}\dot{\vec{M}} + (\omega\hat{O}) \times \vec{M} \tag{159}$$

where ${}^{RCO}\dot{\vec{M}}$ is the derivative of $\vec{M}$ in the *RCO* frame.

$$^{RCO}\dot{\vec{M}} = \dot{r}\hat{R} + \dot{c}\hat{C} + \dot{o}\hat{O} \tag{160}$$

78

$$(\omega\hat{O}) \times \vec{M} = \begin{vmatrix} \hat{R} & \hat{C} & \hat{O} \\ 0 & 0 & \omega \\ k_o + r & c & o \end{vmatrix} = \begin{bmatrix} -\omega c\hat{R} \\ \omega(k_o + r)\hat{C} \\ 0\hat{O} \end{bmatrix} \tag{161}$$

Adding these together yields:

$$\dot{\vec{M}} = (\dot{r} - \omega c)\hat{R} + [\dot{c} + \omega(k_o + r)]\hat{C} + \dot{o}\hat{O} \tag{162}$$

Taking the inertial derivative of Equation 162 yields the acceleration:

$$\ddot{\vec{M}} = {}^{RCO}\ddot{\vec{M}} + (\omega\hat{O}) \times \dot{\vec{M}} \tag{163}$$

where ${}^{RCO}\ddot{\vec{M}}$ is the derivative of $\dot{\vec{M}}$ in the RCO frame.

$$^{RCO}\ddot{\vec{M}} = (\ddot{r} - \omega\dot{c})\hat{R} + (\ddot{c} + \omega\dot{r})\hat{C} + \ddot{o}\hat{O} \tag{164}$$

$$(\omega\hat{O}) \times \dot{\vec{M}} = \begin{vmatrix} \hat{R} & \hat{C} & \hat{O} \\ 0 & 0 & \omega \\ \dot{r} - \omega c & \dot{c} + \omega(k_o + r) & \dot{o} \end{vmatrix} = \begin{bmatrix} [-\omega\dot{c} - \omega^2(k_o + r)]\hat{R} \\ (\omega\dot{r} - \omega^2 c)\hat{C} \\ 0\hat{O} \end{bmatrix} \tag{165}$$

Adding these together yields:

$$\ddot{\vec{M}} = [\ddot{r} - 2\omega\dot{c} - \omega^2(k_o + r)]\hat{R} + (\ddot{c} + 2\omega\dot{r} - \omega^2 c)\hat{C} + \ddot{o}\hat{O} \tag{166}$$

From Appendix A we know that acceleration due to gravity and control (no perturbations) is:

$$\ddot{\vec{M}} = \frac{-\mu\vec{M}}{|\vec{M}|^3} + \vec{v_c} \tag{167}$$

where μ is the gravitational constant and $\vec{v_c}$ is the control acceleration. By Kepler's third law (29)

$$\omega = \sqrt{\frac{\mu}{k_o^3}} \iff \mu = \omega^2 k_o^3 \tag{168}$$

Expanding the magnitude of the position vector

$$|\vec{M}|^3 = \left[\sqrt{(k_o + r)^2 + c^2 + o^2}\right]^3 = \left[(k_o + r)^2 + c^2 + o^2\right]^{\frac{3}{2}} \qquad (169)$$

and using these equalities in Equation 167, we find that

$$\ddot{\vec{M}} = \frac{-\omega^2 k_o^3[(k_o + r)\hat{R} + c\hat{C} + o\hat{O}]}{[(k_o + r)^2 + c^2 + o^2]^{\frac{3}{2}}} + \vec{v_c} \qquad (170)$$

Equating 166 and 170

$$\begin{bmatrix} [\ddot{r} - 2\omega\dot{c} - \omega^2(k_o + r)]\hat{R} \\ (\ddot{c} + 2\omega\dot{r} - \omega^2 c)\hat{C} \\ \ddot{o}\hat{O} \end{bmatrix} = \frac{-\omega^2 k_o^3}{[(k_o + r)^2 + c^2 + o^2]^{\frac{3}{2}}} \begin{bmatrix} (k_o + r)\hat{R} \\ c\hat{C} \\ o\hat{O} \end{bmatrix} + \begin{bmatrix} v_{c_r}\hat{R} \\ v_{c_c}\hat{C} \\ v_{c_o}\hat{O} \end{bmatrix} \qquad (171)$$

Equating scalar terms and simplifying yields the CW equations:

$$\ddot{r} - 2\omega\dot{c} - \omega^2(k_o + r)\left[1 - \frac{k_o^3}{[(k_o + r)^2 + c^2 + o^2]^{\frac{3}{2}}}\right] - v_{c_r} = 0$$

$$\ddot{c} + 2\omega\dot{r} - \omega^2 c\left[1 - \frac{k_o^3}{[(k_o + r)^2 + c^2 + o^2]^{\frac{3}{2}}}\right] - v_{c_c} = 0 \qquad (172)$$

$$\ddot{o} + \omega^2 o\left[\frac{k_o^3}{[(k_o + r)^2 + c^2 + o^2]^{\frac{3}{2}}}\right] - v_{c_o} = 0$$

.

Appendix D. Linear Clohessy-Wiltshire Derivation (Hill's Equations)

Starting with the CW Equations from Appendix C

$$\ddot{r} - 2\omega\dot{c} - \omega^2(k_o + r)\left[1 - \frac{k_o^3}{[(k_o+r)^2+c^2+o^2]^{\frac{3}{2}}}\right] - v_{c_r} = 0$$

$$\ddot{c} + 2\omega\dot{r} - \omega^2 c\left[1 - \frac{k_o^3}{[(k_o+r)^2+c^2+o^2]^{\frac{3}{2}}}\right] - v_{c_c} = 0 \qquad (173)$$

$$\ddot{o} + \omega^2 o\left[\frac{k_o^3}{[(k_o+r)^2+c^2+o^2]^{\frac{3}{2}}}\right] - v_{c_o} = 0$$

The nonlinear part of these equations is

$$NL = [(k_o + r)^2 + c^2 + o^2]^{\frac{3}{2}} = [k_o^2 + 2k_o r + r^2 + c^2 + o^2]^{\frac{3}{2}} \qquad (174)$$

Factoring out an k_o^2

$$NL = \left[k_o^2\left(1 + \frac{2r}{k_o} + \frac{r^2}{k_o^2} + \frac{c^2}{k_o^2} + \frac{o^2}{k_o^2}\right)\right]^{\frac{3}{2}} = k_o^3\left(1 + \frac{2r}{k_o} + \frac{r^2}{k_o^2} + \frac{c^2}{k_o^2} + \frac{o^2}{k_o^2}\right)^{\frac{3}{2}} \qquad (175)$$

Using binomial expansion (13), this becomes

$$NL = k_o^3\left[1 + \frac{3}{2}\left(\frac{2r}{k_o} + \frac{r^2}{k_o^2} + \frac{c^2}{k_o^2} + \frac{o^2}{k_o^2}\right) + \text{H.O.T}\right] \qquad (176)$$

Neglecting higher order terms (H.O.T) and assuming that r, c, and o are appropriately small compared to the radius of the leader orbit (Chapter 1.1) such that

$$\frac{r^2}{k_o^2} \approx \frac{c^2}{k_o^2} \approx \frac{o^2}{k_o^2} \approx 0 \qquad (177)$$

With this assumption, the nonlinear term becomes

$$NL = k_o^3\left(1 + \frac{3r}{k_o}\right) = k_o^3\left(\frac{k_o + 3r}{k_o}\right) \qquad (178)$$

Subbing into Equations 173

$$\ddot{r} - 2\omega\dot{c} - \omega^2(k_o + r)\left[1 - \frac{k_o}{k_o+3r}\right] - v_{c_r} = 0$$

81

$$\ddot{c} + 2\omega\dot{r} - \omega^2 c \left[1 - \frac{k_o}{k_o+3r} \right] - v_{c_c} = 0 \tag{179}$$

$$\ddot{o} + \omega^2 o \left[\frac{k_o}{k_o+3r} \right] - v_{c_o} = 0$$

With some algebra

$$\ddot{r} - 2\omega\dot{c} - \omega^2 (k_o + r) \left[\frac{3r}{k_o+3r} \right] - v_{c_r} = 0$$

$$\ddot{c} + 2\omega\dot{r} - \omega^2 c \left[\frac{3r}{k_o+3r} \right] - v_{c_c} = 0 \tag{180}$$

$$\ddot{o} + \omega^2 o \left[\frac{k_o}{k_o+3r} \right] - v_{c_o} = 0$$

Assuming that r is appropriately small such that

$$k_o + r \approx k_o \tag{181}$$

$$k_o + 3r \approx k_o \tag{182}$$

yeilds

$$\ddot{r} - 2\omega\dot{c} - \omega^2 k_o \left[\frac{3r}{k_o} \right] - v_{c_r} = 0$$

$$\ddot{c} + 2\omega\dot{r} - \omega^2 \left[\frac{3cr}{k_o} \right] - v_{c_c} = 0 \tag{183}$$

$$\ddot{o} + \omega^2 o - v_{c_o} = 0$$

Assuming that r and c are appropriately small such that

$$\frac{cr}{k_o} \approx 0 \tag{184}$$

Yeilds the linearized version of the CW equations

$$\ddot{r} - 2\omega\dot{c} - 3\omega^2 r - v_{c_r} = 0$$

$$\ddot{c} + 2\omega\dot{r} - v_{c_c} = 0 \tag{185}$$

$$\ddot{o} + \omega^2 o - v_{c_o} = 0$$

82

Appendix E. Parametrization of Hill's Equations

Starting with the homogeneous Hill's equations from Appendix D

$$\ddot{r} - 2\omega\dot{c} - 3\omega^2 r = 0$$

$$\ddot{c} + 2\omega\dot{r} = 0 \tag{186}$$

$$\ddot{o} + \omega^2 o = 0$$

Taking the Laplace transform

$$[s^2 R(s) - s r_o - \dot{r_o}] - 2\omega[s C(s) - c_o] - 3\omega^2 R(s) = 0$$

$$[s^2 C(s) - s c_o - \dot{c_o}] + 2\omega[s R(s) - r_o] = 0 \tag{187}$$

$$[s^2 O(s) - s o_o - \dot{o_o}] + \omega^2 O(s) = 0$$

where r_o and $\dot{r_o}$ are the position and velocity initial conditions (ICs) in the radial direction, c_o and $\dot{c_o}$ are the position and velocity ICs in the cross track direction, and o_o and $\dot{o_o}$ are the position and velocity ICs in the out of plane direction. Collecting terms and placing the equations in matrix form

$$
\begin{bmatrix}
s^2 - 3\omega^2 & -2\omega s & 0 \\
2\omega s & s^2 & 0 \\
0 & 0 & s^2 + \omega^2
\end{bmatrix}
\begin{bmatrix}
R(s) \\
C(s) \\
O(s)
\end{bmatrix}
=
\begin{bmatrix}
s r_o + \dot{r_o} - 2\omega c_o \\
s c_o + \dot{c_o} + 2\omega r_o \\
s o_o + \dot{o_o}
\end{bmatrix}
\tag{188}
$$

Finding the inverse and solving for $R(s)$, $C(s)$, $O(s)$

$$
\begin{bmatrix}
R(s) \\
C(s) \\
O(s)
\end{bmatrix}
=
\begin{bmatrix}
\frac{1}{s^2+\omega^2} & \frac{2\omega}{s(s^2+\omega^2)} & 0 \\
\frac{-2\omega}{s(s^2+\omega^2)} & \frac{s^2-3\omega^2}{s^2(s^2+\omega^2)} & 0 \\
0 & 0 & \frac{1}{s^2+\omega^2}
\end{bmatrix}
\begin{bmatrix}
s r_o + \dot{r_o} - 2\omega c_o \\
s c_o + \dot{c_o} + 2\omega r_o \\
s o_o + \dot{o_o}
\end{bmatrix}
\tag{189}
$$

Multiplying this out

$$
\begin{bmatrix} R(s) \\ C(s) \\ O(s) \end{bmatrix} = \begin{bmatrix} \frac{sr_o + \dot{r}_o - 2\omega c_o}{s^2 + \omega^2} + \frac{2\omega(sc_o + \dot{c}_o + 2\omega r_o)}{s(s^2 + \omega^2)} \\ \frac{-2\omega(sr_o + \dot{r}_o - 2\omega c_o)}{s(s^2 + \omega^2)} + \frac{(s^2 - 3\omega^2)(sc_o + \dot{c}_o + 2\omega r_o)}{s^2(s^2 + \omega^2)} \\ \frac{so_o + \dot{o}_o}{s^2 + \omega^2} \end{bmatrix} \tag{190}
$$

Performing partial fraction expansion

$$
\begin{bmatrix} R(s) \\ C(s) \\ O(s) \end{bmatrix} = \begin{bmatrix} \frac{sr_o + \dot{r}_o - 2\omega c_o}{s^2 + \omega^2} + \frac{2\omega^2 c_o - 2s\dot{c}_o - 4s\omega r_o}{\omega(s^2 + \omega^2)} + \frac{2\dot{c}_o + 4\omega r_o}{\omega}\frac{1}{s} \\ \frac{4sc_o + 4\dot{c}_o + 8\omega r_o}{s^2 + \omega^2} + \frac{-2\omega^2 r_o + 2s\dot{r}_o - 4sc_o\omega}{\omega(s^2 + \omega^2)} + \frac{-3\dot{c}_o - 6\omega r_o}{s^2} + \frac{\omega c_o - 2\dot{r}_o}{\omega}\frac{1}{s} \\ \frac{so_o + \dot{o}_o}{s^2 + \omega^2} \end{bmatrix} \tag{191}
$$

Collecting terms

$$
\begin{bmatrix} R(s) \\ C(s) \\ O(s) \end{bmatrix} = \begin{bmatrix} \frac{\left(r_o - \frac{2\dot{c}_o + 4\omega r_o}{\omega}\right)s}{s^2 + \omega^2} + \frac{\left(\frac{\dot{r}_o}{\omega}\right)\omega}{s^2 + \omega^2} + \frac{2\dot{c}_o + 4\omega r_o}{\omega}\frac{1}{s} \\ \frac{2\left(\frac{\dot{r}_o}{\omega}\right)s}{s^2 + \omega^2} + \frac{2\left(\frac{2\dot{c}_o + 4\omega r_o}{\omega} - r_o\right)\omega}{s^2 + \omega^2} - \frac{3\omega}{2}\frac{2\dot{c}_o + 4\omega r_o}{\omega}\frac{1}{s^2} + \frac{\omega c_o - 2\dot{r}_o}{\omega}\frac{1}{s} \\ \frac{so_o}{s^2 + \omega^2} + \frac{\left(\frac{\dot{o}_o}{\omega}\right)\omega}{s^2 + \omega^2} \end{bmatrix} \tag{192}
$$

Taking the inverse Laplace transform

$$
\begin{bmatrix} r(t) \\ c(t) \\ o(t) \end{bmatrix} = \begin{bmatrix} \left[r_o - \frac{2\dot{c}_o + 4\omega r_o}{\omega}\right]\cos(\omega t + \theta) + \frac{\dot{r}_o}{\omega}\sin(\omega t + \theta) + \frac{2\dot{c}_o + 4\omega r_o}{\omega} \\ 2\left(\frac{\dot{r}_o}{\omega}\right)\cos(\omega t + \theta) + 2\left[\frac{2\dot{c}_o + 4\omega r_o}{\omega} - r_o\right]\sin(\omega t + \theta) - \frac{3\omega t}{2}\left(\frac{2\dot{c}_o + 4\omega r_o}{\omega}\right) + \frac{\omega c_o - 2\dot{r}_o}{\omega} \\ o_o\cos(\omega t + \theta) + \frac{\dot{o}_o}{\omega}\sin(\omega t + \theta) \end{bmatrix} \tag{193}
$$

where θ is an initial angle at $t = 0$. Since the ICs and ω do not vary with time, two constants can be defined

$$
a = \frac{2\dot{c}_o + 4\omega r_o}{\omega} \tag{194}
$$

$$
b = \frac{\omega c_o - 2\dot{r}_o}{\omega} \tag{195}
$$

which simplifies Equation 193 to

$$
r(t) = (r_o - a)\cos(\omega t + \theta) + \frac{\dot{r}_o}{\omega}\sin(\omega t + \theta) + a \tag{196}
$$

84

$$c(t) = \frac{2\dot{r_o}}{\omega} \cos(\omega t + \theta) + 2(a - r_o) \sin(\omega t + \theta) - \frac{3\omega a t}{2} + b \tag{197}$$

$$o(t) = o_o \cos(\omega t + \theta) + \frac{\dot{o_o}}{\omega} \sin(\omega t + \theta) \tag{198}$$

For simplicity, $r = r(t)$, $c = c(t)$, $o = o(t)$. Isolating the sinusodal terms in the first two equations.

$$r - a = (r_o - a) \cos(\omega t + \theta) + \frac{\dot{r_o}}{\omega} \sin(\omega t + \theta) \tag{199}$$

$$\frac{c + \frac{3\omega a t}{2} - b}{2} = \frac{\dot{r_o}}{\omega} \cos(\omega t + \theta) + (a - r_o) \sin(\omega t + \theta) \tag{200}$$

Squaring both sides

$$[r - a]^2 = (r_o - a)^2 \cos^2(\omega t + \theta) + \left(\frac{\dot{r_o}}{\omega}\right)^2 \sin^2(\omega t + \theta)$$
$$+ 2(r_o - a)\frac{\dot{r_o}}{\omega} \cos(\omega t + \theta) \sin(\omega t + \theta) \tag{201}$$

$$\frac{[c + \frac{3\omega a t}{2} - b]^2}{4} = \left(\frac{\dot{r_o}}{\omega}\right)^2 \cos^2(\omega t + \theta) + (-1)^2 (r_o - a)^2 \sin^2(\omega t + \theta)$$
$$+ 2(-1)(r_o - a)\frac{\dot{r_o}}{\omega} \cos(\omega t + \theta) \sin(\omega t + \theta) \tag{202}$$

Adding these equations together

$$[r - a]^2 + \frac{[c + \frac{3\omega a t}{2} - b]^2}{4} = \left[(r_o - a)^2 + \left(\frac{\dot{r_o}}{\omega}\right)^2\right] \cos^2(\omega t + \theta) +$$
$$\left[\left(\frac{\dot{r_o}}{\omega}\right)^2 + (r_o - a)^2\right] \sin^2(\omega t + \theta) \tag{203}$$

Pulling out the common coefficient and using the identity $\cos^2(\tau) + \sin^2(\tau) = 1$

$$[r - a]^2 + \frac{[c + \frac{3\omega a t}{2} - b]^2}{4} = (r_o - a)^2 + \left(\frac{\dot{r_o}}{\omega}\right)^2 \tag{204}$$

The right side of this equation has no time varying terms, thus define the constant ρ

$$\rho^2 = (r_o - a)^2 + \left(\frac{\dot{r_o}}{\omega}\right)^2 \tag{205}$$

85

Subsisting and dividing by ρ^2 yields

$$\frac{[r-a]^2}{\rho^2} + \frac{[c + \frac{3\omega at}{2} - b]^2}{4\rho^2} = 1 \qquad (206)$$

This is the standard equation for an ellipse, thus the follower satellite will follow an elliptical path about the leader satellite in the R/C plane (Figure 51). Note that for a stable orbit
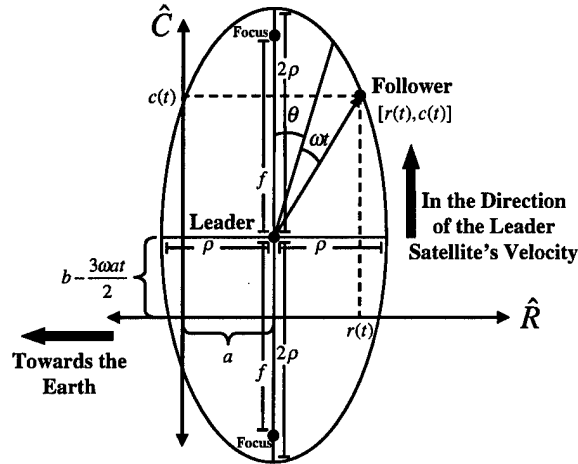
Figure 51   General Follower Orbit in the R/C Plane

(i.e. one that does not drift over time) about the leader satellite, a must equal zero. Ellipses can be parameterized in the general form

$$x - h = A\sin(\alpha)$$

$$y - k = B\cos(\alpha)$$

where A is the semi major or minor axes in the x direction, B is the semi major or minor axes in the y direction, and the center of the ellipse is located at (h,k). Placing Equation 206 in this form

$$r(t) - a = \rho\sin(\omega t + \theta) \qquad (207)$$

$$c(t) + \frac{3\omega at}{2} - b = 2\rho\cos(\omega t + \theta) \qquad (208)$$

86

and solving for $r(t)$ and $c(t)$

$$r(t) = \rho \sin(\omega t + \theta) + a \tag{209}$$

$$c(t) = 2\rho \cos(\omega t + \theta) - \frac{3\omega a t}{2} + b \tag{210}$$

If we visualize the elliptical orbit from Figure 51 rotating about the major or minor axes, it is easy to see it will trace a line in R/O plane (if rotated about the major axis) and the R/C plane (if rotated about the minor axis). Using the equation of a line and adding the effects of a rotation about both major and minor axes

$$o(t) = m[r(t) - a] + n\left[c(t) + \frac{3\omega a t}{2} - b\right] \tag{211}$$

where m and n are the slopes of the lines formed by the rotation about the minor and major axes respectively. Subbing Equations 207 and 208 into the above equation yields:

$$o(t) = m\rho \sin(\omega t + \theta) + 2n\rho \cos(\omega t + \theta) \tag{212}$$

This is the correct form expected from the inverse Laplace transform found in Equation 198 , an oscillatory function with a constant amplitude and a period of ωt.

Of the six constants required to define a relative orbit about a leader satellite, only three have been defined so far (a, b, and ρ). The other three need to be developed in terms of initial conditions. Using Equation 207 and the derivative of Equation 209 (at $t = 0$)

$$r_o - a = \rho \sin(\theta) \tag{213}$$

$$\dot{r}_o = \rho\omega \cos(\theta) \Leftrightarrow \frac{\dot{r}_o}{\omega} = \rho \cos(\theta) \tag{214}$$

and inserting them into Equation 212 and it's derivative (again at $t = 0$)

$$o_o = m\rho \sin(\theta) + 2n\rho \cos(\theta) \tag{215}$$

$$\dot{o}_o = m\rho\omega \cos(\theta) - 2n\rho\omega \sin(\theta) \tag{216}$$

yields

$$o_o = m(r_o - a) + n\left(2\frac{r_o}{\omega}\right) \tag{217}$$

$$\dot{o}_o = m\dot{r}_o - n[2\omega(r_o - a)] \tag{218}$$

In matrix form

$$\begin{bmatrix} o_o \\ \dot{o}_o \end{bmatrix} = \begin{bmatrix} r_o - a & \frac{2\dot{r}_o}{\omega} \\ \dot{r}_o & -2\omega(r_o - a) \end{bmatrix} \begin{bmatrix} m \\ n \end{bmatrix} \tag{219}$$

Solving for m and n by multiplying both sides by the matrix inverse

$$\begin{bmatrix} m \\ n \end{bmatrix} = \begin{bmatrix} \frac{-\omega^2(a-r_o)}{\omega^2 r_o^2 - 2r_o\omega^2 a + \omega^2 a^2 + \dot{r}_o^2} & \frac{\dot{r}_o}{\omega^2 r_o^2 - 2r\omega^2 a + \omega^2 a^2 + \dot{r}_o^2} \\ \frac{\frac{1}{2}\dot{r}_o\omega}{\omega^2 r_o^2 - 2r_o\omega^2 a + \omega^2 a^2 + \dot{r}_o^2} & \frac{\frac{1}{2}(a-r_o)\omega}{\omega^2 r_o^2 - 2r_o\omega^2 a + \omega^2 a^2 + \dot{r}_o^2} \end{bmatrix} \begin{bmatrix} o_o \\ \dot{o}_o \end{bmatrix} \tag{220}$$

Multiplying through and simplifying

$$m = \frac{\dot{o}_o\dot{r}_o - o_o\omega^2(a - r_o)}{\dot{r}_o^2 + \omega^2(a - r_o)^2} \tag{221}$$

$$n = \frac{o_o\dot{r}_o\omega + \dot{o}_o\omega(a - r_o)}{2[\dot{r}_o^2 + \omega^2(a - r_o)^2]} \tag{222}$$

Finally, to find θ divide Equation 213 by Equation 214

$$\frac{r_o - a}{\frac{\dot{r}_o}{\omega}} = \tan(\theta) \tag{223}$$

and solving for θ

$$\theta = \arctan\left[\frac{\omega(r_o - a)}{\dot{r}_o}\right] \tag{224}$$

All parameters can be solved given the relative position and velocity except for θ, so to find θ at any given time, divide Equation 207 by its derivative $\dot{r} = \rho\omega\cos(\omega t + \theta)$

$$\frac{r - a}{\frac{\dot{r}}{\omega}} = \tan(\omega t + \theta) \tag{225}$$

88

using the tan addition identity to expand the right side of the equation (26)

$$\frac{r-a}{\frac{\dot{r}}{\omega}} = \frac{\tan(\omega t) + \tan(\theta)}{1 - \tan(\omega t)\tan(\theta)} \tag{226}$$

With some algebra

$$\omega(r-a) - \dot{r}\tan(\omega t) = \tan(\theta)[\omega(r-a)\tan(\omega t) + \dot{r}] \tag{227}$$

and solving for θ

$$\theta = \arctan\left[\frac{\omega(r-a) - \dot{r}\tan(\omega t)}{\omega(r-a)\tan(\omega t) + \dot{r}}\right] \tag{228}$$

which at $t = 0$ reduces to Equation 224.

E.1 Unit Analysis

Since the initial and final relative orbits are defined in terms of the relative parameters derived above, it is important to understand the proper units for each one. The variables r, c, and o are positions and are defined in terms of *length*. Likewise, $\dot{r}$, $\dot{c}$, and $\dot{o}$ are velocities and are expressed as $\frac{length}{time}$. Finally, ω is the angular frequency of the orbit and is expressed in $\frac{1}{time}$,

$$a = \frac{\frac{length}{time} + \frac{1}{time}length}{\frac{1}{time}} = \frac{\frac{length}{time}}{\frac{1}{time}} = length \tag{229}$$

$$b = \frac{\frac{1}{time}length - \frac{length}{time}}{\frac{1}{time}} = \frac{\frac{length}{time}}{\frac{1}{time}} = length \tag{230}$$

$$\rho = \sqrt{(length - length)^2 + \left(\frac{\frac{length}{time}}{\frac{1}{time}}\right)^2} = \sqrt{length^2 + length^2} = length \tag{231}$$

$$m = \frac{\frac{length}{time}\frac{length}{time} - length\left(\frac{1}{time}\right)^2(length - length)}{\left(\frac{length}{time}\right)^2 + \left(\frac{1}{time}\right)^2(length - length)^2} = \frac{\left(\frac{length}{time}\right)^2 - \frac{length^2}{time^2}}{\left(\frac{length}{time}\right)^2 - \frac{length^2}{time^2}} = unitless \tag{232}$$

$$n = \frac{length\frac{length}{time}\frac{1}{time} + \frac{length}{time}\frac{1}{time}(length - length)}{\left(\frac{length}{time}\right)^2 + \left(\frac{1}{time}\right)^2(length - length)^2} = \frac{\frac{length^2}{time^2} - \frac{length^2}{time^2}}{\left(\frac{length}{time}\right)^2 - \frac{length^2}{time^2}} = unitless \tag{233}$$

$$\theta = \arctan\left[\frac{\frac{1}{time}(length - length)}{\frac{length}{time}}\right] - \frac{1}{time}time = \arctan\left[\frac{\frac{length}{time}}{\frac{length}{time}}\right] = degrees \quad (234)$$

In the simulations run for this thesis, a, b, and ρ are defined in kilometers, θ in degrees, and m and n in terms of a unitless slope.

Appendix F. Inertial to Relative Position and Velocity Transformation

The transformation matrix from the inertial frame to the relative frame is simply the transpose of Equation 14. Let $^{IJK}\vec{L}$, $^{IJK}\dot{\vec{L}}$ and $^{IJK}\vec{M}$, $^{IJK}\dot{\vec{M}}$ be the position and velocity of the leader and follower satellites respectively expressed in the IJK frame.

$$C^{RCO2IJK} = [\hat{R}|\hat{C}|\hat{O}] \tag{235}$$

where

$$\hat{R} = \frac{^{IJK}\vec{L}}{|^{IJK}\vec{L}|} \tag{236}$$

$$\hat{C} = \frac{^{IJK}\dot{\vec{L}}}{|^{IJK}\dot{\vec{L}}|} \tag{237}$$

$$\hat{O} = \hat{R} \times \hat{C} \tag{238}$$

taking the transpose to get the transformation from IJK to RCO

$$C^{IJK2RCO} = [C^{RCO2IJK}]^T = [\hat{R}|\hat{C}|\hat{O}]^T \tag{239}$$

Note that for orthonormal frames $C^{IJK2RCO} * C^{RCO2IJK}$ equals the identity matrix. Equation 18 can then be solved for the relative position

$$\begin{bmatrix} r \\ c \\ o \end{bmatrix} = C^{IJK2RCO}[^{IJK}\vec{M} - ^{IJK}\vec{L}] \tag{240}$$

Solving Equation 25 for relative velocity (ω is calculated with Equation 3)

$$\begin{bmatrix} \dot{r} \\ \dot{c} \\ \dot{o} \end{bmatrix} = C^{IJK2RCO}[^{IJK}\dot{\vec{M}} - ^{IJK}\dot{\vec{L}}] - \begin{bmatrix} -c\omega \\ r\omega \\ 0 \end{bmatrix} \tag{241}$$

Appendix G. LQR Controller Simulation Plots

This appendix presents more detailed data from the simulation discussed in Section 4.4 for an LQR controller. For convenience, Table 37 lists the initial and final relative parameters. The reconfiguration is commanded at 0.05 days (72 minutes) from the start of the simulation. The control weight was varied in order to produce different responses for the LQR controller. High control weight translates to less control usage and lower ΔV with a higher settling time and the reverse for smaller control weights. To show contrast, the low ($R = 10^9$) and the high ($R = 10^{13}$) runs are presented.

	Initial	Final
ρ (km)	0.5	1.5
a (km)	0	0
θ (deg)	45	60
b (km)	0	0
m (slope)	1	1.5
n (slope)	0	1

Table 37   Complex Simulation Initial and Final Parameters

G.1   LQR $R = 10^9$

For the complex simulation, the LQR controller with a gain of $R = 10^9$ required 31.4307824 m/s of ΔV and settled to within +/- 10 meters in each axis after 21.25 minutes. The motion of the follower satellite in the leader centered RCO frame is shown in Figure 52 where the follower starts on the inner ellipse and is commanded onto the outer ellipse. This change in relative parameters translates to a change in the inertial COEs (Figure 53) Changes in each of the COEs is listed in Table 26. The control usage profile necessary to guide the follower onto the desired orbit is displayed in Figure 54. Note that the control inputs are shown in the inertial IJK frame. The absolute value of the control inputs are integrated in order to get the total ΔV expended; their time history is shown in Figure 55 The position error which represents half of the error signal (the other half is the velocity error) and upon which the settling time is based is shown in Figure 56. Finally, the relative parameters (upon which the command signal is based) are shown as a function of time in Figure 57.
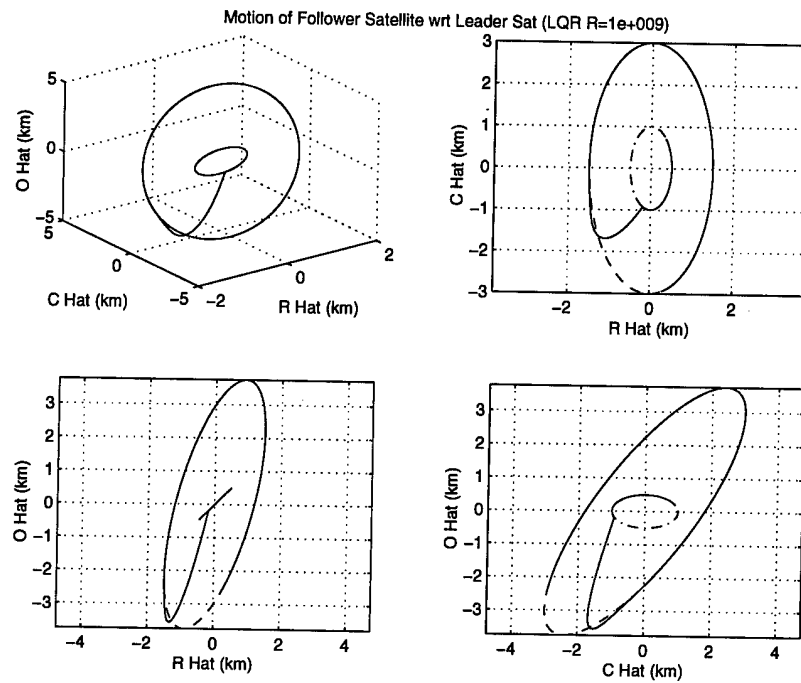
Figure 52   Path of Follower Satellite in RCO Frame (LQR $R = 10^9$)
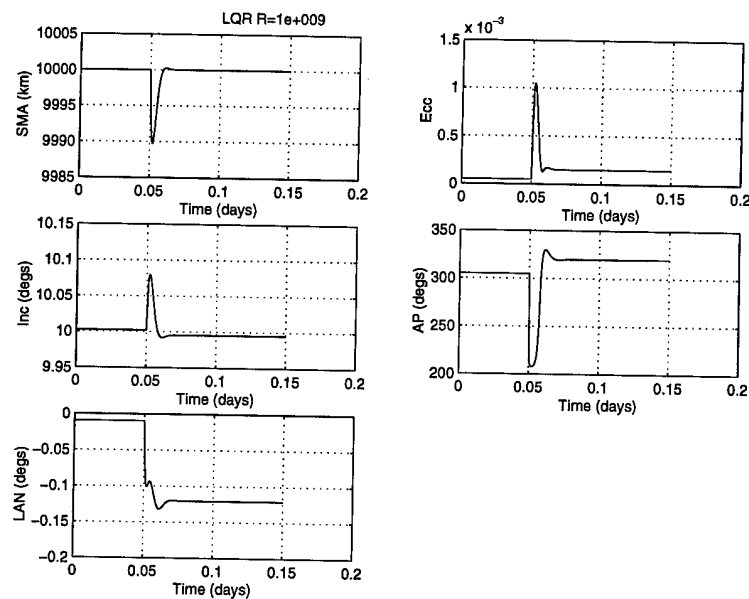
Figure 53   Time History of the Follower Satellite COEs (LQR $R = 10^9$)

93
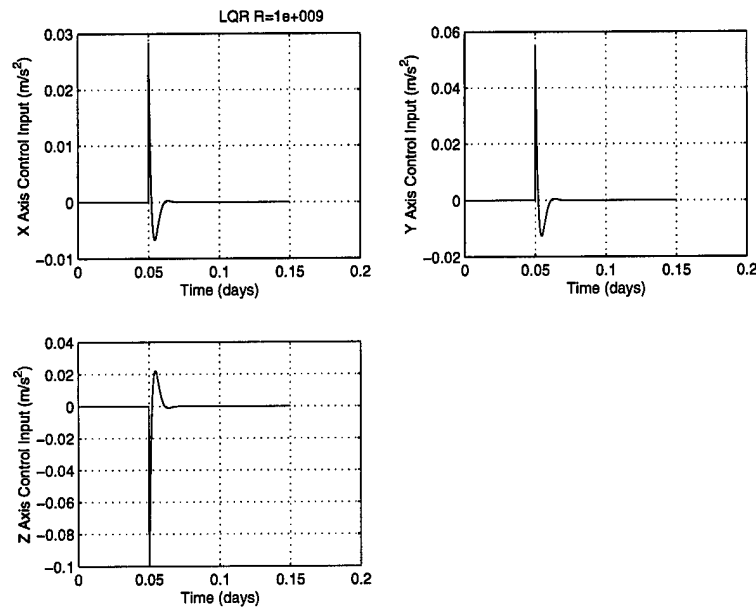
Figure 54   Control Usage (LQR $R = 10^9$)
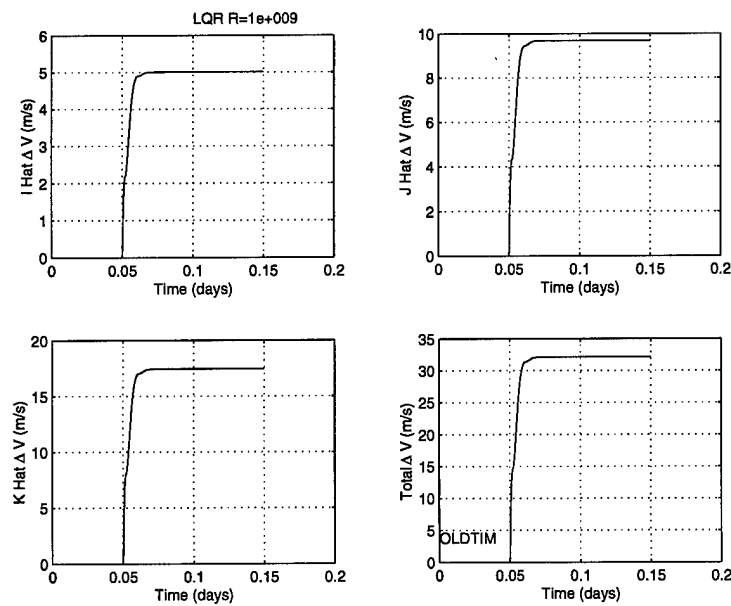

Figure 55 ΔV Time History (LQR $R = 10^9$)
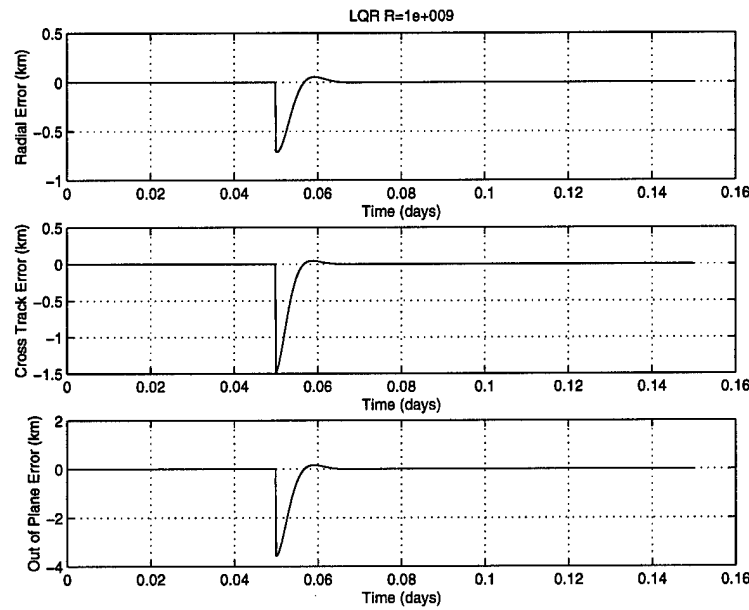
Figure 56   Position Error Time History (LQR $R = 10^9$)
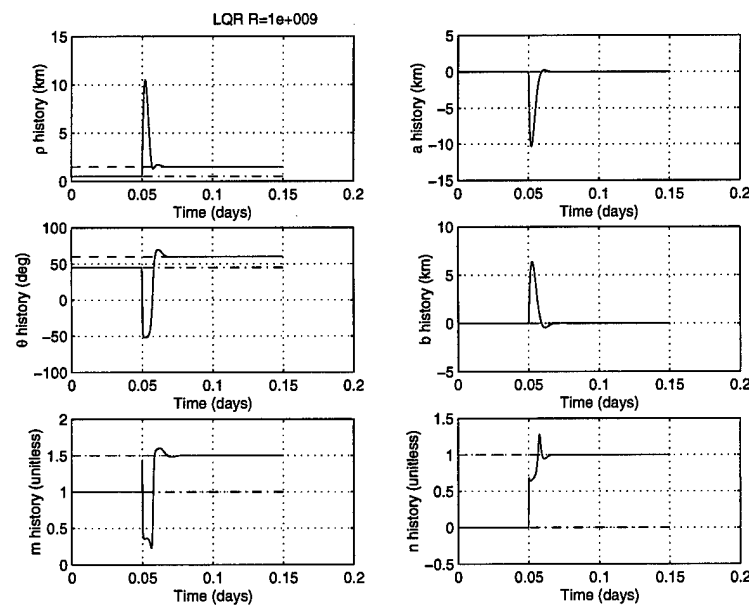
Figure 57   Relative Parameter Time History (LQR $R = 10^9$)

95

For the complex simulation, the LQR controller with a gain of $R = 10^{13}$ required 4.2184381 m/s of ΔV and settled to within +/- 10 meters in each axis after 407.25 minutes. The motion of the follower satellite in the leader centered *RCO* frame is shown in Figure 58 where the follower starts on the inner ellipse and is commanded onto the outer ellipse.
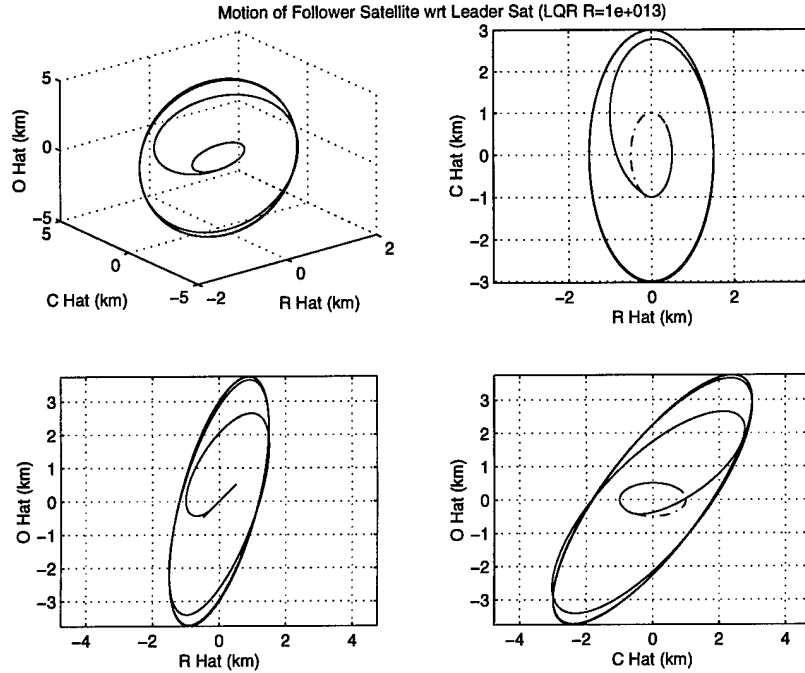
Figure 58   Path of Follower Satellite in *RCO* Frame (LQR $R = 10^{13}$)

This change in relative parameters translates to a change in the inertial COEs (Figure 59) Changes in each of the COEs is listed in Table 26. The control usage profile necessary to guide the follower onto the desired orbit is displayed in Figure 60. Note that the control inputs are shown in the inertial *IJK* frame. The absolute value of the control inputs are integrated in order to get the total ΔV expended; their time history is shown in Figure 61 The position error which represents half of the error signal (the other half is the velocity error) and upon which the settling time is based is shown in Figure 62. Finally, the relative parameters (upon which the command signal is based) are shown as a function of time in Figure 63.
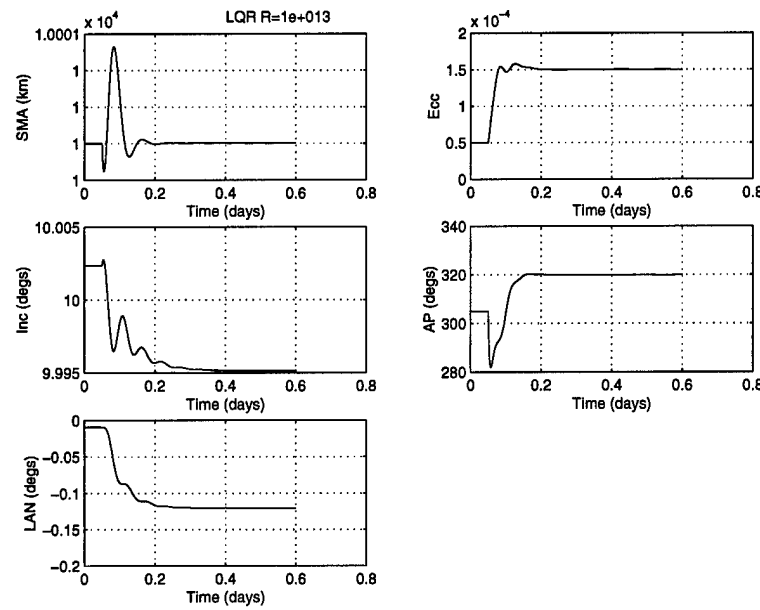
Figure 59   Time History of the Follower Satellite COEs (LQR $R = 10^{13}$)
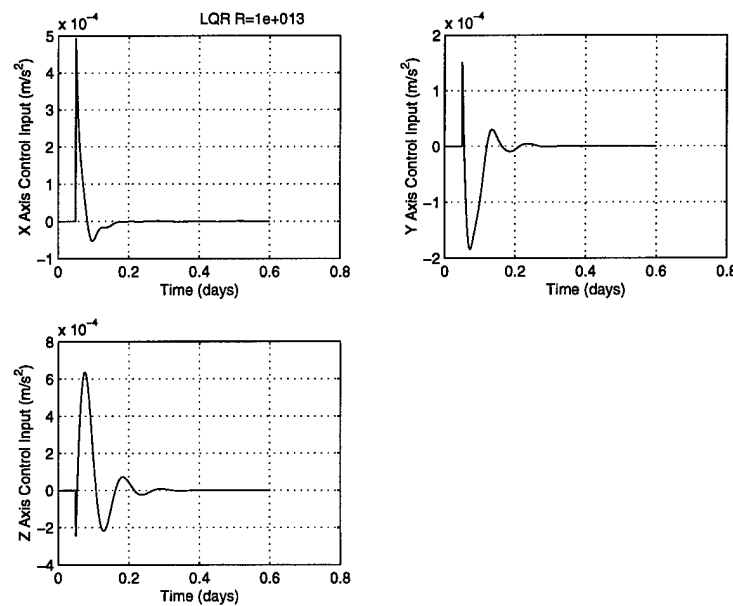
Figure 60   Control Usage (LQR $R = 10^{13}$)

97
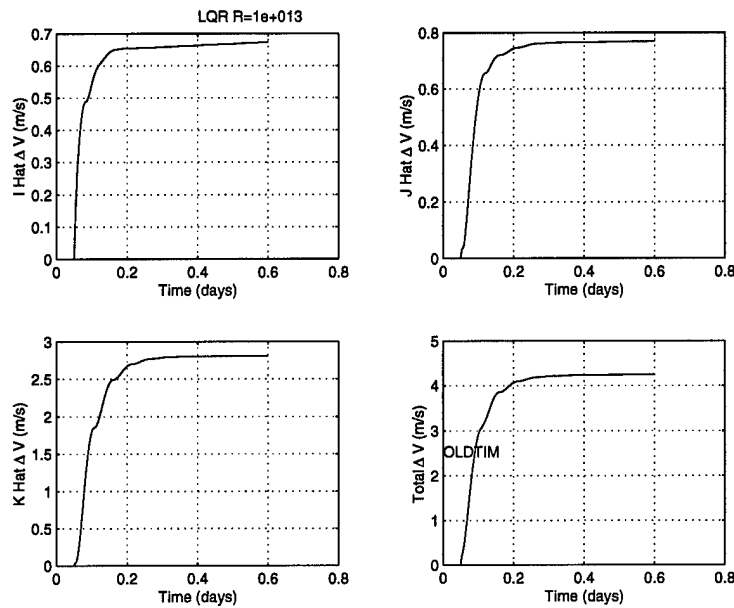
Figure 61 ΔV Time History (LQR $R = 10^{13}$)
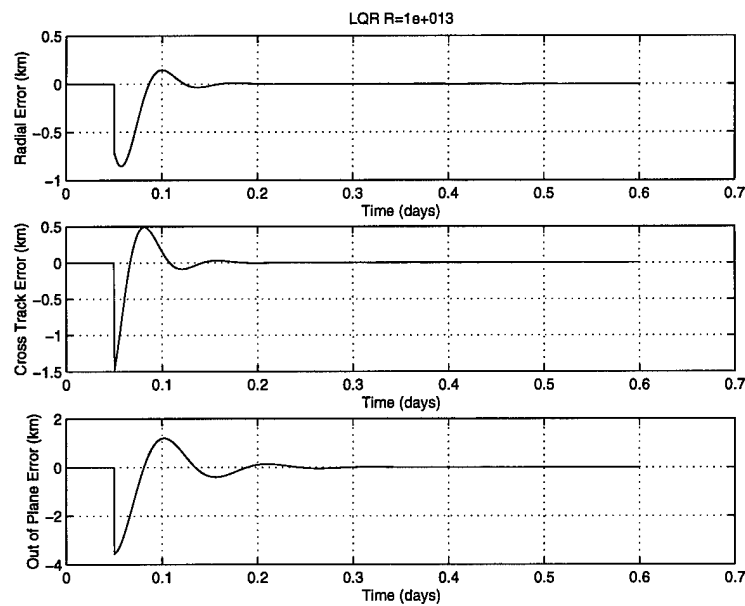
Figure 62   Position Error Time History (LQR $R = 10^{13}$)
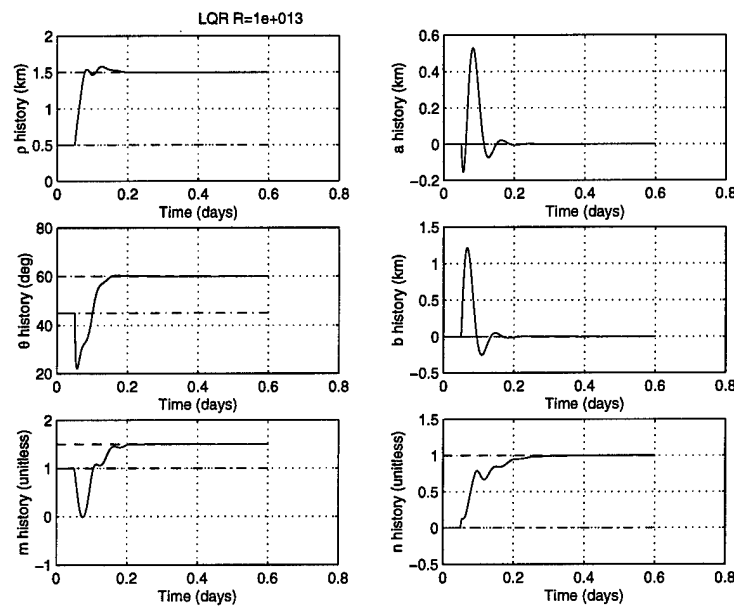
Figure 63   Relative Parameter Time History (LQR $R = 10^{13}$)

Appendix H. LQR with LF Controller Simulation Plots

This appendix presents more detailed data from the simulation discussed in Section 4.4 for an LQR with linearizing feedback (LF) controller. For convenience, Table 38 lists the initial and final relative parameters. The reconfiguration is commanded at 0.05 days (72 minutes) from the start of the simulation. The control weight was varied in order to produce different responses for the LQR with LF controller. High control weight translates to less control usage and lower ΔV with a higher settling time and the reverse for smaller control weights. To show contrast, the low ($R = 10^9$) and the high ($R = 10^{13}$) runs are presented.

	Initial	Final
ρ (km)	0.5	1.5
a (km)	0	0
θ (deg)	45	60
b (km)	0	0
m (slope)	1	1.5
n (slope)	0	1

Table 38   Complex Simulation Initial and Final Parameters

H.1   LQR with LF $R = 10^9$

For the complex simulation, the LQR with LF controller with a gain of $R = 10^9$ required 31.4307616 m/s of ΔV and settled to within +/- 10 meters in each axis after 21.25 minutes. The motion of the follower satellite in the leader centered RCO frame is shown in Figure 64 where the follower starts on the inner ellipse and is commanded onto the outer ellipse. This change in relative parameters translates to a change in the inertial COEs (Figure 65) Changes in each of the COEs is listed in Table 26. The control usage profile necessary to guide the follower onto the desired orbit is displayed in Figure 66. Note that the control inputs are shown in the inertial IJK frame. The absolute value of the control inputs are integrated in order to get the total ΔV expended; their time history is shown in Figure 67 The position error which represents half of the error signal (the other half is the velocity error) and upon which the settling time is based is shown in Figure 68. Finally, the relative parameters (upon which the command signal is based) are shown as a
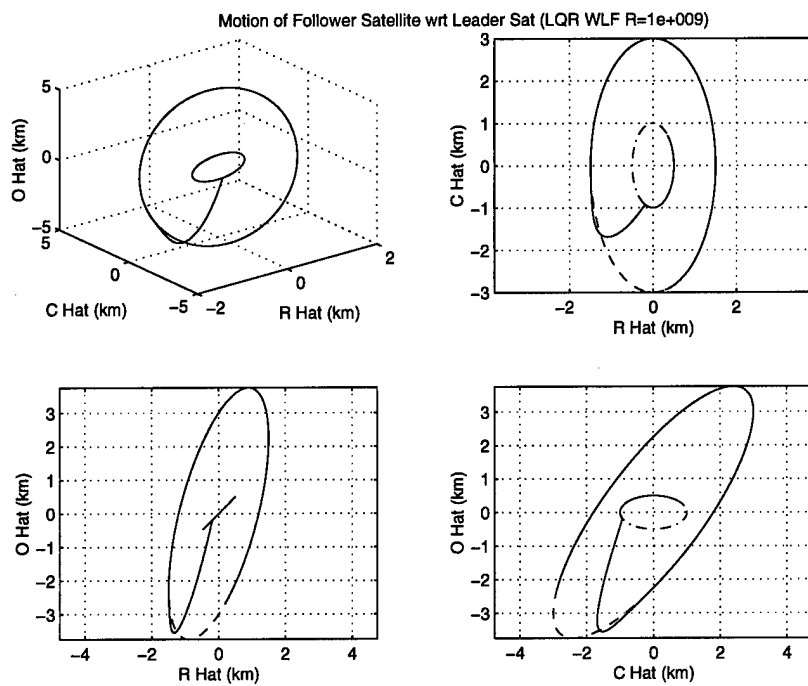
Figure 64   Path of Follower Satellite in RCO Frame (LQRWLF $R = 10^9$)
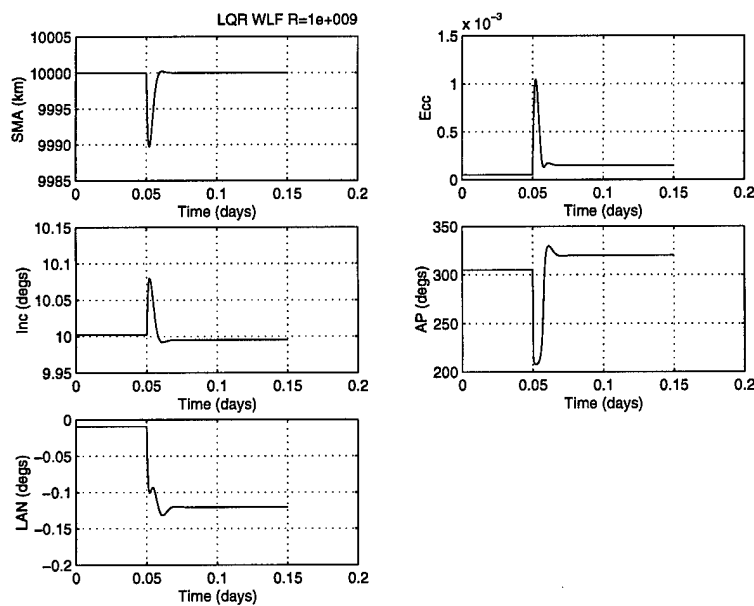
Figure 65   Time History of the Follower Satellite COEs (LQRWLF $R = 10^9$)

101
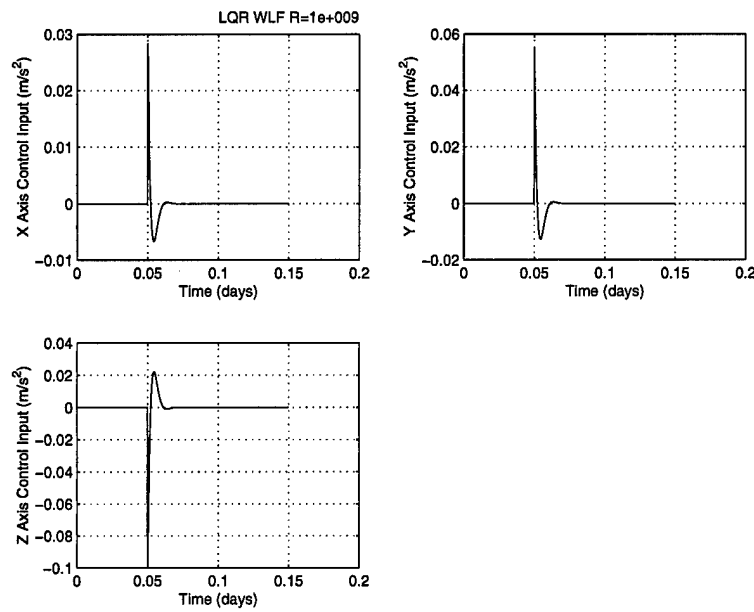
Figure 66   Control Usage (LQRWLF $R = 10^9$)
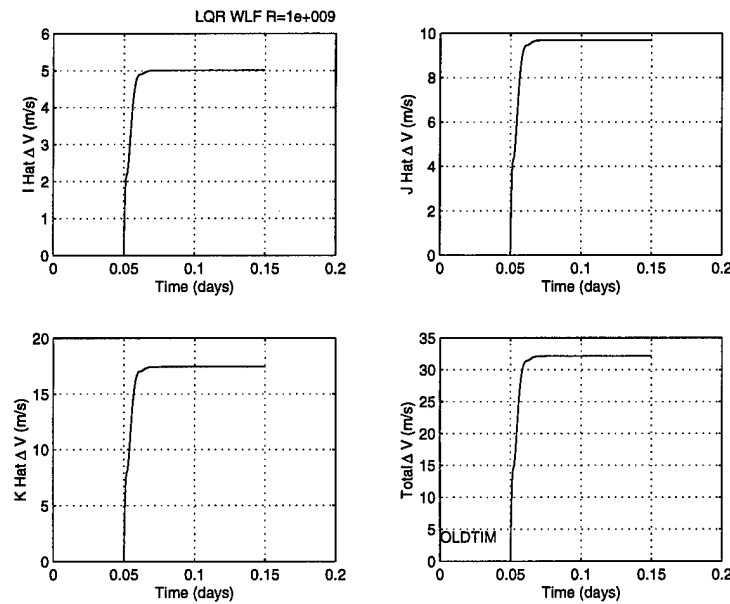
Figure 67 ΔV Time History (LQRWLF $R = 10^9$)
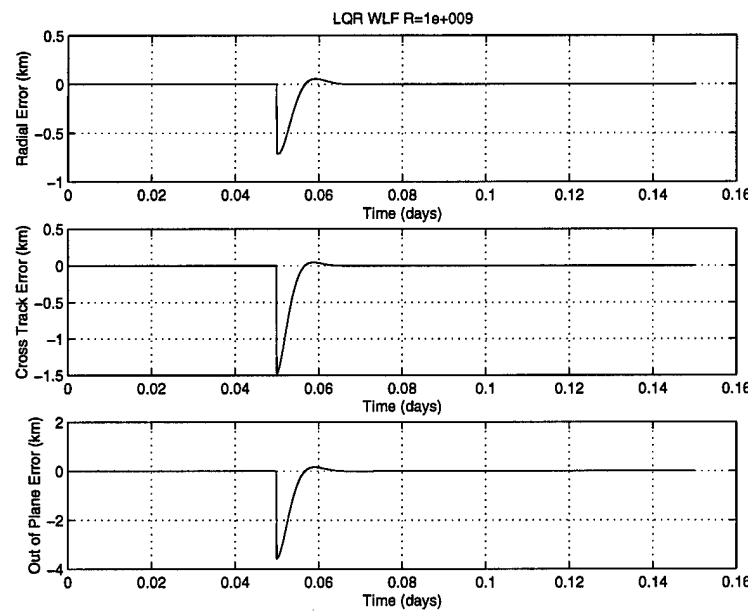
Figure 68   Position Error Time History (LQRWLF $R = 10^9$)

function of time in Figure 69.
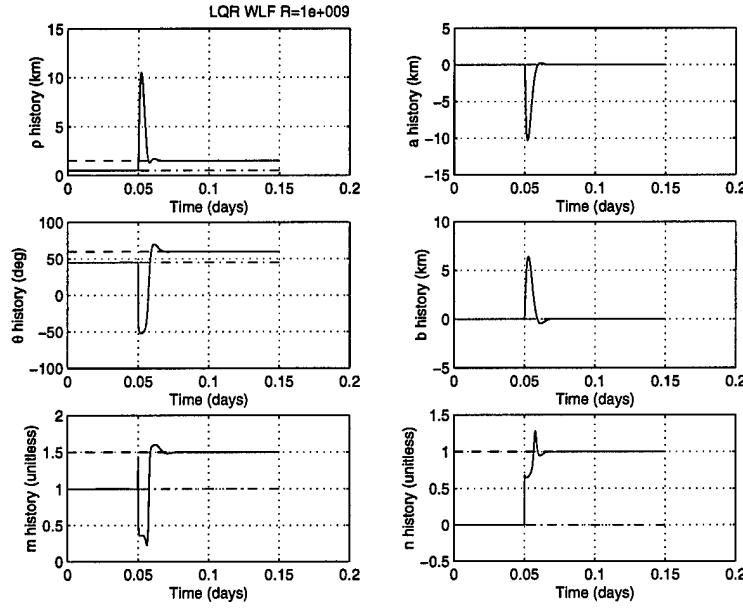
Figure 69   Relative Parameter Time History (LQRWLF $R = 10^9$)

H.2   LQR with LF $R = 10^{13}$

For the complex simulation, the LQR with LF controller with a gain of $R = 10^{13}$ required 4.2181246 m/s of ΔV and settled to within +/- 10 meters in each axis after 407.75 minutes. The motion of the follower satellite in the leader centered RCO frame is shown in Figure 70 where the follower starts on the inner ellipse and is commanded onto the outer ellipse. This change in relative parameters translates to a change in the inertial COEs (Figure 71) Changes in each of the COEs is listed in Table 26. The control usage profile necessary to guide the follower onto the desired orbit is displayed in Figure 72. Note that the control inputs are shown in the inertial IJK frame. The absolute value of the control inputs are integrated in order to get the total ΔV expended; their time history is shown in Figure 73 The position error which represents half of the error signal (the other half is the velocity error) and upon which the settling time is based is shown in Figure 74. Finally, the relative parameters (upon which the command signal is based) are shown as a function of time in Figure 75.
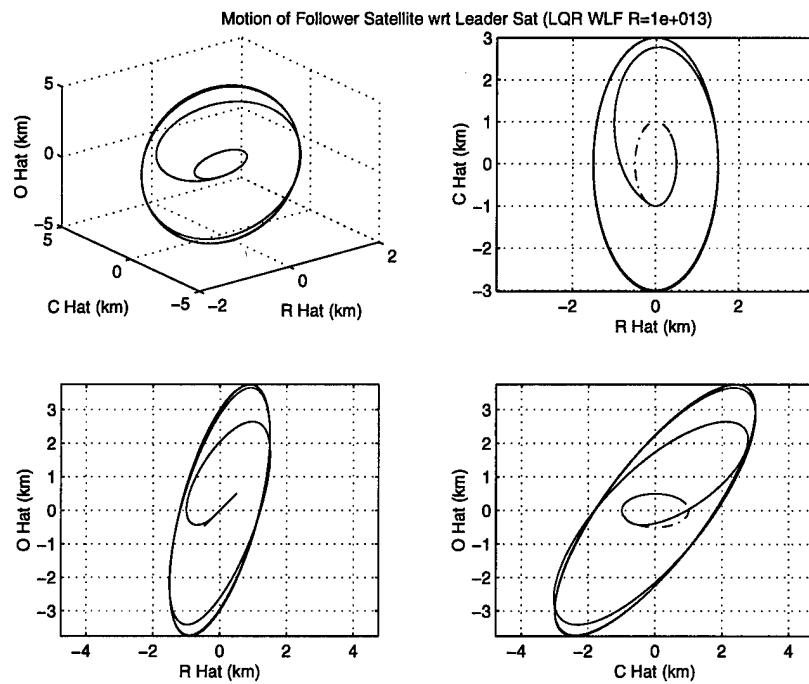
Figure 70   Path of Follower Satellite in RCO Frame (LQRWLF $R = 10^{13}$)
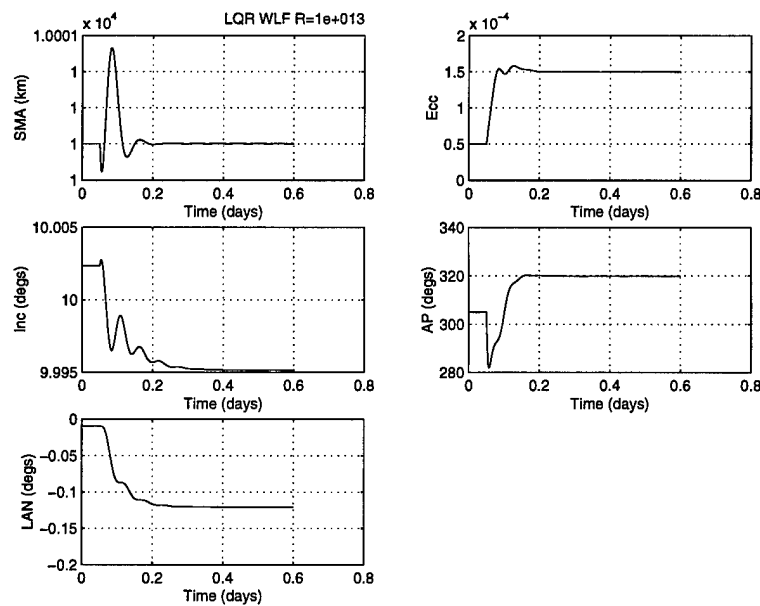
Figure 71   Time History of the Follower Satellite COEs (LQRWLF $R = 10^{13}$)

105
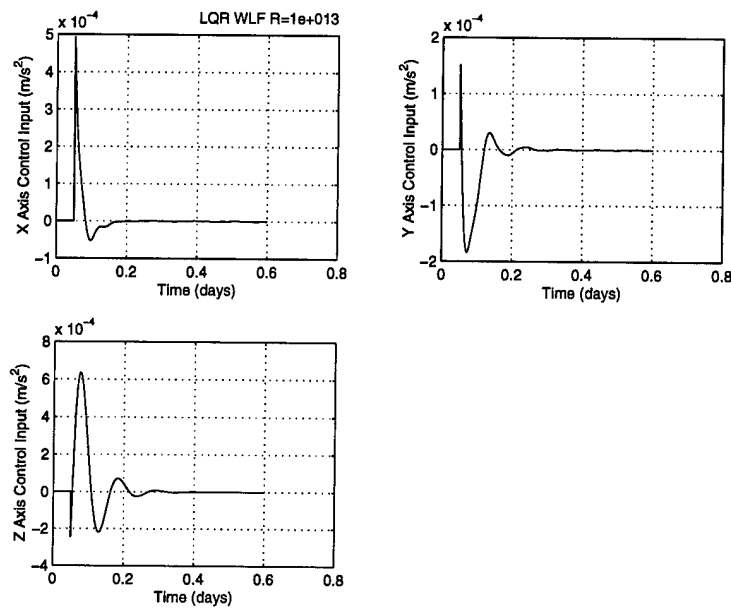
Figure 72   Control Usage (LQRWLF $R = 10^{13}$)
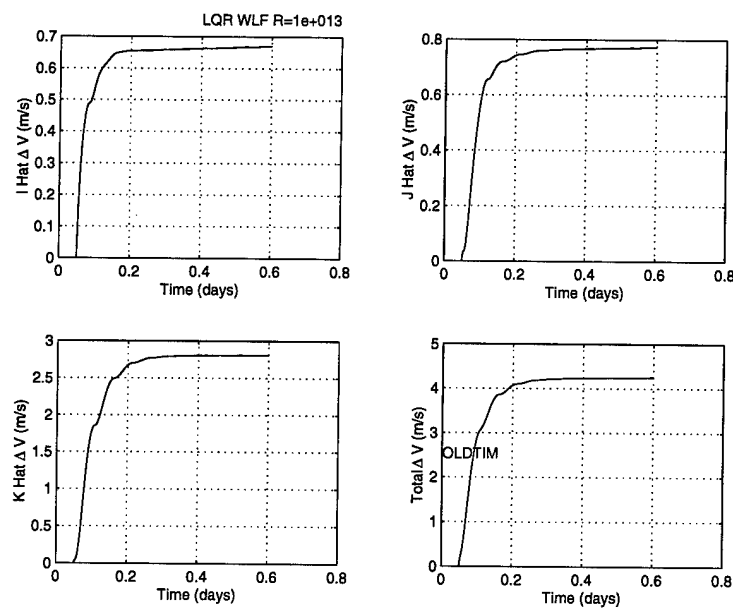
Figure 73 ΔV Time History (LQRWLF $R = 10^{13}$)
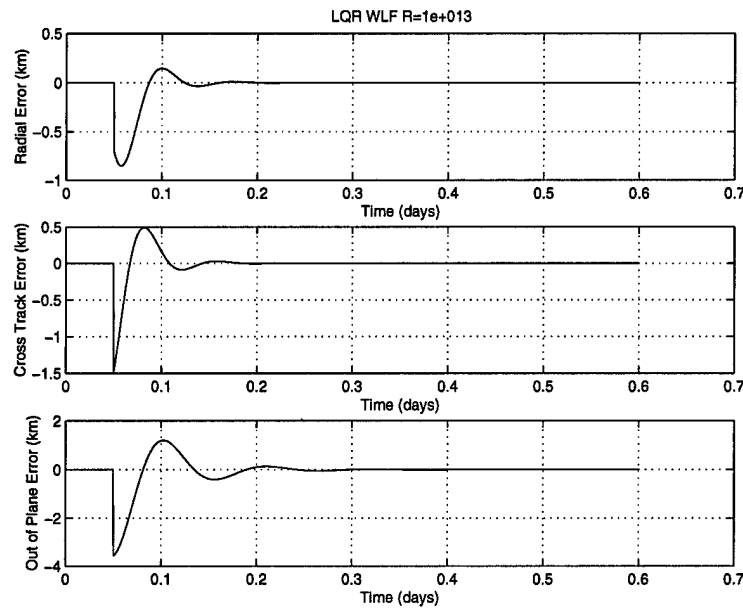
Figure 74   Position Error Time History (LQRWLF $R = 10^{13}$)
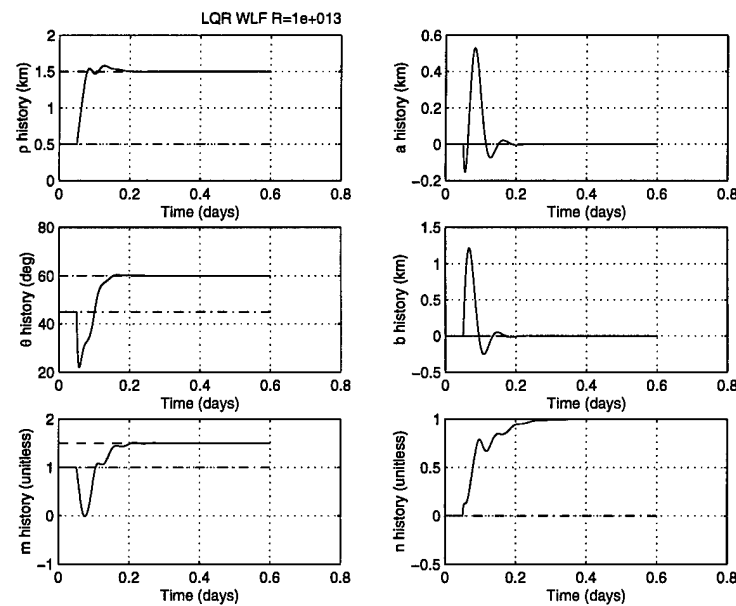
Figure 75   Relative Parameter Time History (LQRWLF $R = 10^{13}$)

Appendix I. SDRE Controller Simulation Plots

This appendix presents more detailed data from the simulation discussed in Section 4.4 for the State Dependent Riccati Equations (SDRE) controller. For convenience, Table 39 lists the initial and final relative parameters. The reconfiguration is commanded at 0.05 days (72 minutes) from the start of the simulation. The control weight was varied in order to produce different responses for the SDRE controller. High control weight translates to less control usage and lower ΔV with a higher settling time and the reverse for smaller control weights. To show contrast, the low ($R = 10^9$) and the high ($R = 10^{13}$) runs are presented.

	Initial	Final
ρ (km)	0.5	1.5
a (km)	0	0
θ (deg)	45	60
b (km)	0	0
m (slope)	1	1.5
n (slope)	0	1

Table 39   Complex Simulation Initial and Final Parameters

I.1   SDRE $R = 10^9$

For the complex simulation, the SDRE controller with a gain of $R = 10^9$ required 31.4307437 m/s of ΔV and settled to within +/- 10 meters in each axis after 21.25 minutes. The motion of the follower satellite in the leader centered RCO frame is shown in Figure 76 where the follower starts on the inner ellipse and is commanded onto the outer ellipse. This change in relative parameters translates to a change in the inertial COEs (Figure 77) Changes in each of the COEs is listed in Table 26. The control usage profile necessary to guide the follower onto the desired orbit is displayed in Figure 78. Note that the control inputs are shown in the inertial IJK frame. The absolute value of the control inputs are integrated in order to get the total ΔV expended; their time history is shown in Figure 79 The position error which represents half of the error signal (the other half is the velocity error) and upon which the settling time is based is shown in Figure 80. Finally, the relative
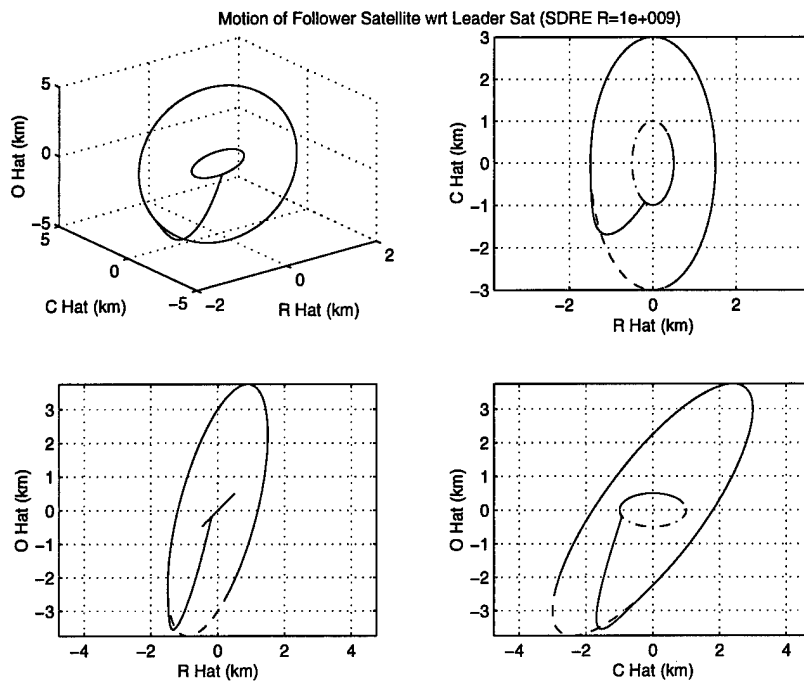
Figure 76   Path of Follower Satellite in RCO Frame (SDRE $R = 10^9$)
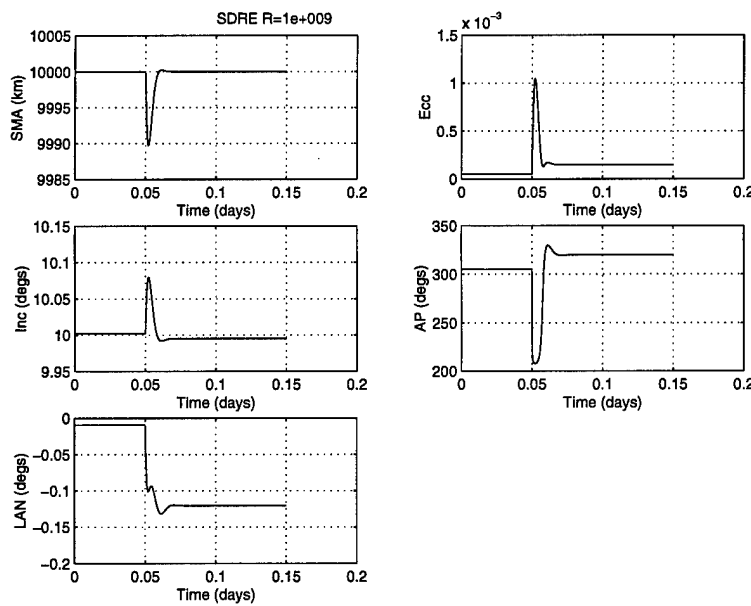
Figure 77   Time History of the Follower Satellite COEs (SDRE $R = 10^9$)

109
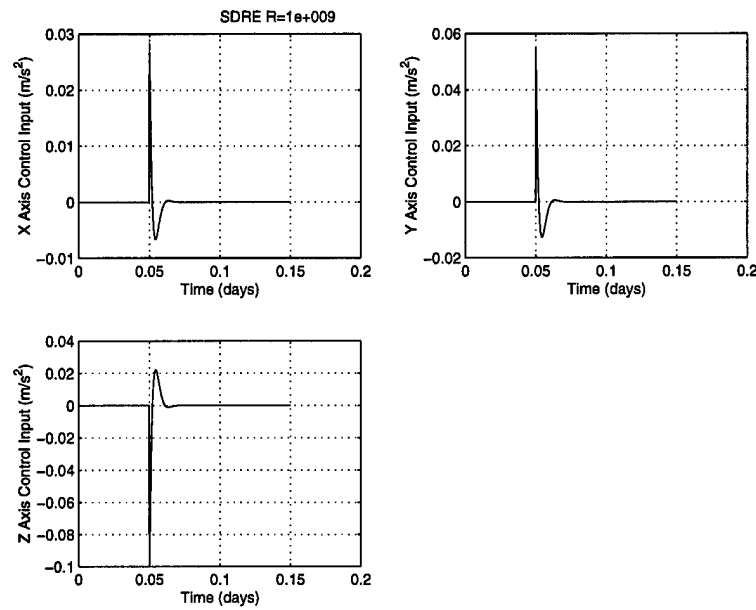
Figure 78   Control Usage (SDRE $R = 10^9$)

Figure 79 ΔV Time History (SDRE $R = 10^9$)

110
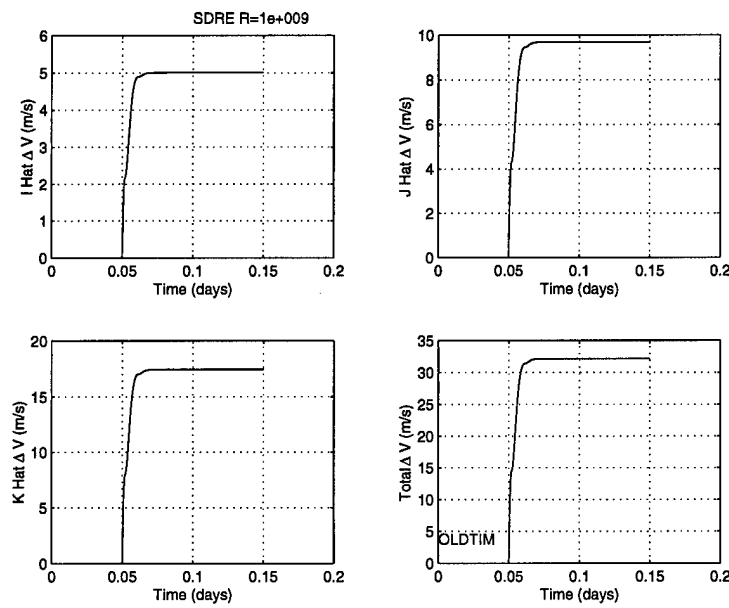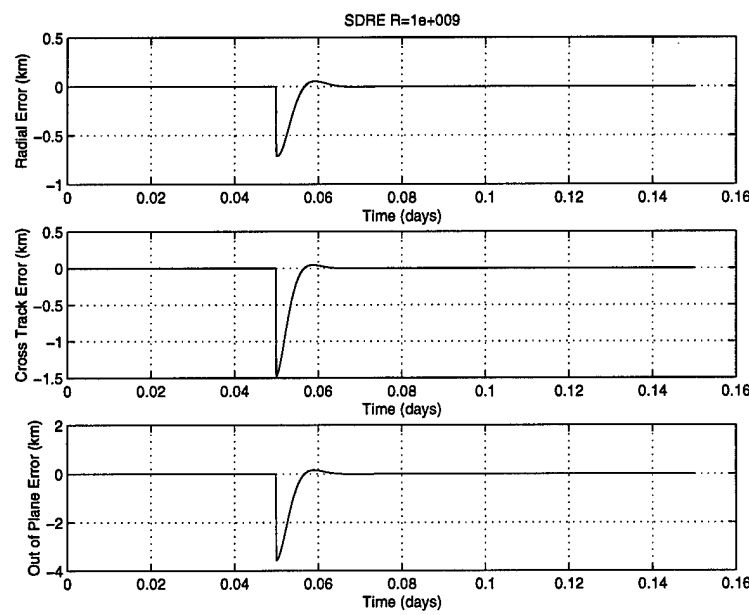
Figure 80   Position Error Time History (SDRE $R = 10^9$)

parameters (upon which the command signal is based) are shown as a function of time in Figure 81.
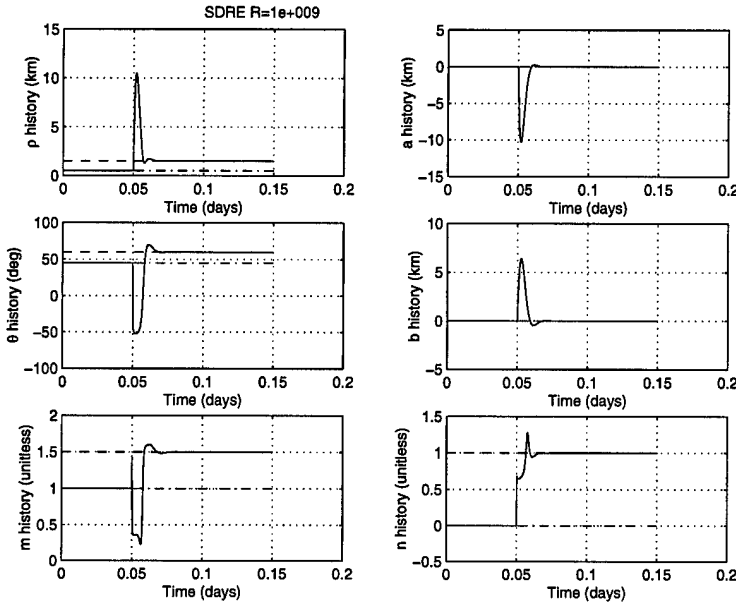
Figure 81   Relative Parameter Time History (SDRE $R = 10^9$)

I.2   SDRE $R = 10^{13}$

For the complex simulation, the SDRE controller with a gain of $R = 10^{13}$ required 4.2185121 m/s of ΔV and settled to within $+/-$ 10 meters in each axis after 407.25 minutes. The motion of the follower satellite in the leader centered RCO frame is shown in Figure 82 where the follower starts on the inner ellipse and is commanded onto the outer ellipse. This change in relative parameters translates to a change in the inertial COEs (Figure 83) Changes in each of the COEs is listed in Table 26. The control usage profile necessary to guide the follower onto the desired orbit is displayed in Figure 84. Note that the control inputs are shown in the inertial IJK frame. The absolute value of the control inputs are integrated in order to get the total ΔV expended; their time history is shown in Figure 85 The position error which represents half of the error signal (the other half is the velocity error) and upon which the settling time is based is shown in Figure 86. Finally, the relative parameters (upon which the command signal is based) are shown as a function of time in Figure 87.
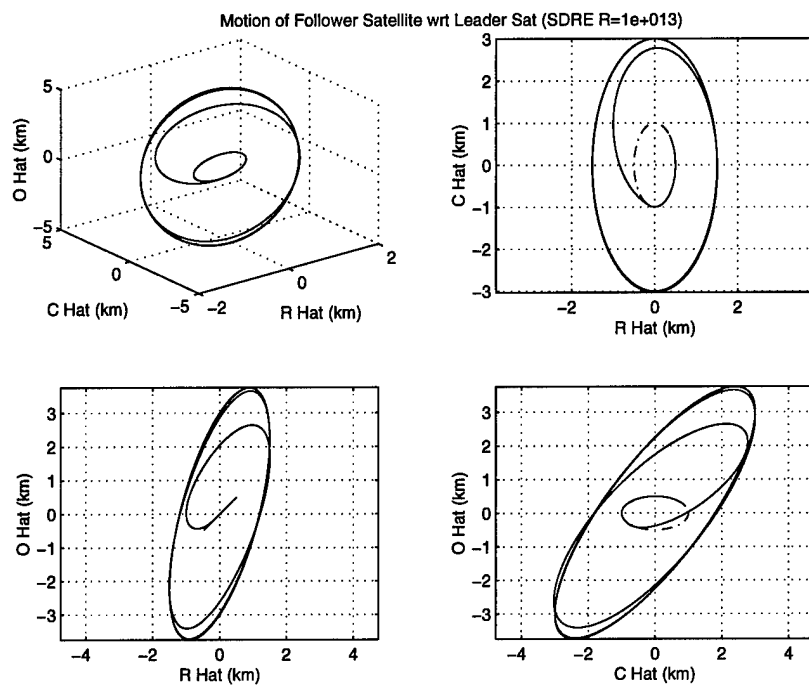
Figure 82   Path of Follower Satellite in RCO Frame (SDRE $R = 10^{13}$)
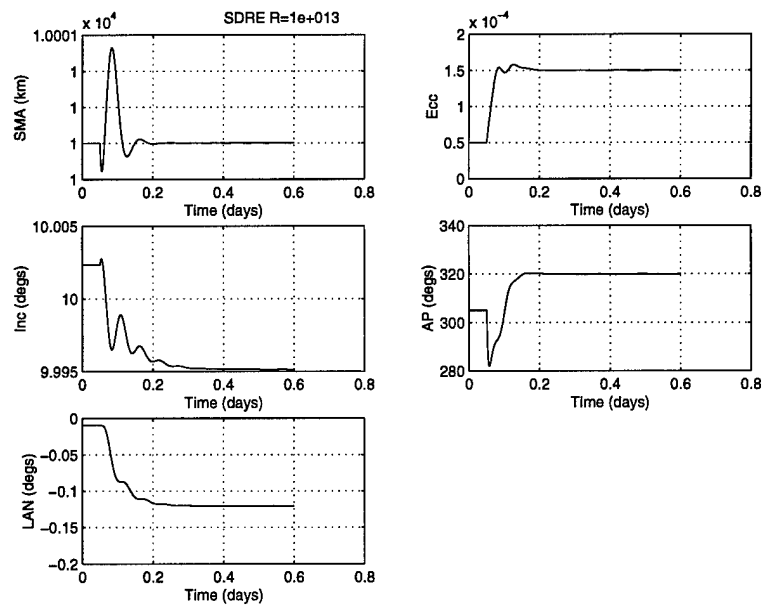
Figure 83   Time History of the Follower Satellite COEs (SDRE $R = 10^{13}$)

113
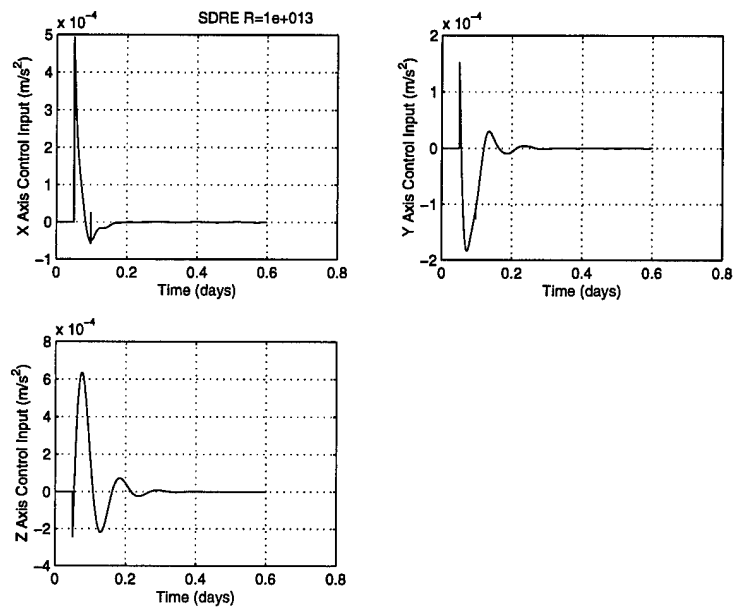
Figure 84   Control Usage (SDRE $R = 10^{13}$)
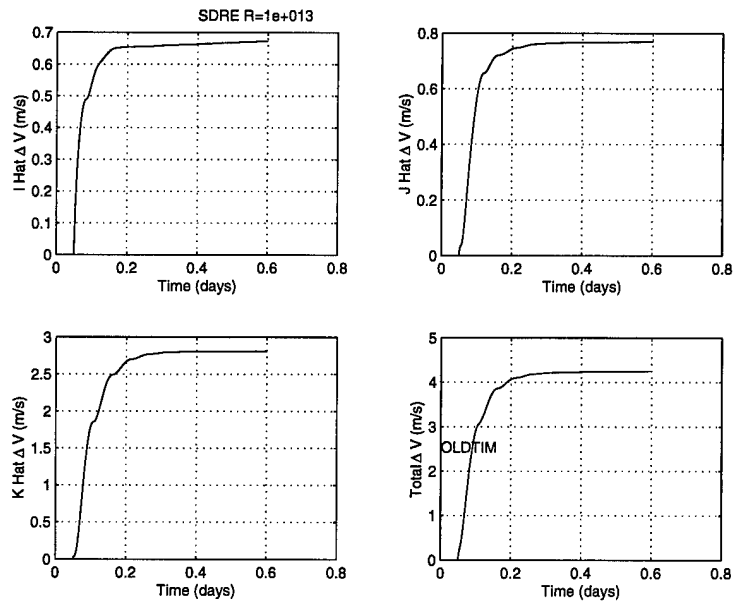
Figure 85 ΔV Time History (SDRE $R = 10^{13}$)
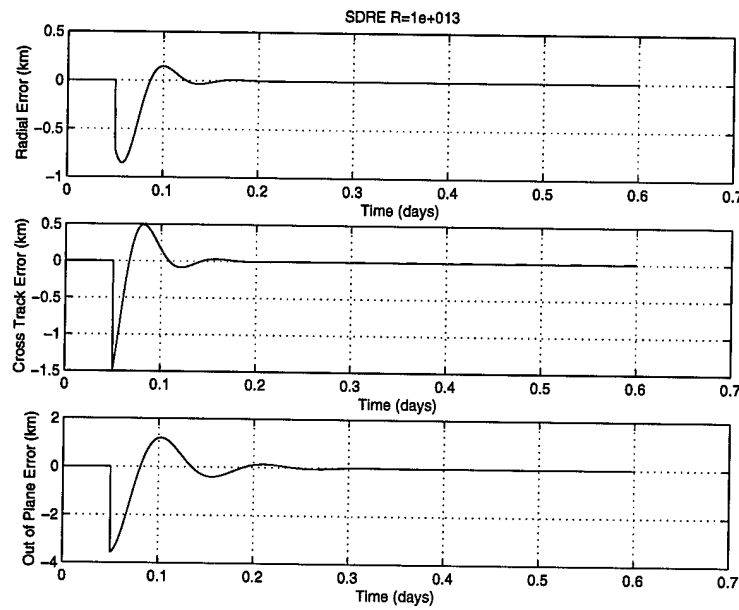
Figure 86   Position Error Time History (SDRE $R = 10^{13}$)
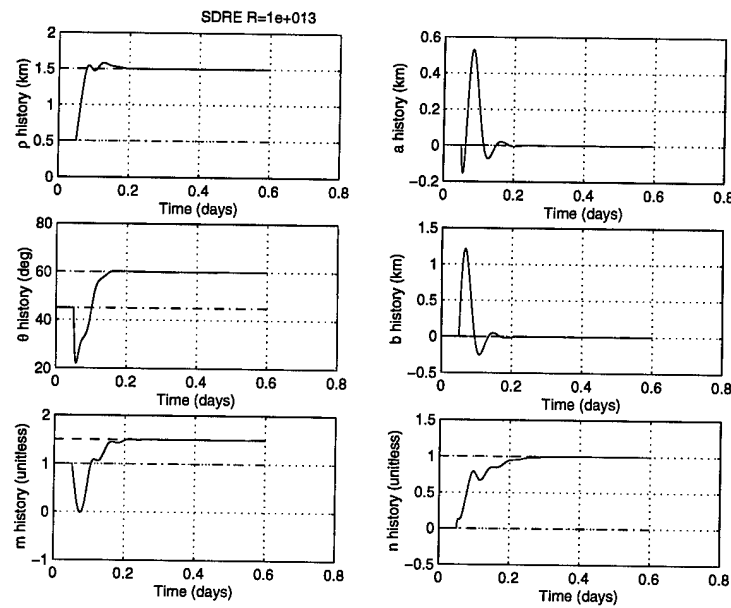
Figure 87   Relative Parameter Time History (SDRE $R = 10^{13}$)

115

Appendix J. SMC Controller Simulation Plots

This appendix presents more detailed data from the simulation discussed in Section 4.4 for the sliding mode controller. For convenience, Table 40 lists the initial and final relative parameters. The reconfiguration is commanded at 0.05 days (72 minutes) from the start of the simulation. The pole position was varied in order to produce different responses for the sliding mode controller. Poles farther from the $j\omega$ axis translate to more control usage and higher ΔV with a lower settling time and the reverse for smaller control weights. To show contrast, the $P = -0.0006$ and $P = -0.0018$ runs are presented.

	Initial	Final
ρ (km)	0.5	1.5
a (km)	0	0
θ (deg)	45	60
b (km)	0	0
m (slope)	1	1.5
n (slope)	0	1

Table 40   Complex Simulation Initial and Final Parameters

J.1   SMC $P = -0.0006$

For the complex simulation, the SMC controller with a gain of $P = -0.0006$ required 40.4172759 m/s of ΔV and settled to within +/- 10 meters in each axis after 166 minutes. The motion of the follower satellite in the leader centered RCO frame is shown in Figure 88 where the follower starts on the inner ellipse and is commanded onto the outer ellipse. This change in relative parameters translates to a change in the inertial COEs (Figure 89) Changes in each of the COEs is listed in Table 26. The control usage profile necessary to guide the follower onto the desired orbit is displayed in Figure 90. Note that the control inputs are shown in the inertial IJK frame. The absolute value of the control inputs are integrated in order to get the total ΔV expended; their time history is shown in Figure 91 The position error which represents half of the error signal (the other half is the velocity error) and upon which the settling time is based is shown in Figure 92. Finally, the relative parameters (upon which the command signal is based) are shown as a function of time in Figure 93.
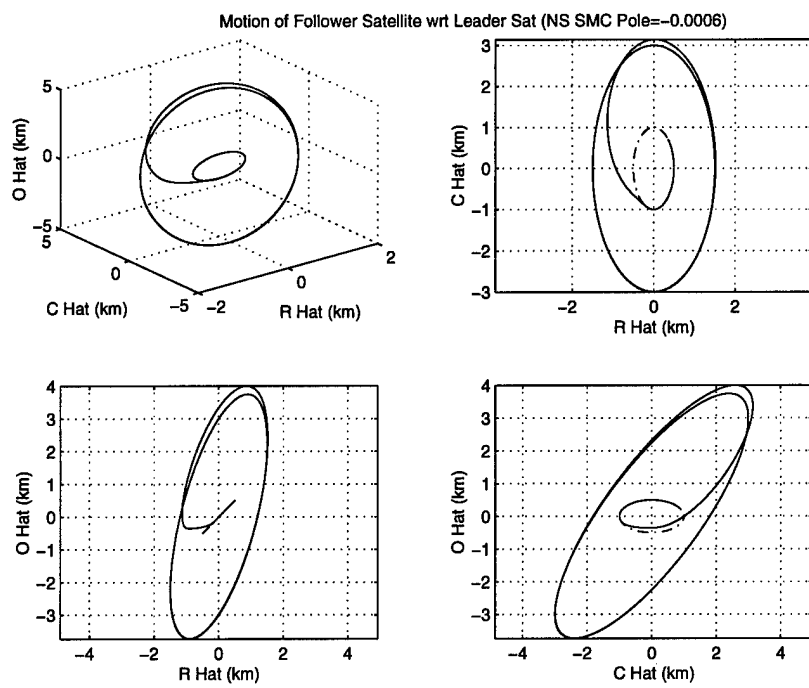
Figure 88   Path of Follower Satellite in RCO Frame (SMC $P = -0.0006$)
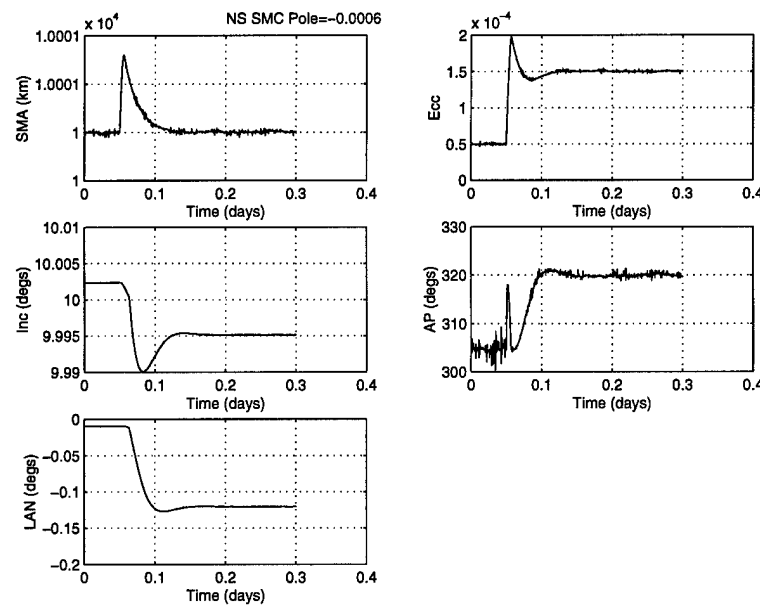
Figure 89   Time History of the Follower Satellite COEs (SMC $P = -0.0006$)

117
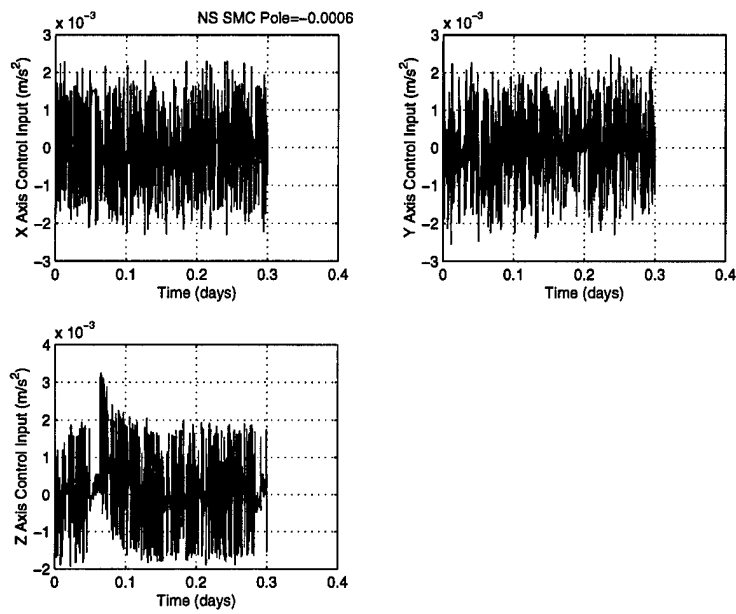
Figure 90   Control Usage (SMC $P = -0.0006$)

Figure 91 ΔV Time History (SMC $P = -0.0006$)

118
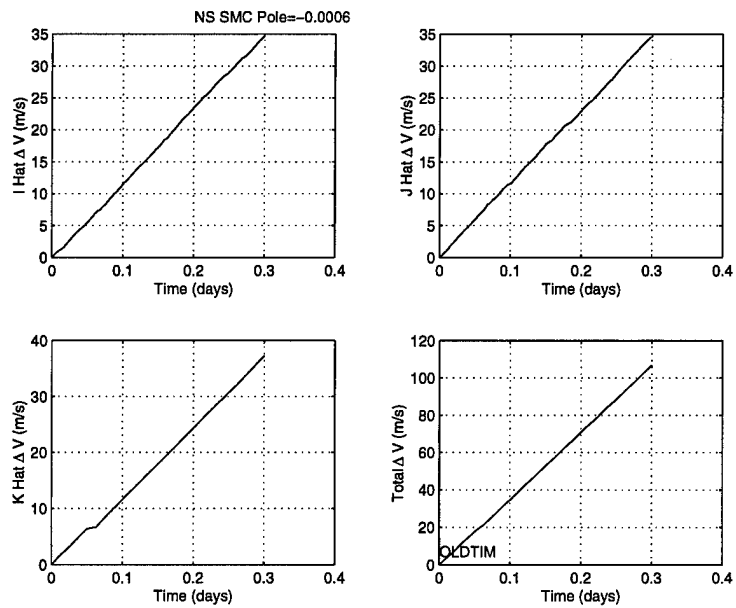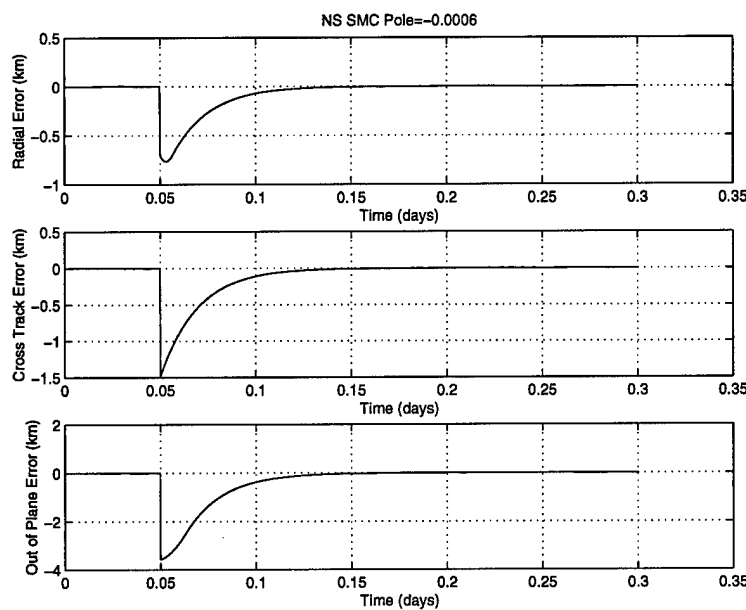
Figure 92   Position Error Time History (SMC $P = -0.0006$)
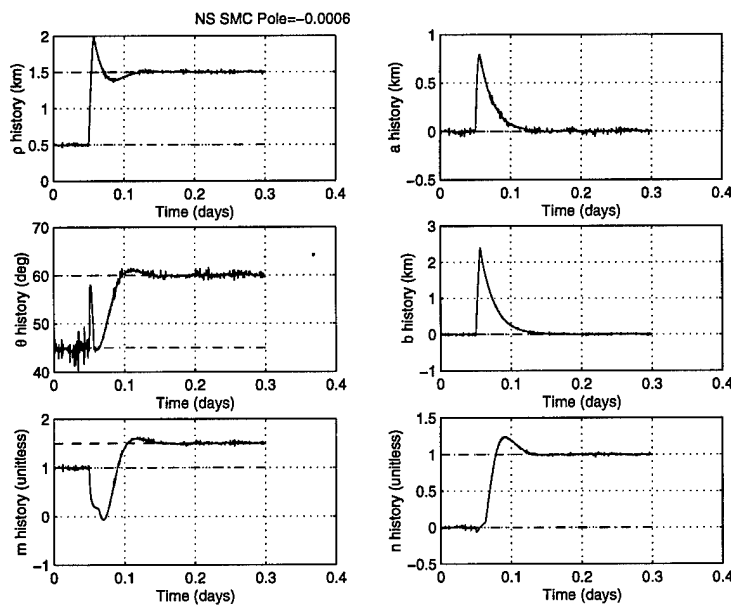
Figure 93   Relative Parameter Time History (SMC $P = -0.0006$)

119

J.2 SMC $P = -0.0018$

For the complex simulation, the SDRE controller with a gain of $P = -0.0018$ required 20.6293084 m/s of ΔV and settled to within $+/-$ 10 meters in each axis after 99 minutes. The motion of the follower satellite in the leader centered RCO frame is shown in Figure 94 where the follower starts on the inner ellipse and is commanded onto the outer ellipse.
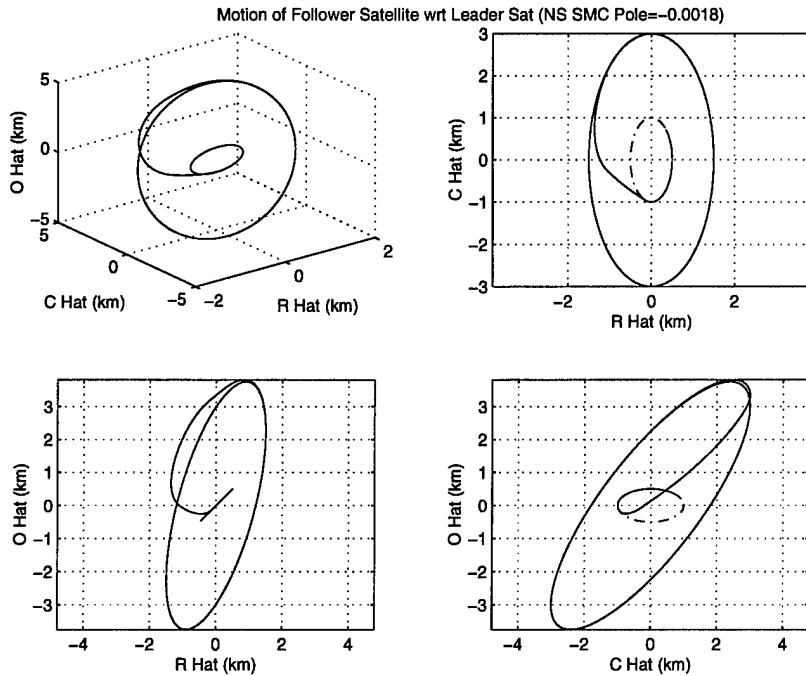

Figure 94   Path of Follower Satellite in RCO Frame (SMC $P = -0.0018$)

This change in relative parameters translates to a change in the inertial COEs (Figure 95) Changes in each of the COEs is listed in Table 26. The control usage profile necessary to guide the follower onto the desired orbit is displayed in Figure 96. Note that the control inputs are shown in the inertial IJK frame. The absolute value of the control inputs are integrated in order to get the total ΔV expended; their time history is shown in Figure 97 The position error which represents half of the error signal (the other half is the velocity error) and upon which the settling time is based is shown in Figure 98. Finally, the relative parameters (upon which the command signal is based) are shown as a function of time in Figure 99.
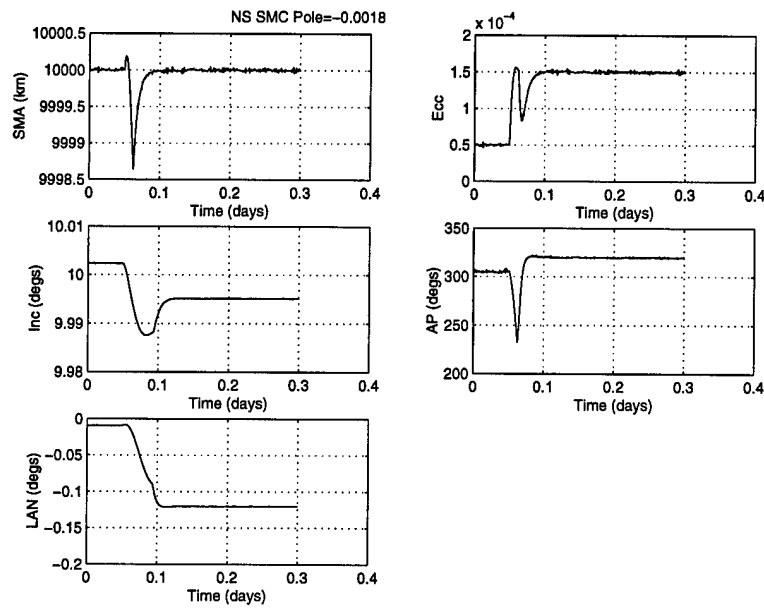
Figure 95   Time History of the Follower Satellite COEs (SMC $P = -0.0018$)
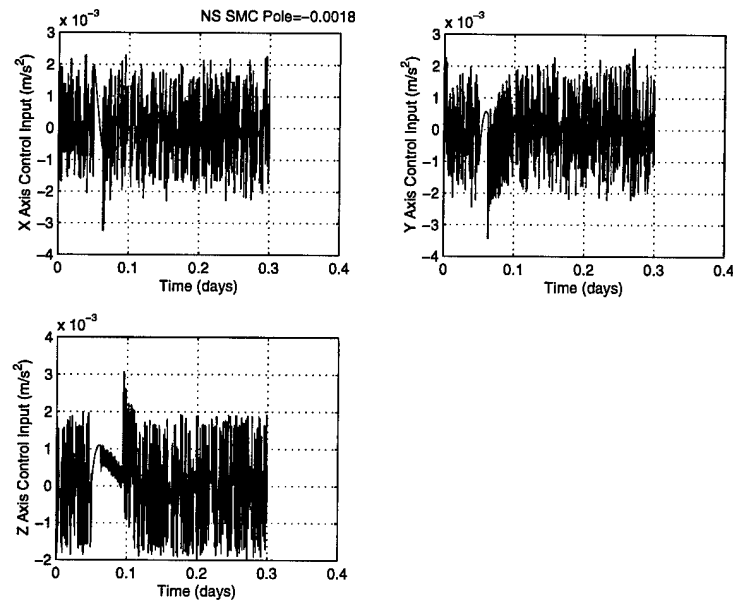
Figure 96   Control Usage (SMC $P = -0.0018$)

121
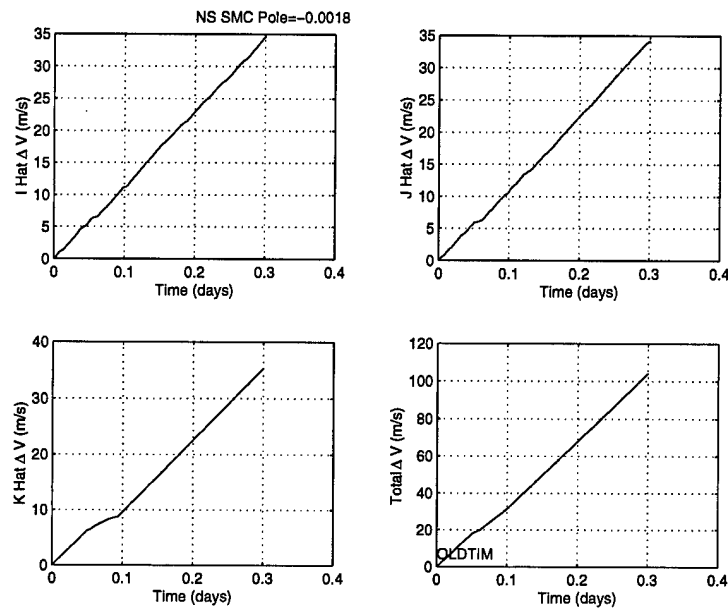
Figure 97　ΔV Time History (SMC $P = -0.0018$)
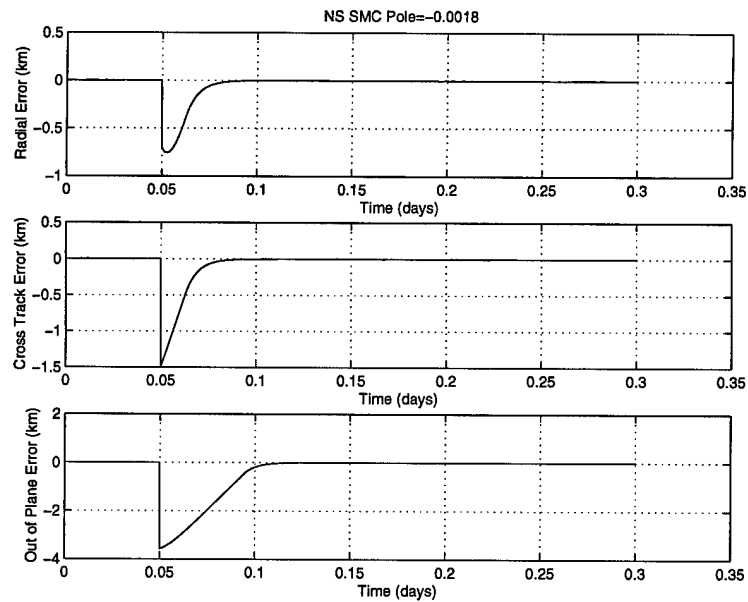
Figure 98　Position Error Time History (SMC $P = -0.0018$)

122
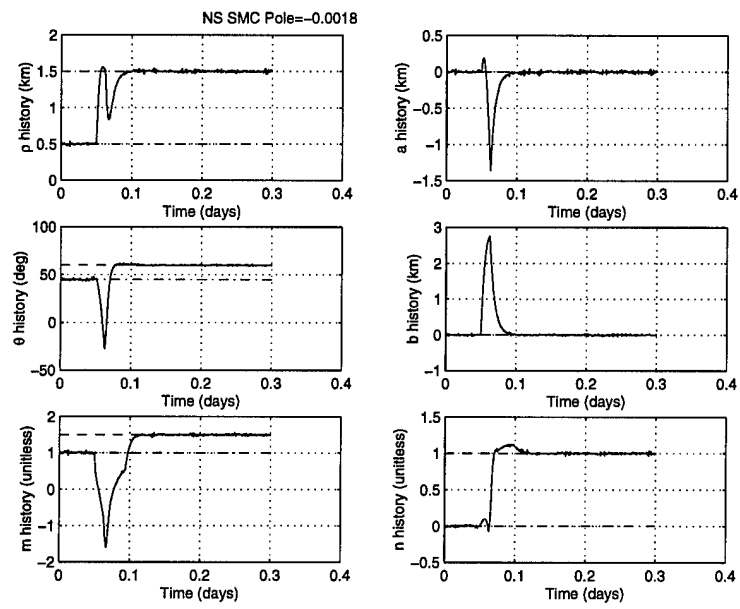
Figure 99   Relative Parameter Time History (SMC $P = -0.0018$)

Appendix K. LQR Simulink Diagram
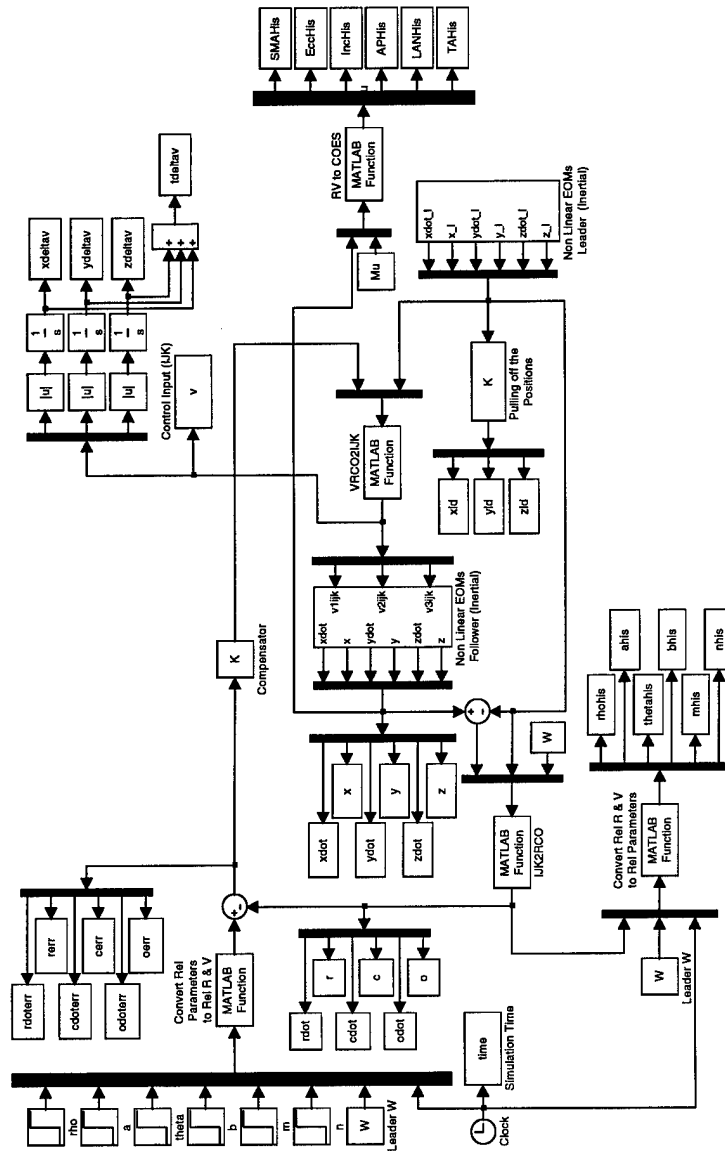
Figure 100   LQR Simulink Diagram

Figure 101   LQR With Linearizing Feedback Simulink Diagram
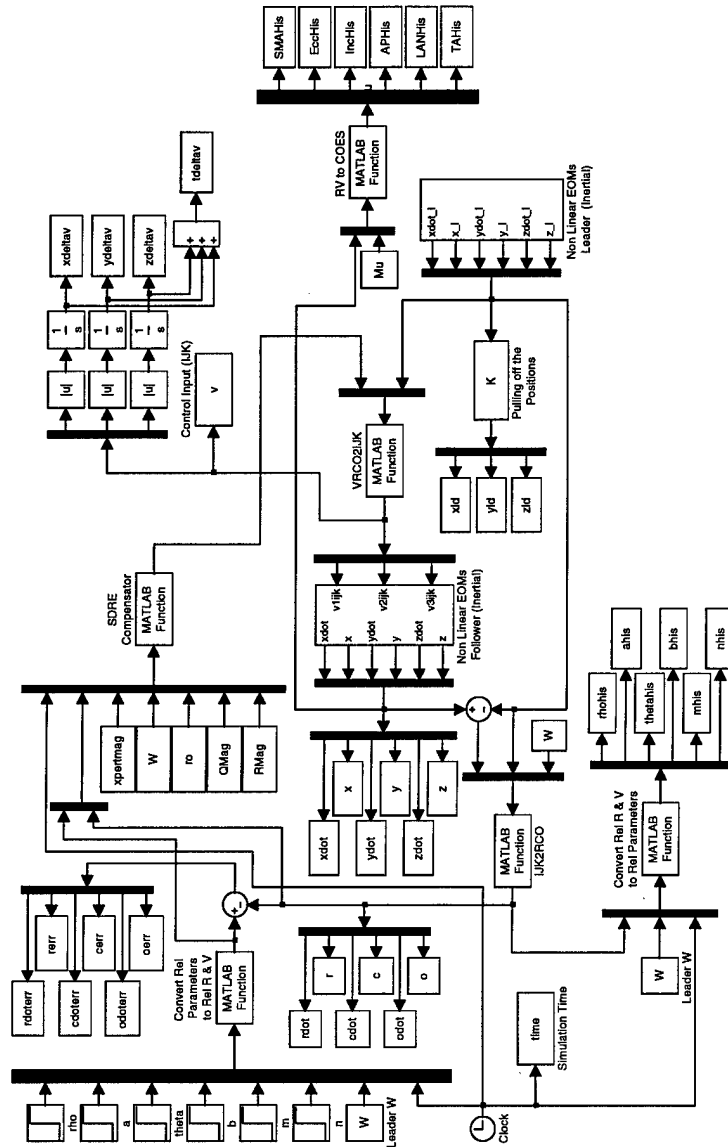
Figure 102   SDRE Simulink Diagram
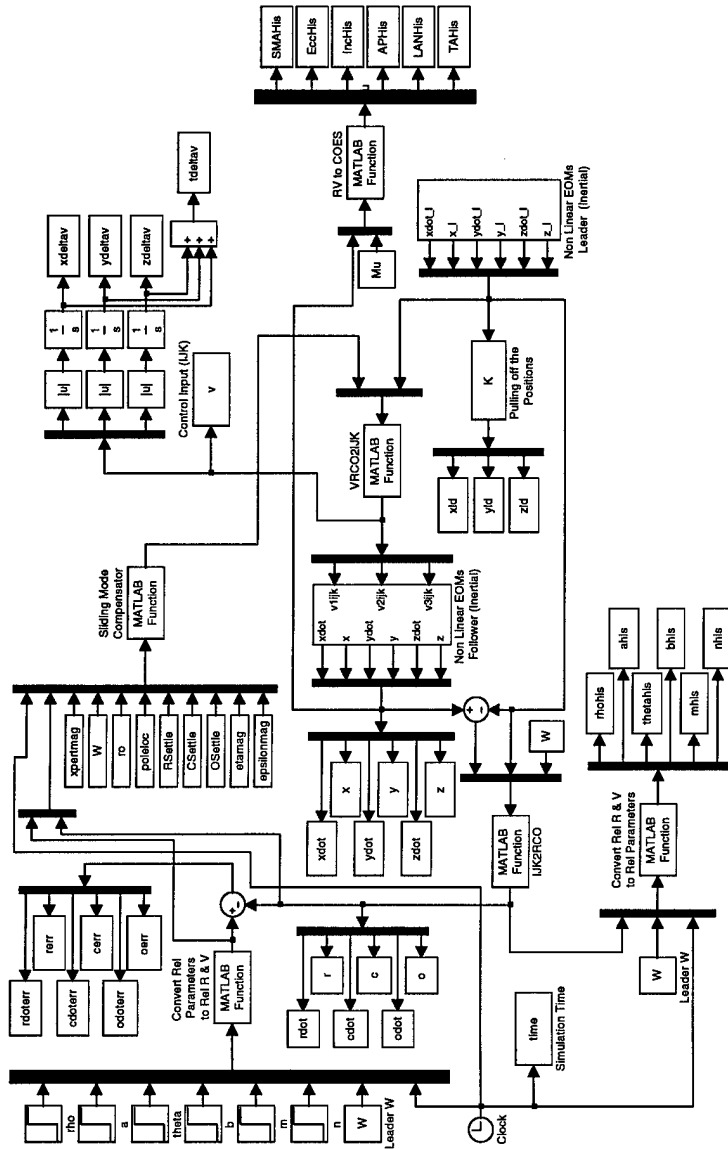
Figure 103   Sliding Mode Simulink Diagram

Bibliography

1. Agency, European Space. "Cluster II Homepage." http://sci.ea.int/cluster, February 2001.

2. Avanesov, Guenrikh A: and others. "LOCSS (Local Space Service program) and its Implementation on the Basis of a Small Satellite Cluster," *Acta Astronautica, 39*:1025–1032 (December 1996).

3. Baker, David (ed). *Jane's Space Directory* (16th Edition). Alexandria, VI: Jane's Information Group Inc., 2000.

4. Chao, C.C. and others. "Dynamics and Control of Cluster Orbits for Distributed Space Missions." *Proceedings of the AAS/AIAA Space Flight Mechanics Meeting.* 355–374. 1999.

5. Chobotov, Vladimir A. (ed). *Orbital Mechanics* (1st Edition). Washington D.C.: American Institue of Aeronautics and Astronautics, Inc., 1991.

6. Clohessy, W.H. and R.S. Wiltshire. "Terminal Guidance System for Satellite Rendezvous," *Journal of the Aerospace Sciences, 27*:653–658 (September 1960).

7. Filer, Sherrie Norton. *Investigation of the Observability of a Satellite Cluster in a Near Circular Orbit.* MS thesis, AFIT/GA/ENY/89D-2, Graduate School of Engineering, Air Force Institute of Technology (AETC), Wright-Patterson AFB OH, March 1989 (AD-A216224).

8. Frayssinhes, Eric and Erick Lansard. "Designing Clusters of Satellites for Radiolocalisation Purposes." *Proceedings of the AAS/AIAA Astrodynamics Conference.* 521–533. 1996.

9. Ganz, Aura and Bo Li. "Design and Analysis of Satellite Clusters." *IEEE Global Telecommunications Conference.* 1–32. 1991.

10. Garrison, James L. and Penina Axelrad. "Application of the Extended Kalman Filter for Relative Navigation in an Elliptical Orbit." *Proceedings of the 6th AAS/AIAA Spaceflight Mechanics Conference.* 693–712. 1996.

11. Kang, Wei and others. "Multi-Satellite Formation and Reconfiguration." *Proceedings of the American Control Conference.* 379–383. 2000.

12. Kreyszig, Erwin. *Advanced Engineering Mathematics* (7th Edition). New York: John Wiley and Sons Inc., 1993.

13. Larson, Roland E. and Robert P. Hostetler. *Calculus with Analytic Geometry* (3rd Edition). Lexington, MA: D.C. Heath and Company, 1986.

14. Larson, Wiley J. and James R. Wertz (ed). *Space Mission Analysis and Design* (Second Edition). Torrance, CA: Microcosm, Inc. and Kluwer Academic Publishers, 1992.

15. Martin, Maurice and Michael J. Stallard. "Distributed Satellite Missions and Technologies - The TechSat 21 Program." *AIAA Space Technology Conference and Exposition.* 1999.

16. Menon, P.K. and others. *Nonlinear Synthesis Tools User's Manual* (1st Edition). Los Altos, CA: Optimal Synthesis Inc, 1998.

17. Middendor, J.T. *Navigation of a Satellite Cluster with Realistic Dynamics*. MS thesis, AFIT/GA/ENY/91D-5, Graduate School of Engineering, Air Force Institute of Technology (AETC), Wright-Patterson AFB OH, March 1991 (AD-A243897).

18. Ogata, Katsuhiko. *Modern Control Engineering* (3rd Edition). Upper Saddle River, NJ: Prentice-Hall Inc., 1997.

19. Serway, Raymond A. *Physics for Scientists and Engineers with Modern Physics* (2nd Edition). Philadelphia, PA: Saunders College Publishing, 1986.

20. Sidi, Marcel J. *Spacecraft Dynamics and Control* (1st Edition). New York: Cambridge University Press, 1997.

21. Slotine, Jean-Jacques E. and Wieping Li. *Applied Nonlinear Control* (1st Edition). Englewood Cliffs, New Jersey: Prentice Hall, 1991.

22. Space Vehicles Directorate, AFRL. "TechSat 21 - Space Missions Using Satellite Clusters." http://www.vs.afrl.af.mil/TechProgs/TechSat21/NGSC.html, December 2000.

23. Sparks, Andrew and others. "Coordinated Control of Multi-Satellite Systems." Submitted to Journal of Guidance and Control, January 2000.

24. Sparks, Anthony. "Satellite Formationkeeping Control in the Presence of Gravity Pertubations." *Proceedings of the American Control Conference*. 844–848. 2000.

25. Swinerd, G.G. and J. Murdoch. "An Assessment of Satellite-to-Satellite Tracking Applied to Satellite Clusters." *Proceedings of the Astrodynamics Conference*. 1001–1018. 1985.

26. Tallarida, Ronald J. *Pocket Book of Integrals and Mathematical Formulas* (2nd Edition). Boca Raton, FL: CRC Press, 1992.

27. Vassar, Richard H. and Richard B. Sherwood. "Formationkeeping for a Pair of Satellites in a Circular Orbit," *Journal of Guidance, Navigation, and Control*, 8:235–242 (March 1985).

28. Ward, Michael L. *Estimated Satellite Cluster Elements in Near Circular Orbit*. MS thesis, AFIT/GA/AA/88D-13, Graduate School of Engineering, Air Force Institute of Technology (AETC), Wright-Patterson AFB OH, March 1988 (AD-A202938).

29. Wiesel, William E. *Spaceflight Dynamics* (Second Edition). Boston, MA: Irwin McGraw-Hill, 1997.

30. Yan, Qiguo and others. "Nonlinear Dynamics and Output Feedback Control of Multiple Spacecraft in Elliptical Orbits." *Proceedings of the American Control Conference*. 839–843. 2000.

31. Yeh, Hsi-Han and Andrew Sparks. "Geometry and Control of Satellite Formations." *Proceedings of the American Control Conference*. 384–388. 2000.

Vita

David J. Irvin Jr. was born in Honolulu, HI into an Army family stationed at Scholfield Barracks. He attended high school at South Caldwell H.S. in Hudson, NC and entered the U.S. Air Force Academy in June 1992 where he graduated with a Bachelor of Science degree in Astronautical Engineering.

His first assignment was to Cape Canaveral AS, FL in August 1996 where he served under U.S. Space Command as an Upper Stage Mechanical Engineer for the Titan IV program. After two years, he was reassigned to the 45th Space Wing Command Post located at Patrick AFB, FL where he remained until his entrance into the Air Force Institute of Technology at Wright Patterson AFB, OH in August 1999. Upon graduation, he will be assigned to the Air Force Research Lab at Eglin AFB, FL.

REPORT DOCUMENTATION PAGE

Form Approved
OMB No. 0704-0188

1. REPORT DATE *(DD-MM-YYYY)*	2. REPORT TYPE	3. DATES COVERED *(From - To)*
08-03-2001	Thesis	Mar 2000 - Mar 2001

4. TITLE AND SUBTITLE	5a. CONTRACT NUMBER
A STUDY OF LINEAR VS. NONLINEAR CONTROL TECHNIQUES FOR THE RECONFIGURATION OF SATELLITE FORMATIONS	
	5b. GRANT NUMBER
	5c. PROGRAM ELEMENT NUMBER

6. AUTHOR(S)	5d. PROJECT NUMBER
David J. Irvin, Jr., Captain, USAF	
	5e. TASK NUMBER
	5f. WORK UNIT NUMBER

7. PERFORMING ORGANIZATION NAME(S) AND ADDRESS(ES)	8. PERFORMING ORGANIZATION REPORT NUMBER
Air Force Institute of Technology Graduate School of Engineering and Management 2920 P Street, Building 640 WPAFB OH 45433-7765	AFIT/GA/ENY/01M-02

9. SPONSORING/MONITORING AGENCY NAME(S) AND ADDRESS(ES)	10. SPONSOR/MONITOR'S ACRONYM(S)
AFOSR/NM Dr. Marc Jacobs 801 North Randolph Rm 732 Arlington, VA 22203-1977	
	11. SPONSOR/MONITOR'S REPORT NUMBER(S)

12. DISTRIBUTION/AVAILABILITY STATEMENT
APPROVED FOR PUBLIC RELEASE; DISTRIBUTION UNLIMITED

13. SUPPLEMENTARY NOTES

14. ABSTRACT
This thesis investigates several linear and nonlinear feedback control methods for satellite formation reconfigurations and compares them to a near optimal open loop, discrete-time, impulsive maneuver. The reconfigurations are done in terms of a set of relative parameters that define an orbit about the leader satellite (or center reference position if a leader satellite does not exist at the center of the formation). The purpose of the study is two-fold, to compare the control usage of continuous feedback control methods versus a discrete burn method and to determine if nonlinear control techniques offer significant improvement over more conventional linear control laws. Linear Quadratic Regulators (LQR), LQR with linearizing feedback, State Dependent Riccati Equation (SDRE) and sliding mode controllers are considered. Simulations showed that reconfigurations for small relative orbits were adequately controlled using linear techniques.

15. SUBJECT TERMS
Satellite Formations, Relative Satellite Navigation, Reconfiguration, Satellite Formation Flying, LQR, SDRE

16. SECURITY CLASSIFICATION OF:			17. LIMITATION OF ABSTRACT	18. NUMBER OF PAGES	19a. NAME OF RESPONSIBLE PERSON
a. REPORT	b. ABSTRACT	c. THIS PAGE			Lt Col David Jacques, AFIT/ENY
U	U	U	UU	150	19b. TELEPHONE NUMBER *(Include area code)* (937)255-3636 x4723

Standard Form 298 (Rev. 8/98)
Prescribed by ANSI Std. Z39.18